Cubatic Phase in Complex Liquids

Foto omslag: A. Blaak

Cubatic Phase in Complex Liquids

Cubatische Fase
in
Complexe Vloeistoffen

(met een samenvatting in het Nederlands)

Proefschrift

ter verkrijging van de graad van doctor aan de Universiteit Utrecht op gezag van de Rector Magnificus, Prof. dr. H.O. Voorma, ingevolge het besluit van het College van Decanen in het openbaar te verdedigen op maandag 15 september 1997 des namiddags te 4.15 uur

door

Ronald Blaak

geboren op 8 september 1970 te Etten-Leur

Promotor: Prof. dr. D. Frenkel
Faculteit der Scheikunde van de Universiteit Utrecht en
FOM-Instituut voor Atoom- en Molecuulfysica te Amsterdam

Copromotor: Dr. B.M. Mulder
FOM-Instituut voor Atoom- en Molecuulfysica te Amsterdam

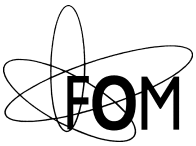

The work described in this thesis was performed at the FOM-Institute for Atomic- and Molecular Physics, Kruislaan 407, 1098 SJ, Amsterdam, The Netherlands. The work is part of the research program of the Stichting voor Fundamenteel Onderzoek der Materie (FOM) and was made possible by financial support from the Nederlandse Organisatie voor Wetenschappelijk Onderzoek (NWO).

ISBN 90-393-1961-8

Subject headings: density functional theory / computer simulations / liquid crystals / phase transitions

Contents

Chapter 1 General Introduction **1**
1.1 Gas, Liquid and Solid 1
1.2 Liquid Crystals 4
1.3 Cubatics 5

Chapter 2 Technical Introduction **9**
2.1 Statistical Mechanics 9
2.2 Density Functional Theory 12
2.3 Excluded Volume 15
2.4 Bifurcation Theory 16
2.5 Thermodynamics 19
2.6 NPT-Simulations 21

Chapter 3 Theory of Crosses **25**
3.1 Introduction 25
3.2 Free Energy 27
3.3 Analysis 28
3.4 Bifurcation Analysis 32
3.5 Trial Functions 39
3.6 Gaussian Approximation 44
3.7 Discussion 49

Chapter 4 Simulation of Crosses **53**
4.1 Introduction 53
4.2 Virial Coefficients 54
4.3 Parameter Hopping 60
4.4 Cubatic order 62
4.5 High density phases 63
4.6 Simulation results 64
4.7 Discussion 69

Chapter 5 Monodisperse Cylinders **71**
5.1 Introduction 71
5.2 Excluded Volume 72
5.3 Series Expansion 74
5.4 Free Energy 75
5.5 Bifurcation Analysis 77
5.6 Trial Functions 81
5.7 Discussion 87

Chapter 6 Assembly and Polydispersity of Cylinders **89**
6.1 Introduction 89

6.2 Aggregation 89
6.3 The Isotropic Phase 92
6.4 Bifurcation Analysis 95
6.5 Polydispersity 98
6.6 Discussion 101

Chapter 7 Simulation of Cylinders 103
7.1 Introduction 103
7.2 Overlap Criterion 104
7.3 Virial coefficients 105
7.4 The Flip-move 106
7.5 Crystal Phases 107
7.6 Simulation Results 108
7.7 Free Energy Calculation 115
7.8 Polydispersity 116
7.9 Discussion 118

Appendix A Special Functions 121
A.1 $\mathcal{D}^l_{m,n}$-functions 121
A.2 Symmetry adapted functions 123
A.3 $\Delta^l_{m,n}$-functions 124
A.4 $C_{l,m}$-functions 125

Bibliography 127

Summary 129

Samenvatting voor Iedereen 131

Nawoord 135

Curriculum Vitae 137

1 General Introduction

In this introduction we give a brief overview of the history of complex liquids. We start with familiar substances and proceed in small steps to more complicated systems, to end finally with the subject of this thesis, the cubatic phase in complex liquids.

1.1 Gas, Liquid and Solid

Most of us never wonder about common things such as sitting on chairs, drinking beer or breathing air. Yet we can only sit on chairs because they are made from *solid* materials as wood, drink beer because it is a *liquid* and breathe air because it is a *gas*. It would be rather difficult to breathe lumps of oxygen, to drink beer which, as a gas, would escape from our glass or to attempt siting on a liquid chair.

Yet under special conditions these changes might actually happen. If one cools oxygen to temperatures below -183^oC it becomes liquid and below -219^oC it even becomes solid. By heating beer most of it will evaporate, and although the chair, if made from wood, will not melt, our glass might.

The existence of these three different forms of a given substance is more commonly known for water. If the temperature is below 0^oC it freezes to form solid ice, it is liquid in the temperature range from 0 to 100^oC and becomes a vapor above 100^oC , all measured at normal pressure. Because if one would check this on the top of a high mountain, where the pressure is lower, these temperatures are a bit lower for boiling and slightly higher for freezing.

These different manifestations of the same material are referred to as *phases*. Many materials are able to exhibit a gas, liquid and solid phase, although most of them, in daily life, will only be found in one phase. By changing the temperature we can influence the phase, for instance melting a solid. This change in appearance is what we call a *phase transition*. The phase transitions we are interested in are reversible, which means that if you change from a liquid to a solid, you can also do the reverse and go back to the liquid again. This is not always possible, for instance if an egg is boiled (long enough) is becomes solid but cannot go back to its initial liquid-like state. The absence of reversibility means that something else is changed in the process too. In contrast, water can freeze to ice and melt back to water as many times we like.

The different phases have also different properties. There is of course the obvious difference between a solid and liquid or gas. Whereas we can sit on anything solid (as long as it is strong enough), we cannot do this with a liquid or gas. A gas can easily be compressed by a pump while for liquids and solids this is very difficult.

The property that we are after is that of the structure of a phase, in other words how do we describe one of the three phases. In order to do so we need to describe a substance in general, and more precisely what it is it made of. Greek philosophers already wondered about this question and one of them, Democritus ($\pm 400 BC$), thought that each material was made from small particles which could not be divided anymore, *atoms*. This speculative idea was in the 19th century used by Avogadro and others, leading to periodic system of Mendelejev, which lists the different atoms. These atoms can be chemically bonded with each other to form larger particles or *molecules*. Any pure substance consists of many identical molecules. The existence of atoms was, in the begin of this century, confirmed by the experiments of Perrin.

But already before this result, the assumption was used and led to the formulation of the kinetic gas theory by Maxwell. This theory assumes that gas consists out of many small identical particles which fly randomly through space and only bounce off the container wall. Although these particles also collide among each other this is neglected which, in the case of an dilute gas, is justified. This apparent random movement of the particles leads to a homogeneous distribution of particles over the available volume. A gaseous phase is therefore characterized by the absence of any structure.

This is very similar to a liquid phase. Also a liquid phase is completely disordered, but at a much higher density than a gas. In contrast with a gas, the collisions and interactions between particles can no longer be neglected. Particles are still able to move freely through the available volume, but as they hinder each other considerably it takes a much longer time to travel from one side to the other side of the container. This interaction also leads to some local order which might extend over a few times the size of the particles. But since there is no long range order, also the liquid, although at a much higher density, is a homogeneous phase.

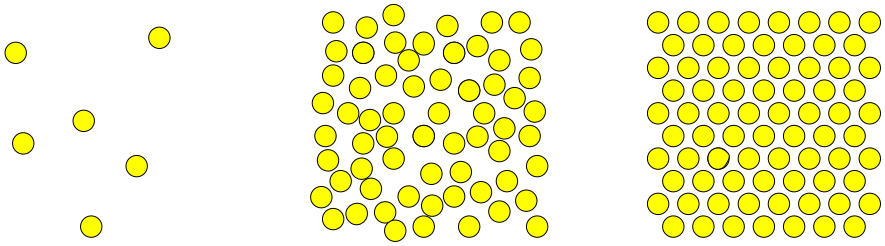

Figure 1.1: A schematic drawing of the three different phases in two dimensions, from left to right a gas, liquid and solid.

Solids, however, are different from gases and liquids in the sense they are not homogeneous at all, they are ordered. This was already suggested in the 18th century by mineralogists, based on their discovery that the direction of all faces of a crystal, like quartz, can be described by integer numbers. From this observation they concluded that a crystal a three-dimensional periodic arrangement (lattice) of identical particles is. This was later, in the beginning of this century, confirmed by X-ray experiments of Friedrich and Knipping, and the theoretical work of Von Laue and Bragg. The particles in a crystal are not able to move freely anymore but can only vibrate about their equilibrium lattice positions, which are correlated over large distances.

In figure 1.1 these three different phase are visualized in two dimensions, where we used disks to denote the particles. The gas and liquid are disordered and differ only in density, the crystal is a nicely ordered structure.

Although the gas and liquid appear in only one form, for crystals there are many different regular arrangements of the particles. Carbon for instance is known in three different structures, diamond, graphite and more recently crystals of Bucky-balls. A solid is however not always crystalline. Glass for instance is an example of a solid which does not have any long-range order. These solids are known as an amorphous solids or *glasses*.

So far we only discussed the structural differences between phases, but not for what reason these phases exist. The major breakthrough was made by Van der Waals. By assuming that particles at short-range repel each other and attract each other at long distances he was able to explain the difference between a gas and a liquid. For low temperatures the attractive forces keep particles together, but not too close due to the repulsion, to form a liquid. On heating particles begin to move faster and the attraction is not strong enough anymore to maintain particles together and they will fly apart to form a gas.

The repulsion for these classical systems could be understood by the assumption of hard spherical objects for the atoms and molecules. The explanation of the true nature of this force, however, had to wait until the beginning of this century and the development of quantum mechanics, which showed that the repulsion is a consequence of the Pauli exclusion principle. The long range attractions, which now are known as Van der Waals forces, are due to the presence of dipole-dipole interactions.

As different molecules have different strengths of interactions, materials will in general have different properties like the boiling temperature but the general scenario for the gas-liquid transition remains the same.

By going to lower temperatures the rate at which particles move decreases and the attractive forces become strong enough to keep particles close together. In fact the forces become so strong that particles cannot escape from their neighbors anymore, what in a liquid phase is still possible, and a solid is formed.

In order to explain these phenomena we used the presence of attracting forces, but in 1957 Alder and Wainwright performed computer simulations on a system of hard spheres [1], in which case particles do not attract each other at all, but only collide with each other like billiard balls. Surprisingly these simulations showed that such a system crystallizes as well. In other words a crystal can be formed by particles which only repel each other.

More recently other interesting discoveries have been made with respect to the interaction between molecules. Computer simulations of C_{60} indicated that these particles do have a gas and solid phase but might not have a liquid phase [2].

Other simulations on a system of hard spheres showed that if the attraction becomes very short-range there exist two solid phases having the same structure but different densities, which is analogous to the gas and liquid phase [3].

1.2 Liquid Crystals

In the previous section particles or molecules are described as spherical objects. But in general molecules are not spherical at all, but can have various shapes. An oxygen molecule in air for instance, is made from two identical oxygen atoms, and a water molecule is formed by one oxygen and two hydrogen atoms. Although each atom in first approximation is spherical, combinations of them are not. The larger molecules are the more complex they can be in shape. There are flat or disk-like particles like clay or benzene aggregates and rod-like particles such as cholesterol. These particles are stiff in the sense that their shape is more or less fixed. But there are also chain-like molecules, as found in plastics, which do not have a specific shape, but are flexible and can form coils.

This opens a much broader perspective with respect to the different phases discussed in the previous section. Particles now do not only have the possibility to order their positions but also their orientations. Or combinations, phases in which particles are ordered with respect to orientation but disordered as far as their positions are concerned. Or phases for which the positions of the particles are ordered, but only in one dimension and disordered in the other two dimensions. This is the field of *liquid crystals*, in which a phase can have properties which remind us of a solid structure combined with properties found for liquids.

Similar to the freezing of hard spheres, these new phases can also be formed in absence of long-range attraction. In this thesis we will focus on these liquid crystals, in which the particles can be described by hard particles, like billiard balls, but now with other shapes. At first glance this seems an highly idealized version of real particles and interactions, but there are experimental systems available in which only these hard interactions are present. One such example is the the tobacco mosaic virus (TMV), which under the appropriate experimental conditions behave as a hard rod-like particle. This particle is about 300 nm long and 18 nm wide, but can be altered in aspect ratio by end-to-end aggregation, to make longer particles, or by sonic fragmentation, to make smaller particles.

Similar to spherical particles at low densities, also rod-like particles will have no positional order in a dilute solution. And since particles are far away from each other they can rotate freely and have no preferred direction. This homogeneous liquid phase with no orientational order is known as the *isotropic* phase, and is schematically represented in figure 1.2.

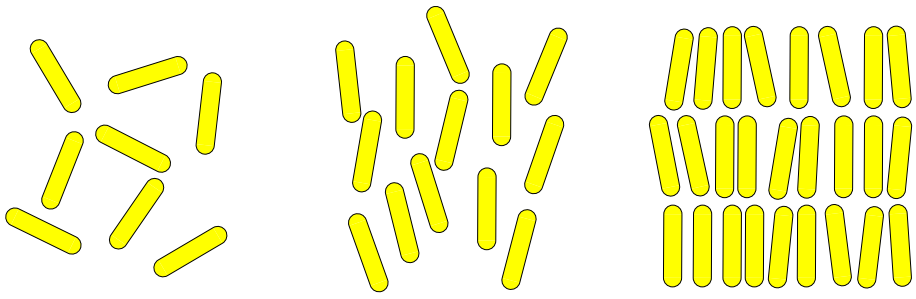

Figure 1.2: A schematic drawing of the three different phases of rod-like particles, from left to right the isotropic a nematic and a smectic phase.

There are two ways in which we can now alter the phase of such a system, either we change the pressure or we change the temperature. If we increase the pressure or decrease the temperature the density, in such an isotropic phase for rod-like particles, will increase and the interaction becomes stronger in the sense that particles hinder each other more in their movement. If the density is high enough the rods will align and form an ordered phase. On average all particles are pointing in the same direction and the system is invariant under rotations about this direction. The positions of the centers of mass, however are still homogeneously distributed over the available volume. Such a phase in which there is only orientational and no positional order is called a *nematic* phase, and more precisely a uniaxial nematic, where uniaxial is referring to the fact that there is one preferred direction. This nematic phase illustrated in figure 1.2.

It was Onsager who in 1949 showed that this isotropic-to-nematic phase transition can be explained by assuming that the interaction between the particles is purely repulsive [4].

As we continue to increase the pressure, the system becomes even denser. At first the particles get more and more aligned, but it turns out that the nematic phase at high enough density, also undergoes a phase transition. And this time the positions of the particles become ordered as well. But instead of forming a three-dimensional crystal, particles will arrange themselves in layers. In these layers the particles are still distributed homogeneously, while the orientations are aligned and are perpendicular to the layers. This phase, which schematically is depicted in figure 1.2, is called the *smectic-A* phase, in which particles are orientationally, and in one dimension positionally, ordered and disordered in the other two dimensions.

This is still not the end of the story, because finally the particles in the layers will also order and form a three-dimensional crystal. So an apparently simple rod-like particle is able to form four different phases.

But there are many more phases possible. By changing the aspect ratio or going to more complicated shapes we can form many other liquid crystalline phases. As the name uniaxial nematic already implied there are also non-uniaxial nematics. This phase, also called the *biaxial* phase, has more than one preferred direction, and can for instance be found in mixtures of rod- and disk-like particles. Both rods and disks prefer to be aligned with particles of the same species but do not like to point in the same direction as particles of a different species. This leads a phase with one preferred direction for the rods and another perpendicular direction for the disks. Also different smectic phases exist, the direction of the orientations for instance can be tilted with respect to the layers or be different in successive layers.

1.3 Cubatics

Computer simulations have contributed to the understanding of the phase transitions in liquid crystals, because they showed that many of these phases can be explained by hard-core repulsion only.

In order to study disk-like particles Eppenga and Frenkel simulated infinitely thin platelets [5]. These particles form a nematic phase but when aligned these particles will not notice each other anymore, preventing other transitions to happen.

Mulder and Frenkel used oblate ellipsoids [6, 7], which also formed an nematic phase. As soon as these particles are aligned however, this system can be scaled along the average direction of the particles and the system can be mapped upon a hard sphere system. Also this system therefore does not show any other liquid crystalline phases.

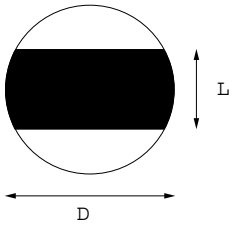

Figure 1.3: A schematic drawing of a cut-sphere, with thickness L and diameter D.

Veerman and Frenkel [8] performed computer simulations of cut-spheres (figure 1.3). These particles are formed by removing everything which is further away from the equatorial plane than a distance $\frac{1}{2}L$. By tuning the ratio of L and the diameter D these particles can go from infinitely thin to complete spheres.

For thin particles they found a isotropic-to-nematic, and nematic-to-*columnar* phase transition. The latter is a formed by particles in columns, for which the columns are ordered in a two-dimensional crystal and the particles inside a column behave as a one-dimensional liquid. For high enough densities the system forms a solid. Thick particles do not show a nematic phase, instead the isotropic phase freezes directly to a solid.

Figure 1.4: Snapshot of a cubatic phase for cut-spheres.

For an intermediate value of $L/D = 0.2$, Veerman and Frenkel unexpectedly discovered a new phase, of which figure 1.4 shows a snapshot. It turned out that this phase did not have any positional order and therefore is a liquid. There is also no preferred orientation of the particles, and therefore it is also not a normal nematic phase. But order is clearly visible. The symmetry of the orientational order is cubic. Instead of one preferred direction of the particles, there are now three different directions, which are perpendicular and have equal strength. It is in fact a triaxial nematic phase, because it is a special form of the biaxial phase. Two perpendicular directions automatically define

the third direction and they will in general have different strengths. In this case however they are identical. Analogous the the name nematic, Veerman and Frenkel named this phase the *cubatic* phase and this phase is the subject of the present thesis.

2 Technical Introduction

In this chapter we introduce all standard concepts and techniques which are used in this thesis. These are both theoretical and simulation techniques. We introduce the density functional theory and the idea of bifurcation analysis, which despite its simplicity is a powerful tool to study phase transitions. Further more we give a brief introduction in the concept of computer simulation and a more specifically the NPT-ensemble.

2.1 Statistical Mechanics

If we have two masses interacting through gravitational forces we can still exactly predict what is going to happen at any point in the future or calculate backwards to any point in history. But adding one extra mass makes it impossible to solve the time evolution of the new system. Although we know exactly how the masses interact with each other and what the equations of motion are there is, in general, no way of telling whether they will collide and if so at which instant in time or if they will eventually fly apart (provided this is allowed by the total amount of energy present). Only by numerically solving the equations of motion for short successive intervals of time can this problem be tackled.

It is therefore quite surprising that we can actually tell something about the behavior of systems which have millions of particles all interacting with each other. This is the theory of statistical mechanics. It connects the microscopic interactions of the particles, which determine the equations of motion, with the macroscopic properties of the complete system.

The connection goes via the Helmholtz free energy $F(N, V, T)$, which depends on the number of particles N, the volume V and the temperature T of the system. We assume that the particles are identical, but the analysis can easily be extended to systems which contain different species of particles. Note that the free energy does not contain any detailed information on the particles. That information determines the microscopic state of the system. It consists of two parts, $q^N = \{q_1, q_2, \cdots, q_N\}$ the coordinates of all N particles and $p^N = \{p_1, p_2, \cdots, p_N\}$ the conjugate momenta of the particles. The precise form of these coordinates and momenta depends on the particles we want to describe. For the simple system of point-particles these are only the usual positional coordinates and linear momenta of the particles. If a particle has a finite size however,like spheres and rigid rods, we need to include orientation and angular momentum. In case of polymers and flexible rods we also need to describe the internal structure by including

the internal degrees of freedom. The microscopic state of the system is collectively denoted by $\Gamma = \{q^N, p^N\}$.

The interaction between the particles is included via the Hamiltonian $H_N(q^N, p^N)$ of the system, which is identical to the total energy for the given state Γ. It allows us in principle to solve all equations of motion and therefore to predict how the microstate of the system will evolve in the future. But as already mentioned, if that problem cannot be solved for a relative simple system of three masses only interacting via gravity then it is impossible to do this for millions of particles. A numerical method would also fail given the large number of equations which have to be solved for each small step in time.

Macroscopic observables however are not determined by the exact motion of all particles at each point in time but are obtained from long time averages and are independent of the initial state of the system. Statistical mechanics makes use of these notions by taking a weighted average over all microstates. If we work in the canonical ensemble, which means that we describe the macroscopic system by the number of particles N, the volume V and the temperature T, the weight function which is used is called the Boltzmann weight and is proportional to $\exp(-H_N(\Gamma)/k_BT)$, where k_B is the Boltzmann constant. Any observable A of the macroscopic system can now be obtained by integrating over all microstates Γ

$$< A >= \frac{\int d\Gamma A \exp(-\beta H_N(\Gamma))}{\int d\Gamma \exp(-\beta H_N(\Gamma))} \tag{2.1}$$

where we used $\beta = 1/k_BT$. The quantity we are interested in, the Helmholtz free energy, is directly related to the canonical partition function $Z(N, V, T)$. This is the integral over all different microstates of the particles

$$Z(N, V, T) = \frac{1}{N!h^{3N}} \int d\Gamma \exp(-\beta H_N(\Gamma)) \tag{2.2}$$

The factor $1/N!$ is a consequence indistinguishability of the particles. The factor $1/h^{3N}$ is needed to make the partition function dimensionless. This is done using h, which according to quantum mechanics should be the Planck constant and has the dimension of angular momentum. The actual value is, as far as classical systems are concerned, not relevant, since all observables (2.1) are independent of h. The power of h which is needed depends on the number of degrees of freedom which the particles of the system have. If they have position and orientation this is h^6 per particle. For point-particles, which do not have any orientation this is only h^3.

The Helmholtz free energy can now be obtained from the canonical partition function by taking the logarithm

$$\beta F(N, V, T) = -\log(Z(N, V, T)) \tag{2.3}$$

In simple systems we can split the Hamiltonian in a part containing the potential energy U_N, which only depends on the coordinates of the particles, and a part containing the kinetic energy T_N, which only depends on the momenta

$$H_N(q^N, p^N) = U_N(q^N) + T_N(p^N) \tag{2.4}$$

Point-particles are described completely by their position (x, y, z) in a Cartesian reference frame. The generalized momenta are the usual linear momenta (p_x, p_y, p_z), hence the kinetic energy of one of these particles is given by

$$T = \frac{p_x^2}{2m} + \frac{p_y^2}{2m} + \frac{p_z^2}{2m} \tag{2.5}$$

Note that the integrals over the momenta can be performed analytically. This allows us to write the partition function as

$$Z(N, V, T) = \frac{1}{N! \mathcal{V}_T^N} Q(N, V, T) = \frac{1}{N! \mathcal{V}_T^N} \int dq^N \exp(-\beta U_N(q^N)) \tag{2.6}$$

where we implicitly introduced the configurational integral $Q(N, V, T)$ and where $\mathcal{V}_T$ is the thermal volume defined by

$$\mathcal{V}_T = \sqrt{\frac{h^6 \beta^3}{(2\pi)^3 m^3}} \tag{2.7}$$

For particles with a finite size we need to include the orientation and angular momentum. There are now 6 generalized coordinates needed $q = (\vec{r}, \Omega)$, the 3 position coordinates $\vec{r}$ and in general three angles Ω, for instance the Euler angles, in order to describe the orientation. The kinetic energy of the particles has to be extended with the rotational kinetic energy

$$T^{rot} = \tfrac{1}{2} I_x \omega_x^2 + \tfrac{1}{2} I_y \omega_y^2 + \tfrac{1}{2} I_z \omega_z^2 \tag{2.8}$$

where I_x, I_y and I_z are the principal moments of inertia and ω_x, ω_y and ω_z are the angular velocities of the particle around the appropriate axis. Also the integration over these extra generalized momenta can be performed analytically. As a consequence the thermal volume has to be extended to

$$\mathcal{V}_T = \sqrt{\frac{h^{12} \beta^6}{(2\pi)^6 m^3 I_x I_y I_z}} \tag{2.9}$$

In the simple case of an not interacting system (ideal gas), the configurational integral (2.6) can be evaluated analytically. Since there is no interaction the energy $U_N(q^N)$ is zero and we obtain

$$Z(N, V, T) = \frac{1}{N! \mathcal{V}_T} (8\pi^2 V)^N \tag{2.10}$$

where each integral over the position coordinates gives a factor V, the volume, and each integral over the Euler angles gives a contribution $8\pi^2$. In general however the integral cannot be evaluated analytically and has to be estimated.

Suppose that the potential energy of the system is pair-wise additive. Then we can write the total potential energy as a sum of all pair contributions $u(q_i, q_j)$ depending only on the coordinates of the particles

$$U_N(q^N) = \sum_{i<j} u(q_i, q_j) \tag{2.11}$$

If we also introduce the Mayer-function [9] defined by

$$f_{ij} \equiv \exp(-\beta u(q_i, q_j)) - 1 \tag{2.12}$$

we can express the configurational integral in terms of the Mayer-functions

$$\begin{aligned} Q(N,V,T) &= \int dq^N \prod_{i<j}(1 + f_{ij}) \\ &= \int dq^N \left(1 + \sum_{i<j} f_{ij} + \cdots\right) \end{aligned} \tag{2.13}$$

Taking the thermodynamic limit where the number of particles is going to infinity this expansion can be used to obtain an expression for the Helmholtz free energy in the form of a virial series in the low density limit

$$\begin{aligned} \beta F =& N\left(\log(\rho \mathcal{V}_T) - 1\right) - \tfrac{1}{2}\rho^2 \int dq_1 dq_2 f_{12} \\ & - \tfrac{1}{6}\rho^3 \int dq_1 dq_2 dq_3 f_{12} f_{23} f_{31} + \mathcal{O}(\rho^4) \end{aligned} \tag{2.14}$$

where $\rho \equiv N/(8\pi^2 V)$ is the one-particle distribution function of a homogeneous and isotopic liquid. The first term is the ideal gas contribution of the non-interacting system. The second and third term are proportional to the second virial coefficient B_2 and third virial coefficient B_3, respectively

$$\begin{aligned} B_2 &= -\frac{1}{2(8\pi^2)^2 V} \int dq_1 dq_2 f_{12} \\ B_3 &= -\frac{1}{3(8\pi^2)^3 V} \int dq_1 dq_2 dq_3 f_{12} f_{23} f_{31} \end{aligned} \tag{2.15}$$

Note that in this derivation we assumed that the particles do not have any preferred position or orientation. Hence this formulation is only correct for the positionally and orientationally disordered phase and serves as a correction to the ideal gas.

2.2 Density Functional Theory

The formulation for the Helmholtz free energy (2.14) is only valid for the homogeneous isotropic phase, as was already mentioned in the previous section. What we need, however, is the ability to describe ordered phases as well. Therefore we have to

generalize the derivation of the previous section and we arrive at the density functional theory.

For a more detailed description of density functional theory we refer to Evans [10]. Here we will only give a brief overview of the main results.

In order to describe the ordered system we define the one-particle distribution function (ODF), which we will denote by $\rho(q) = \rho(\vec{r}, \Omega)$. It is proportional to the fraction of particles with given position $\vec{r}$ and orientation Ω and is normalized to the total number of particles when integrated over q

$$\int dq\rho(q) = N \tag{2.16}$$

In case of a homogeneous isotropic phase this function reduces to the constant number density $\rho = N/(8\pi^2 V)$ as was found in the previous section.

For a classical many particle system, density functional theory asserts that there exists a functional $W[\rho]$ of the ODF for which the following two properties hold

1. For all ODF ρ, we have the inequality $\mathcal{W}[\rho] \geq \mathcal{W}[\rho_{eq}]$, where ρ_{eq} is the equilibrium ODF.
2. $\mathcal{W}[\rho_{eq}] = \mathcal{W}_{eq}$ where $\mathcal{W}_{eq}$ is the equilibrium value of the grand canonical potential.

Although the statements are correct, they do not provide a way to explicitly construct the functional $\mathcal{W}[\rho]$. Nevertheless we continue to follow along this line of reasoning. The grand canonical potential W can be related to the Helmholtz free energy F by the thermodynamic relation $W = F - \mu N$, where μ is the chemical potential, hence we can write the functional in the form

$$\mathcal{W}[\rho] = \mathcal{F}[\rho] - \mu \int dq\rho(q) \tag{2.17}$$

where we introduced the functional $\mathcal{F}[\rho]$, which corresponds to the Helmholtz free energy of the system. In equilibrium this functional reduces to the true minimum of the free energy $\mathcal{F}[\rho_{eq}] = F$. We can split the free energy functional in an ideal contribution and an excess term $\Phi[\rho]$ which contains all contributions of the interacting particles in the system

$$\beta\mathcal{F}[\rho] = \int dq\rho(q)(\log(\rho(q)\mathcal{V}_T) - 1) - \Phi[\rho] \tag{2.18}$$

where the first term is a generalization of the ideal gas contribution in (2.14). In order to obtain the equilibrium ODF we need to find the minimum of the grand canonical potential. By taking the functional derivative with respect to the ODF we get the stationarity equation, which is necessary but not sufficient to guarantee a minimum

$$\left.\frac{\delta\mathcal{W}[\rho]}{\delta\rho(q)}\right|_{\rho=\rho_{eq}} = \left.\frac{\delta\mathcal{F}[\rho]}{\delta\rho(q)}\right|_{\rho=\rho_{eq}} - \mu = 0 \tag{2.19}$$

for fixed values of μ. Note that μ in this equation for the free energy functional serves as a Lagrange multiplier to constrain the integral of the ODF as defined by (2.16).

We are left with the problem of determining the excess free energy $\Phi[\rho]$. We could for instance use the virial expansion. Throughout this thesis however we will approximate it by the second virial term only, which is also known as the Onsager approximation, and is obtained by expanding excess term $\Phi[\rho]$ in equilibrium in the low density limit

$$\begin{aligned}\Phi[\rho] =&\Phi[\rho=0] + \int dq\rho(q)\left.\frac{\delta\Phi}{\delta\rho(q)}\right|_{\rho=0} + \\ &\tfrac{1}{2}\int dq_1 dq_2 \rho(q_1)\rho(q_2)\left.\frac{\delta^2\Phi}{\delta\rho(q_1)\delta\rho(q_2)}\right|_{\rho=0}\end{aligned} \tag{2.20}$$

The first term on the right-hand side is a constant as therefore has no observable effect. In order to have a stable phase the second term is zero by definition. The third term can be identified with

$$\Phi[\rho] = \tfrac{1}{2}\int dq_1 dq_2 \rho(q_1)\rho(q_2) f_{12}(q_1, q_2) \tag{2.21}$$

It is the first correction on the ideal gas system and was used by Onsager to explain the isotropic-to-nematic phase transition in a system of hard elongated particles [4]. For this system it can be shown explicitly that the third and higher virial coefficients of infinitely long rods can be neglected and hence the theory is exact in the isotropic phase, but in general higher virial coefficients are relevant. One can however hope that the second virial approach will give a qualitatively correct description of the system.

Attempting to minimize the free energy functional in the complete available function space for the ODF is a time consuming and elaborate task that usually involves evaluating high dimensional integrals in an iterative scheme. Difficulties will arise especially when the equilibrium ODF is not a smooth but a fluctuating or strongly peaked function. Instead of solving the complete problem one could try to use trial functions.

Trial functions are a way to reduce the infinite dimensional function space for the ODF to a finite dimensional, preferably single parameter space. In this parameter space we then minimize the free energy. Although the corresponding free energy in general will not be the true free energy, by choosing proper trial functions we obtain a good estimate. The choice of trial functions is arbitrary as long as they are relevant to the problem and they are chosen on basis of convenience, which is best illustrated by an example.

Suppose for instance that we would like to describe Onsager's system of long rods [4]. The equilibrium ODF $\psi(\theta)$, now only depending on the angle θ of the particles with respect to the nematic director, can always be expanded in terms of Legendre polynomials, denoted by $P_l(\cos(\theta))$. As a trial function we could truncate the expansion after the fourth Legendre polynomial

$$\psi(\theta) = \sum_{l=0}^{4} a_l P_l(\cos(\theta)) \tag{2.22}$$

where the constants a_l are the not yet determined parameters. This particular choice has two drawbacks. The first one is that the ODF, during the process of minimizing

the free energy, might become negative. This is unphysical and should be avoided. The second problem is that this trial function is not capable of forming a strongly peaked ODF as it should be in the case of elongated particles. Both problems can easily be solved by using a trial function like

$$\psi(\theta) = \exp\left[a_2 P_2(\cos(\theta))\right] \tag{2.23}$$

Trial functions are strongly dependent on the system one is interested in and some insight in its behavior is essential for the choice of appropriate and convenient functions.

2.3 Excluded Volume

In the previous section we obtained an expression for the free energy functional $\mathcal{F}[\rho]$ of an order system as function of the ODF $\rho(q)$. We are going to apply this formalism to systems of hard particles. Moreover we will focus on systems which have no positional order but might possibly be orientationally ordered. We therefore define the orientational distribution function which we will denote by $\psi(\Omega)$

$$\rho(\vec{r}, \Omega) = n\psi(\Omega) \tag{2.24}$$

where $n = N/V$ is the number density and $\int d\Omega\psi(\Omega) = 1$. If we fill this in the free energy expression (2.18), perform the integration over the spatial coordinates and divide by the number of particles we obtain the free energy per particle

$$\begin{aligned}\frac{\beta\mathcal{F}[\psi]}{N} =& \log(n\mathcal{V}_T) - 1 + \int d\Omega\psi(\Omega)\log(\psi(\Omega)) \\ &+ \tfrac{1}{2}n\int d\Omega d\Omega'\psi(\Omega)\psi(\Omega')\mathcal{E}(\Omega,\Omega')\end{aligned} \tag{2.25}$$

where $\mathcal{E}(\Omega,\Omega')$ is defined via the Mayer-function f, which still depends on the pair potential energy of the particles

$$\mathcal{E}(\Omega,\Omega') = -\frac{1}{V}\int d\vec{r}d\vec{r}\,' f(\Omega,\vec{r},\Omega',\vec{r}\,') \tag{2.26}$$

For hard-core interactions the only restriction on the particles is that they are not allowed to overlap. Hence the potential energy for overlapping particles has to be infinite and for non overlapping particles the potential is an arbitrary constant which can be chosen to be zero. Hence the Mayer-function has a simple form

$$f = \begin{cases} 0 & \text{if no overlap} \\ -1 & \text{if overlap} \end{cases} \tag{2.27}$$

As a consequence the integral (2.26) reduces to the integral

$$\mathcal{E}(\Omega,\Omega') = \int_{overlap} d\vec{r} \tag{2.28}$$

which is the excluded volume. It is the volume from which the second particle is excluded for the given orientations in order to avoid overlap of the two particles, as is illustrated in figure 2.1.

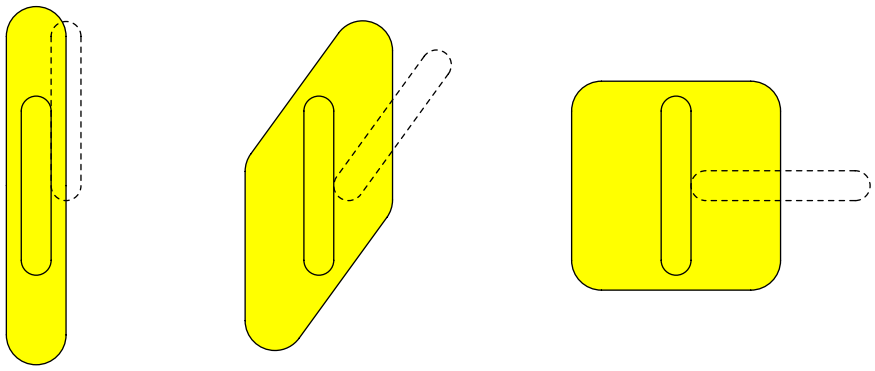

Figure 2.1: The excluded volume of two particles (gray area) for three different relative orientations. If the center of mass of the second particle is in this volume, the particles will overlap.

The excluded volume is in general a complicated function $\mathcal{E}(\Omega)$ of the relative orientation of two particles, and only for simple particles is known analytically.

The free energy (2.25) has to be minimized for the equilibrium ODF. The first integral is the orientational entropy of the system and is minimal for the isotropic phase. It will therefore try to keep the system disordered. The second integral is translational entropy of the system and is proportional to the density. In order to minimize the free energy it will tend to minimize the excluded volume. According to the Brunn-Minkowski theorem, this minimum excluded volume for convex particles is reached for parallel orientations [11].

These opposite forces will determine the phase behavior of the system. For low densities the first term is dominant, favoring an isotropic phase. On increasing the density this last term becomes more important and will drive the system to an more ordered phase.

We will use the excluded volume not only as a function of the relative orientation of two particles but also in the form of a functional of an ODF ψ

$$\mathcal{E}[\psi] = \int d\Omega' \psi(\Omega') \mathcal{E}(\Omega, \Omega') \tag{2.29}$$

This definition will allow us not only to formulate the equations in a more compact way, but also to derive a number of interesting and useful properties.

2.4 Bifurcation Theory

In the section 2.2 we have seen that the equilibrium distribution function can be found by minimizing the Helmholtz free energy functional. This is in general difficult task and usually one needs to solve the problem numerically. There is however an

alternative path which allows us to get some insight in the behavior of the system, the so-called bifurcation analysis. This technique was for the first time applied on liquid crystals in 1978 by Kayser and Raveché for the isotropic-to-nematic phase transition in a system of long rods [12], and later extended by Mulder [13].

Instead of minimizing the free energy functional (2.25) with respect to the normalized ODF ψ, we can also solve the stationarity equation. The stationarity equation is now obtained by taking the functional derivative of the free energy (2.25) with respect to the ODF ψ

$$\log(\psi) + 1 + n\mathcal{E}[\psi] - \mu = 0 \tag{2.30}$$

This equation has the trivial solution $\psi_0 = 1/(8\pi^2)$, which corresponds to the isotropic phase. As was already mentioned, being a solution of the stationarity equation does not necessarily mean that it is also the minimum of the free energy, it might also be a maximum or saddle point. It is obvious that for sufficiently low densities the interaction between the particles is negligible and therefore the isotropic phase is the equilibrium state. On increasing the density, however, the particles will start to interact more strongly and the system will undergo a phase transition. The isotropic phase will therefore no longer be the real minimum of the free energy. In fact at high enough density it will even cease to be a local minimum of the free energy and will change to a local maximum. But this means that the isotropic phase becomes unstable and any small variation in the ODF will lead to a lower free energy. The density at which this happens is called the bifurcation density and is an upper limit for the phase transition.

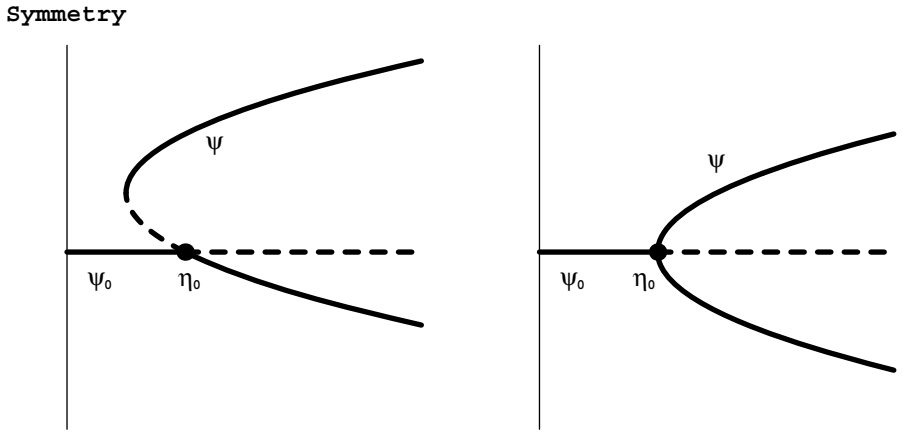

Figure 2.2: Generic bifurcation diagrams for a first order (left) and continuous (right) phase transition. The lines represent the solutions of the stationarity equation. The solid curves are corresponding to minima in the free energy, dashed lines to maxima. n_0 is the bifurcation density.

In figure 2.2 the idea of bifurcation is schematically illustrated. ψ_0 is a local minimum of the free energy up to the density n_0, where it becomes unstable with respect to the solution ψ. This solution is characterized by a different symmetry than ψ_0. In the case of a first order phase transition the initial branch corresponds to a maximum and only later on becomes a true minimum of the free energy. Only in the case of a continuous

phase transition the solution ψ is immediately stable and is the bifurcation density corresponding to the true transition density.

In order to calculate the bifurcation density we solve the stationarity equation (2.30) near this point. We expand both the ODF and number density in a small parameter ε around the isotropic ODF ψ_0 and the unknown bifurcation density n_0

$$\begin{aligned} \psi &= \psi_0 + \varepsilon\psi_1 + \varepsilon^2\psi_2 + \cdots \\ n &= n_0 + \varepsilon n_1 + \varepsilon^2 n_2 + \cdots \end{aligned} \tag{2.31}$$

The ODF ψ has to be normalized to unity. This has already been taken care of by the first term ψ_0. As a consequence all other functions ψ_i have to be normalized to zero. Filling these expansions into (2.30) and expanding in ε we obtain a coupled non-linear set of equations in the functions ψ_i and coefficients n_i. These equations are the bifurcation equations. The first order equation is given by

$$\frac{\psi_1}{\psi_0} + n_0\mathcal{E}[\psi_1] = 0 \tag{2.32}$$

This equation has the form of an eigenvalue problem, and in order to solve it we need to determine the eigenfunctions and eigenvalues of the excluded volume $\mathcal{E}$. Since this function in principle is known, we can solve this equation. For each eigenfunction and corresponding eigenvalue λ the remaining equation is $1/\psi_0 + n_0\lambda = 0$. Since we are interested in the lowest density at which the isotropic phase becomes unstable we need to find that eigenvalue of the excluded volume that is negative and largest in absolute value.

As we will see later on there might be several different eigenfunctions corresponding to the same eigenvalue. In order to determine the function ψ_1 we therefore need to go to the second bifurcation equation

$$\frac{\psi_2}{\psi_0} - \tfrac{1}{2}\left(\frac{\psi_1}{\psi_0}\right)^2 + n_0\mathcal{E}[\psi_2] + n_1\mathcal{E}[\psi_1] = -\tfrac{1}{2}\int \frac{d\Omega}{8\pi^2}\left(\frac{\psi_1}{\psi_0}\right)^2 \tag{2.33}$$

This equation determines ψ_2 in terms of ψ_1. The right-hand side of the equation is a constant, obtained by integrating the left-hand side over $d\Omega/(8\pi^2)$, which ensure the normalization of ψ_2.

This equation allows us also to determine the precise form of ψ_1. The solutions of ψ_1 come in families which, within a family, all have the same symmetry but are rotated with respect to each other. Solving higher order bifurcation equations would lead to a branch of solutions of the stationarity equation in the ODF-density space emerging from the bifurcation point and parameterized by ε.

Note that in (2.33) we can always add to ψ_2 a term proportional to ψ_1. In fact this is true for all other ψ_i as well. This would therefore suggest that the functions ψ_i are not completely determined by the bifurcation equations. This is not the case, one needs to realize that the branch of solutions is parameterized by ε, but any monotonic function of ε would do as well. By changing the expansion parameter ε to ν, we can always ensure that ψ_1 is orthogonal to ψ_2 and all other higher terms in the expansion of the ODF. If we expand ε in terms of the new parameter ν

$$\varepsilon = \sum_{k\geq 0} a_k \nu^k \tag{2.34}$$

where the coefficients a_k are yet undetermined, substitute this for ε in (2.31) and combine terms in the same power of ν, we can write the ODF as

$$\begin{aligned} \psi &= \psi_0 + a_1\psi_1\nu + \left(a_2\psi_1 + a_1^2\psi_2\right)\nu^2 + \cdots \\ &= \psi_0 + \tilde{\psi}_1\nu + \tilde{\psi}_2\nu^2 + \cdots \end{aligned} \tag{2.35}$$

where $\tilde{\psi}_i$ are the expansion term of the ODF if it is expanded in term of ν. Since each coefficient in front of ν^n is linear in a_n and contains the term $a_n\psi_1$ we can choose the value of a_n in order to satisfy orthogonality with ψ_1. Further more we can choose a_1 as we like, determining all coefficients a_i in a unique way. We can therefore impose, without loss of generality, the following constraints on the ODF

$$\begin{aligned} \int d\Omega\psi_i(\Omega) &= \delta_{i,0} \qquad &\text{for } i \geq 0 \\ \int d\Omega\psi_i(\Omega)\psi_1(\Omega) &= \delta_{i,0} \qquad &\text{for } i \geq 1 \end{aligned} \tag{2.36}$$

with $\delta_{i,0}$ the Kronecker delta.

The bifurcation analysis provides us with a bifurcation density, at which the isotropic phase becomes unstable, and the formal solution of the ODF and number density as function of ε. This branch of solutions of the stationarity equation starts at the bifurcation point. The symmetry of the ODF is determined by the symmetry of ψ_1 and gives an indication of what the symmetry of the equilibrium phase might be.

The bifurcation analysis is however not capable of predicting what the the real equilibrium phase is. Its solutions are only an indication of what might happen. The obtained bifurcation density is, for the functional in question, a true upper limit for the stability of the isotropic phase. Only in case of a continuous phase transition this density will coincide with the actual density at the transition.

It is possible that the bifurcation equations give rise to more then one family of solutions with different symmetries. In such a case the theory cannot determine in a simple way what the most stable solution will be.

Despite its simplicity bifurcation theory is a very powerful tool as it gives us a glance at the actual phase behavior of the system. Although explained here in order to determine the stability of the isotropic phase, this theory can also be used to study the stability of ordered phases. The generalization of the equations is straightforward, but will lead to more complicated expressions. The main problem is here to determine the ODF ψ_0 as function of the density for an ordered phase. In general this ODF is not known but one can apply numerical methods in such cases.

2.5 Thermodynamics

By solving the stationarity equation for the free energy functional we obtain families of solutions for the ODF as function of the density. For a given density there is in

general only one ODF corresponding to the true minimum of the free energy. It is possible however that there are several other locally stable solutions as well. Suppose that we have only two stable solutions of the free energy and label them by A and B. We can make a plot of the free energy as function of the inverse number density $v = 1/n$ as is done in figure 2.3.

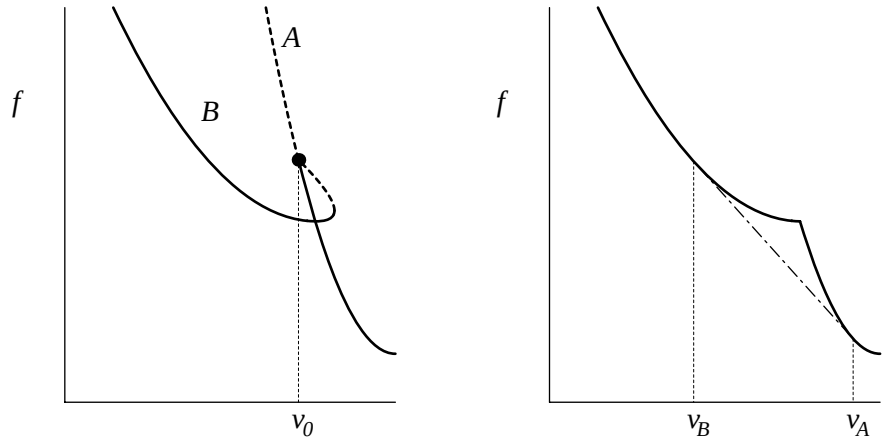

Figure 2.3: The free energy f as function of $v = 1/n$ the inverse number density. The solid lines correspond to minima in the free energy, dashed lines to maxima. The phase B branches of at the bifurcation point v_0. On the right site we plotted only the minimum of the free energy and performed the comment tangent construction (dotted-dashed line).

In the left figure we plotted the free energies for both solutions A and B of the stationarity equation. At $n_0 = 1/v_0$, the bifurcation density, the solution B branches of from A, which becomes unstable. The true free energy corresponds to the minimum of all solutions and is plotted in the right part of the figure. It is however possible to construct an even lower free energy as is indicated by the dotted-dashed line.

Instead of having a single phase we can also divide the system in two parts having a different symmetry. If we split the total system with volume V and N particles in an A-phase region with volume V_A and N_A particles and B-phase region with volume V_B and N_B particles.

For large number of particles N and large volumes V the Helmholtz free energy is extensive, which allows us to write the free energy in terms of the free energy f per particle

$$F(N, V, T) = Nf(v, T) \tag{2.37}$$

If we neglect the effects of the interface we can write the total free energy of the combined system as

$$F = N_A f(v_A) + N_B f(v_B) \tag{2.38}$$

If we minimize the total free energy with respect to V_A and N_A, taking into account the two constraints $N = N_A + N_B$ and $V = V_A + V_B$, we get two equations

$$\left.\frac{\partial f}{\partial v}\right|_{v_a} = \left.\frac{\partial f}{\partial v}\right|_{v_b} \tag{2.39}$$

and

$$f(v_A) - v_A \left.\frac{\partial f}{\partial v}\right|_{v_a} = f(v_B) - v_B \left.\frac{\partial f}{\partial v}\right|_{v_b} \tag{2.40}$$

These equations can be interpreted in a simple way by recognizing that in equilibrium the pressure P of a system is defined by

$$P = -\left(\frac{\partial F}{\partial V}\right)_{N,T} = -\left(\frac{\partial f}{\partial v}\right) \tag{2.41}$$

and the chemical potential μ by

$$\mu = \left(\frac{\partial F}{\partial N}\right)_{V,T} = f(v) - v\left(\frac{\partial f}{\partial v}\right) \tag{2.42}$$

In order words the conditions for the coexistence between the two phases, both in equilibrium, are equal pressure and and chemical potential. Inserting these results back in the total free energy of the combined system will reveal that the free energy as function of the overall inverse density v is a straight line, connecting the two free energies of the phases A and B at v_A and v_B. Moreover the line is tangent at both points to the free energy curve which follows from (2.39). This line is the so-called common tangent construction (dotted-dashed line in figure 2.3).

2.6 NPT-Simulations

As we have mentioned it seems impossible to solve the equations of motion of a system and following in time as it moves through its phase space. Nevertheless this is exactly what people nowadays try to do with computer simulations. There are obvious limitations to the number of particles that can be used, depending on the type of interaction and of course the combination of computer power and time available.

The first computer simulations on this type of systems were performed by Metropolis *et al* [14] in 1953, introducing the Metropolis Monte Carlo (MC) method. In the beginning simple models were used, in which molecules were represented by hard spheres and disks. But a few years later already, in 1957, Wood and Parker [15] used the Lennard-Jones potential in their MC-simulation, making it possible to compare data obtained from simulation and experiments on for instance liquid Argon.

In 1957 Alder and Wainwright [1] used the Molecular Dynamics (MD) method on a system of hard spheres, showing that hard spheres have a freezing transition. The first time the MD method was used to simulate a real liquid was in 1964 by Rahman [16], who simulated Argon using a system of Lennard-Jones particles.

Since then both simulation methods have been applied to a wide range of systems. Starting with simple hard particles, but soon on more complicated systems with soft interactions and non-spherical objects, like water, proteins and polymers.

Only in MD simulations one tries to solve the equations of motion. For hard spheres this is simple and can be done without any approximation, because they move at constant velocities between elastic collisions. But if soft interactions are included, approximations have to be made, because the forces on the particles change continuously. By making small steps in time, the equations of motion can be solved numerically. Depending on the complexity of the system, simulations up to several millions of particles can at present be done. In general a smaller number of particles (100-10000) will already describe the behavior of an infinite system quite well. All macroscopic observables are computed by a time average, and since the time evolution of the system is followed, we are also able to study dynamical quantities.

In a MC-simulation the equation of motions are not solved and as a consequence dynamical information is lost. Instead we try to evaluate the average (2.1) directly, by sampling configurations in phase space randomly. Each generated configuration is weighted proportional to the Boltzmann factor $\exp(-\beta U)$. These weights can however, depending on the type of system, differ orders of magnitude. As a consequence a lot of time can be spend on generating configurations with relatively low weights. Metropolis *et al* [14] developed a different method in which the configurations are chosen from a distribution, such that by the end of the simulation each state occurred according their probability of existence. This is achieved by growing a Markov chain of configurations. Starting with an arbitrary configuration, a new one is generated, by random translation and/or rotation of particles. The new configuration is accepted according to the transition probability of going from the old to the new state, given by $\min(1, \exp(-\beta\Delta U))$. The limiting distribution of configurations in a Markov chain, fulfills precisely the requirement needed. Observables can therefore be obtained by an unweighted average over the generated configurations.

In the last 40 years many new simulation techniques have been developed for both methods, for which we refer the reader to the books of Allen and Tildesley [17], and more recently Frenkel and Smit [18].

In this thesis we describe MC-simulations performed on systems of hard particles. Although there are no forces in these system due to interaction of the particles, the particle shapes we will study will make it a tedious task to calculate the collisions between the particles. The MC method is therefore much simpler because we only need to calculate the potential energy of a configuration. This is for hard particles very simple, as the potential energy of a configuration is zero if there is no overlap in the system and infinite if there is an overlap. Hence in MC simulation we only thing need to calculated whether there are overlaps or not.

We are going to work in the isothermal-isobaric constant-NPT ensemble. This means that the number of particles N, the pressure P and the temperature T are fixed. Since the system is now described by the pressure P and not the volume V, we should not use the Helmholtz free energy, but we have to use the Gibbs free energy $G = F + PV$. In this ensemble the average of an observable A is weighted with a slightly different function than the one described in section 2.1, namely $\exp(-\beta(H + PV))$

$$< A >= \frac{1}{Z_{NPT}} \int dV \exp(-\beta PV) \int d\vec{r}^N d\Omega^N A \exp(-\beta U(\vec{r}^N, \Omega^N)) \qquad (2.43)$$

where Z_{NPT} is the appropriate configurational integral. In order to change the configuration we can do two different moves. We can change the position and/or orientation of the particles or we can change the volume of the simulation box in order to allow the system to relax for given pressure. In the case of moving a hard particle this is simply checking whether the new position and/or orientation cause an overlap in the system. If this is so then the difference in energy is infinite and the move is rejected. If it does not cause an overlap the energy difference is zero and the move is alway accepted.

For a volume move this is slightly more complicated, because a change in volume also affects the particle positions and hence the integrals over $\vec{r}$ in (2.43). It is therefore more convenient to express the particle positions in scaled coordinates $\vec{s}$ defined by

$$\vec{s} = L^{-1}\vec{r} \tag{2.44}$$

where we assumed to have a cubic simulation box with sides $L = V^{\frac{1}{3}}$. We can now rewrite the average (2.43) as

$$< A >= \frac{1}{Z_{NPT}} \int dV \exp(-\beta PV) V^N \int d\vec{s}^N d\Omega^N A \exp(-\beta U(\vec{s}^N, \Omega^N)) \tag{2.45}$$

The simplest way to incorporate a volume move is by attempting an isotropic expansion or compression of the system, for which the volume changes from V to $V' = V + \Delta V$ and ΔV is chosen uniformly from an interval $[-\Delta V_{max}, \Delta V_{max}]$. Since the weight of a microstate according to (2.45) is proportional to $V^N \exp(-\beta PV)$ the probability of accepting the move, if it does not produce overlaps, is given by

$$\min(1, \exp[-\beta P(V' - V) + N \log(V'/V)]) \tag{2.46}$$

The maximum volume change ΔV_{max} is chosen such that the acceptance of a volume move is between the 35 and 50 per cent [19]. During simulations this acceptance ratio is continuously monitored and if necessary the value of ΔV_{max} is adjusted.

An alternative way to sample the volumes was introduced by Eppenga and Frenkel [5]. Instead of making random changes in V it might be useful to change $\log(V)$, by choosing a random value $\Delta \log V$ uniformly from the interval $[-\Delta \log V_{max}, \Delta \log V_{max}]$. The acceptance probability for a volume move has to be changed to

$$\min(1, \exp[-\beta P(V' - V) + (N + 1) \log(V'/V)]) \tag{2.47}$$

It is straightforward to generalize the volume sampling to non-cubic boxes or to include potential energies. A volume move is however computationally more expensive, because it can cause overlaps for particles close together and all pairwise potentials, if included, are affected. In general a volume move will therefore be attempted with a lower frequency than the normal particle moves.

3 Theory of Crosses

In this chapter we investigate the phase behavior of a non-convex particle made up by connecting three perpendicular elongated rods to form what we will call an Onsager cross. We will show that, depending on the actual shape, it is possible for some of these particles to form a cubatic phase. By means of three methods we will draw a schematic phase diagram of the phase behavior of this class of particles, restricting ourselves to homogeneous orientationally ordered phases.

3.1 Introduction

In order to understand the behavior of complex liquids, like liquid crystals, on a molecular basis one is forced, by the sheer complexity of the molecules involved, to adopt highly simplified models of inter-particle interactions. These model interactions are chosen to represent as well as possible the general nature, or at least some aspect, of the true interactions involved. In the case of liquid crystals it was Onsager who already in 1942 pioneered the description in terms of hard non-spherical particles [4] . He showed that a system of very elongated hard rods would at high enough density form a uniaxially anisotropic orientationally ordered liquid phase: a nematic liquid crystal. The origin of this ordering process lies in the fact that the system can gain translational entropy by aligning the particles and hence decreasing the excluded volume. At high enough density this gain will outweigh the loss in orientational entropy incurred by aligning the particles and the resultant ordered phase will have a lower free energy than the isotropic state. Of course a description in terms of hard interactions is directly applicable only to lyotropic liquid crystals like the tobacco mosaic virus (TMV), which, in a suitably chosen salt solution, actually behaves like a hard rod. Nevertheless, even in thermotropic liquid crystals, where phase transitions are induced by decreasing the temperature, the short range repulsive interactions must also play a role in determining the phase behavior. This is true *a fortiori* under typical liquid densities, as the theory of simple fluids strongly suggest that at least the local structure of a fluid is nearly completely determined by the short-ranged repulsions. In this case a hard model system can function as a reference systems to which other aspects of the true interactions (soft cores, dispersion interactions, intra-molecular conformational energies) can be added as a perturbation. To date the hard particle approach to modeling liquid crystalline behavior has yielded the insight that most of the common liquid crystalline phases can be understood as the effect of packing entropy alone. Moreover, as models go, they are both easily specified and often quite tractable.

Figure 3.1: Onsager cross for $L/D = 5$

Given the success of hard particle theories in *describing* the known liquid crystalline phases, one can ask if it is possible to use these models to *predict* novel phases that have not yet been observed in nature. Apart from the intrinsic fundamental interest of this question, this would also represent a first step towards the "molecular engineering" of new materials with novel and possibly interesting properties. The aim of this chapter is to work out a test case of this approach. We have chosen as our example a model due to Frenkel, which we have dubbed Onsager crosses. They consist of three elongated hard rods rigidly connected to each other in their centers so as to form a cross with three mutually orthogonal "beams" (figure 3.1). If the three component rods are equally long, Frenkel argued, such a system should form a nematic phase with cubic orientational order, a claim which he backed up with an approximate calculation [20]. His argument for the occurrence of this novel "cubatic" phase is based on the fact that if, at a given density any of the particle's axes would prefer to order, the remaining axes which by symmetry are completely equivalent will do so too. Since they are rigidly connected at right angles to each other, the resultant phase will have three equivalent orthogonal ordering directions and hence have cubic symmetry. Here we consider a generalization of the original symmetric crosses by allowing the ratios of the lengths of the components rods to vary. In this way we obtain a family of particles containing the symmetric crosses as a special case, which as it turns out has a rather rich phase diagram. As a side product we re-confirm Frenkel's conjecture within the context of a more detailed calculation.

In section 3.2 we introduce the Helmholtz free energy as functional of the one-particle orientational distribution function and derive some basic results from symmetries of our model.

We will analyze the behavior of our particles in three different ways. In section 3.4 we will use a bifurcation analysis which gives a global idea of the phase diagram concerning the transition from an isotropic phase to ordering. In section 3.5 try to find numerical solutions which minimize the free energy using trial functions and by analyzing the distribution functions we obtain the symmetry of the phases and find series of transitions. As a third method we solve the model in section 3.6 within a Gaussian approximation which means that we assume that the distribution functions will be sharply peaked.

In section 3.7 we will summarize and combine our results obtained by the different methods. We will discuss the validity of some of our assumptions and give a few suggestions for further research.

3.2 Free Energy

In order to study our system we will need an appropriate free energy functional. Onsager showed that, at least for a fluid of very elongated rods, the excess free energy can be effectively be truncated at second virial coefficient level, yielding a theory with the formal structure of a mean-field theory. Even in the cases were the truncation is not *a priori* justified, this approximation still contains the essential ingredients of the physics of such systems viz. the competition between orientational and translational entropy.

Though our particles are no longer the elongated rods as in Onsager's original model, they do consist of three of these kind of objects. They form together a very open structure. This means that the probability of multiple overlaps between two particles in general will be very small. As a consequence we might expect that the rods act independently of each other, which allows us to use a similar reasoning as Onsager did and truncate the free energy expansion in virial coefficients after the second virial coefficient. This leads to the following free-energy functional

$$\beta f[\psi] = \int d\Omega \psi(\Omega) \ln \psi(\Omega) + \frac{1}{2}\rho \int d\Omega_1 \int d\Omega_2 \psi(\Omega_1)\psi(\Omega_2)\mathcal{K}(\Omega_1,\Omega_2) + \beta \hat{f} \tag{3.1}$$

Here f is the free energy per particle which is a functional of ψ the orientational distribution function (ODF). This ODF is a measure for the fraction of particles with an orientation Ω in a fixed reference frame and is normalized to unity. $\beta = (k_B T)^{-1}$ the inverse temperature.

The first term of the free energy functional is associated with the orientational entropy of the system. The second term takes into account the interaction between the particles, described by $\mathcal{K}(\Omega_1, \Omega_2)$, being the excluded volume of two particles with given orientations. The last term is the ideal gas term and does not depend on the the ODF.

In general we need three parameters to describe any orientation Ω. For this we make use of the Euler-angles (α, β, γ) describing an arbitrary rotation in 3-dimensional space.

A necessary condition for an equilibrium ODF of a system described by a free energy functional is that it satisfies the stationarity condition

$$\frac{\delta}{\delta\psi(\Omega)} \left\{ f[\psi] - \mu \int d\Omega \psi(\Omega) \right\} = 0 \tag{3.2}$$

where the second term takes care of the normalization of the ODF. To ensure that the solution is stable we need to check whether it is a minimum of the free energy and in case of phase coexistence to equate the chemical potentials and pressures of the different phases.

The most important contribution to the excluded volume of two elongated rods with lengths L_1 and L_2 and diameters D_1 and D_2 is given by

$$v_{excl} = L_1 L_2 (D_1 + D_2) |\sin\gamma| \tag{3.3}$$

where γ is the angle between the long axis of the particles. We assume that the infinitely long rods of our cross-like particles contribute independently to the excluded volume and neglect the fact that the rods are physically connected. The first assumption is based on the fact that the probability for multiple overlaps between two crosses will be small compared to that of a single overlap. The last assumption can be justified since the overlap volume of the rods is of $\mathcal{O}(D^3)$ and hence its effect on the excluded volume is an order $\mathcal{O}(D/L)$ smaller compared to the contribution of the rods.

If we denote the lengths of the three rods by L_1, L_2 and L_3 pointing respectively in the x, y and z direction of a particle fixed frame and take equal diameters D for all rods we obtain for the leading term in the excluded volume of two cross-like particles

$$v_{\text{cross}} = \sum_{i,j} 2 L_i^{(1)} L_j^{(2)} D |\sin\gamma_{ij}| = 2L^2 D \sum_{i,j} l_i^{(1)} l_j^{(2)} |\sin\gamma_{ij}| \tag{3.4}$$

where $l_i = L_i/L$ and the sum of the lengths of the rods is given by $L = L_1 + L_2 + L_3$. It is convenient to express the density in terms of the second virial coefficient, which is half of the mean of the excluded volume in the isotropic phase

$$B_2 = \frac{1}{2} < v_{\text{cross}} >_I = \frac{\pi}{4} L^2 D \tag{3.5}$$

We now introduce a reduced density $\eta \equiv B_2 \rho$. Since the excluded volume interaction between two particles only depends on their mutual orientation $\Omega_{12} = \Omega_2^{-1}\Omega_1$ we define the reduced excluded volume interaction by

$$\mathcal{E}(\Omega_{12}) \equiv \frac{\mathcal{K}(\Omega_1, \Omega_2)}{B_2} = \frac{8}{\pi} \sum_{i,j} l_i^{(1)} l_j^{(2)} |\sin\gamma_{ij}| \tag{3.6}$$

3.3 Analysis

In general any function of Ω can be expanded in the rotation matrix elements $\mathcal{D}^l_{m,n}(\Omega)$. However in this case it is convenient to exploit the extra symmetries in our problem in order to obtain a smaller subset of symmetry adapted functions. The particles, and therefore the interaction as well, are invariant under rotations over an angle π about any of the three axes in the particle fixed frame. Together with the identity these three rotations form the group $D_2 = \{1, R_x(\pi), R_y(\pi), R_z(\pi)\}$ and lead to the definition of the $\Delta^l_{m,n}$-functions (see appendix)

$$\Delta^l_{m,n} = \left(\frac{1}{\sqrt{2}}\right)^{2+\delta_{m,0}+\delta_{n,0}} \left\{\mathcal{D}^l_{m,n} + (-)^l \mathcal{D}^l_{m,-n} + (-)^l \mathcal{D}^l_{-m,n} + \mathcal{D}^l_{-m,-n}\right\} \tag{3.7}$$

Both m and n are even and chosen to be non-negative. In case of odd values for l both indices need to be positive in order to define a non-zero function as can be seen directly form this definition.

To give an impression what these functions look like we here list the four with $l = 2$, first discussed by Straley [21]

$$\begin{aligned}
\Delta^2_{0,0}(\Omega) &= \tfrac{1}{2}(3\cos^2\beta - 1) \\
\Delta^2_{0,2}(\Omega) &= \tfrac{1}{2}\sqrt{3}\sin^2\beta\cos 2\gamma \\
\Delta^2_{2,0}(\Omega) &= \tfrac{1}{2}\sqrt{3}\sin^2\beta\cos 2\alpha \\
\Delta^2_{2,2}(\Omega) &= \tfrac{1}{2}(1+\cos^2\beta)\cos 2\alpha\cos 2\gamma - \cos\beta\sin 2\alpha\sin 2\gamma
\end{aligned} \tag{3.8}$$

We are now able to expand the excluded volume interaction (3.6) in these symmetry adapted $\Delta^l_{m,n}$-functions

$$\mathcal{E}(\Omega) = \sum_{l,m,n} \frac{2l+1}{8\pi^2} E_{l,m,n}\Delta^l_{m,n}(\Omega) \tag{3.9}$$

where the coefficients $E_{l,m,n}$ are formally given by

$$E_{l,m,n} = \int d\Omega \mathcal{E}(\Omega)\Delta^l_{m,n}(\Omega) \tag{3.10}$$

and are symmetric in m and n ($E_{l,m,n} = E_{l,n,m}$) because the interaction is invariant under interchanging the particles. In order to calculate these coefficients $E_{l,m,n}$ we need to evaluate integrals of the type

$$\int d\Omega |\sin\theta_{ij}| \Delta^l_{m,n}(\Omega) = \int d\Omega |\hat{\mathbf{e}}^{(\mathbf{1})}_{\mathbf{i}} \times \hat{\mathbf{e}}^{(\mathbf{2})}_{\mathbf{j}}| \Delta^l_{m,n}(\Omega) \tag{3.11}$$

where $\hat{\mathbf{e}}^{(\mathbf{k})}_{\mathbf{i}}$ is the unit vector pointing along the rod l_i of particle k. This can be achieved by introducing the rotations q_i about the axes of the particle fixed frame

$$\begin{aligned}
q_1 &= R_y(\pi/2) \\
q_2 &= R_x(-\pi/2) \\
q_3 &= \mathbf{1}
\end{aligned} \tag{3.12}$$

and using them as coordinate transformations in order to redirect the rods $l^{(1)}_i$ and $l^{(2)}_j$ along the z-axis which enables us to obtain a more convenient form for the integrals (3.11)

$$\begin{aligned}
\int d\Omega |q_i\hat{\mathbf{e}}^{(\mathbf{1})}_{\mathbf{z}} \times q_j\hat{\mathbf{e}}^{(\mathbf{2})}_{\mathbf{z}}| \Delta^l_{m,n}(\Omega) &= \int d\Omega |\hat{\mathbf{e}}^{(\mathbf{1})}_{\mathbf{z}} \times \hat{\mathbf{e}}^{(\mathbf{2})}_{\mathbf{z}}| \Delta^l_{m,n}(q_j^{-1}\Omega q_i) \\
&= \sum_{m',n'} \int d\Omega |\sin\beta| \Delta^l_{m,m'}(q_j^{-1})\Delta^l_{m',n'}(\Omega)\Delta^l_{n',n}(q_i) \\
&= \sum_{m',n'} \Delta^l_{m,m'}(q_j^{-1})\Delta^l_{n',n}(q_i) \int d\Omega |\sin\beta| \Delta^l_{m',n'}(\Omega)
\end{aligned} \tag{3.13}$$

After performing the coordinate transformation in the first line we used the properties (A.20) of the $\Delta^l_{m,n}$-functions, which state that they form a closed set under the symmetry operations of the cubic group O.

The integral in the last line of (3.13) can be calculated exactly and is only nonzero for $m' = n' = 0$ and even values of l [22, 7.132.1]

$$\begin{aligned}\mu_{2l} &= \int_0^{2\pi} d\alpha \int_0^{2\pi} d\gamma \int_0^{\pi} d\beta \sin\beta |\sin\beta| \Delta^{2l}_{0,0}(\alpha,\beta,\gamma) \\ &= (2\pi)^2 \int_0^{\pi} d\beta \sin^2\beta P_{2l}(\cos\beta) \\ &= -\frac{2\pi^3}{(l+1)(2l-1)2^{4l}} \left(\begin{array}{c} 2l \\ l \end{array} \right)^2 \\ \mu_{2l+1} &= 0\end{aligned} \tag{3.14}$$

Using the property of the $\Delta^l_{m,n}$-functions for the inverse rotation (A.19) this gives us the final result for the coefficients $E_{l,m,n}$

$$E_{l,m,n} = \frac{8}{\pi}\mu_l \sum_{i,j} l_i l_j \Delta^l_{0,m}(q_j)\Delta^l_{0,n}(q_i). \tag{3.15}$$

In table 3.1 the values of $\Delta^l_{0,n}(q_i)$ are listed for $l = 2$ and $l = 4$.

	q_1	q_2	q_3
$\Delta^2_{0,0}$	$-\frac{1}{2}$	$-\frac{1}{2}$	1
$\Delta^2_{0,2}$	$\frac{1}{2}\sqrt{3}$	$-\frac{1}{2}\sqrt{3}$	0
$\Delta^4_{0,0}$	$\frac{3}{8}$	$\frac{3}{8}$	1
$\Delta^4_{0,2}$	$-\frac{1}{4}\sqrt{5}$	$\frac{1}{4}\sqrt{5}$	0
$\Delta^4_{0,4}$	$\frac{1}{8}\sqrt{35}$	$\frac{1}{8}\sqrt{35}$	0

Table 3.1: The most important values of $\Delta^l_{0,n}$ as function of the three different rotations q_i.

It is convenient to introduce some shorthand notations analogous to [12]. We define the following inner product for real functions f and g of Ω,

$$< f|g > \equiv \int f(\Omega)g(\Omega)d\Omega \tag{3.16}$$

We can also define a functional in this space of real functions by

$$f[g](\Omega) = \int d\Omega' f(\Omega'^{-1}\Omega)g(\Omega'). \tag{3.17}$$

If we apply this last definition to $\mathcal{E}$ and use that it only depends on relative orientations we obtain

$$< f|\mathcal{E}[g] > = \int d\Omega_1 \int d\Omega_2 \mathcal{E}(\Omega_2^{-1}\Omega_1)f(\Omega_1)g(\Omega_2) = < \mathcal{E}[f]|g > . \tag{3.18}$$

With this new notation we can write the free energy functional (3.1) in a more compact form as

$$\beta f[\psi] =< \psi|\ln\psi > +\frac{1}{2}\eta < \psi|\mathcal{E}[\psi] > +\beta\hat{f} \tag{3.19}$$

In order to understand the behavior of the excluded volume as a functional we let (3.9) work on a $\Delta^l_{m,n}$-function. If we now use (A.22) we immediately obtain

$$\mathcal{E}[\Delta^l_{m,n}] = \sum_p E_{l,n,p}\Delta^l_{m,p}. \tag{3.20}$$

This means that the total space $\mathcal{S}_\Omega$ of the $\Delta^l_{m,n}$ is decomposed into invariant subspaces $\mathcal{S}^l_m$ by the excluded volume interaction. Moreover (3.20) shows that for fixed l the action of $\mathcal{E}$ is represented by the same matrix $(E_l)_{n,p}$, in all the subspaces $\mathcal{S}^l_m$ labeled by $m = 0, 2, \cdots, l$.

We now go back to the stationarity equation (3.2). With our new notation we can perform the functional derivative explicitly and write it compact as

$$\ln\psi + \eta\mathcal{E}[\psi] - \beta\mu = 0 \tag{3.21}$$

where the ODF ψ satisfies the normalization $< 1|\psi >= 1$. Any solution which minimizes the free energy surely has to be a solution of this equation. We assume that the ODF possesses the same symmetry D_2 as our particles and hence can be expanded in the $\Delta^l_{m,n}$-functions

$$\psi(\Omega) = \sum_{l,m,n} \frac{2l+1}{8\pi^2}\psi_{l,m,n}\Delta^l_{m,n}(\Omega) \tag{3.22}$$

with some constant coefficients $\psi_{l,m,n}$. Intuitively this seems justified as a homogeneous phase with symmetry lower than that of the constituent particles seems implausible. To our knowledge however no rigorous proof exists for this statement.

We are going to use three different methods to study the behavior of our system. First we will use a bifurcation analysis to study the transition of the isotropic phase to some other orientational ordered phase. This is a fast method which gives an global description of the phase behavior and tells us some of the symmetries of the phases we might expect. However two problems might occur, it is possible to obtain several phases with different symmetries and the predicted phase is not necessarily the thermodynamically most stable phase.

The second method we will use is minimizing the free-energy functional by solving the stationarity condition (3.21) numerically. This involves integration which we can only hope to do properly if they ODF is a not too strongly peaked function. So the results are useful only for low densities when phases probably are not yet strongly ordered. For higher densities the results, though might be an indication, are not reliable in predicting the densities for phase transitions. For these densities we will use a third method, which is a so called Gaussian approximation. We will assume that for higher densities the ODF becomes strongly peaked and can be approximated by a combination of Gaussians.

3.4 Bifurcation Analysis

3.4.1 Method

The isotropic phase is of course a solution of (3.21), at least for low densities. In that case the ODF is merely a constant, which is the trivial solution, $\psi_0 = 1/8\pi^2$. If we increase the density η, the isotropic phase remains a solution of the stationarity condition, but fails to be a minimum for the free energy. This means that there is a certain density η_0 at which ψ_0 stops being a local minimum and becomes a local maximum of the free energy. In other words any anisotropic perturbation would destroy the isotropy of the system. The density where this occurs is called the bifurcation density and is explicitly calculated. But in fact the requirement on the equilibrium ODF is stronger since it has to be the absolute minimum of the free-energy. So the real density at which the isotropic phase becomes thermodynamically unstable will usually be lower than the bifurcation density. This implies that the bifurcation density is an upper limit for the density at which the phase transition will occur and only in case of a continuous transition gives the right value.

To calculate the bifurcation density we try to find a parameter family of solutions satisfying (3.21), by means of the following expansion in some small parameter ε

$$\begin{aligned} \psi &= \psi_0 + \varepsilon\psi_1 + \varepsilon^2\psi_2 + \cdots \\ \eta &= \eta_0 + \varepsilon\eta_1 + \varepsilon^2\eta_2 + \cdots \end{aligned} \tag{3.23}$$

We want ψ to remain normalized to unity which leads to $< 1|\psi_i >= \delta_{i,0}$. Furthermore we assume that $< \psi_1|\psi_i > \propto \delta_{i,1}$, which always can be achieved by rescaling the parameter ε.

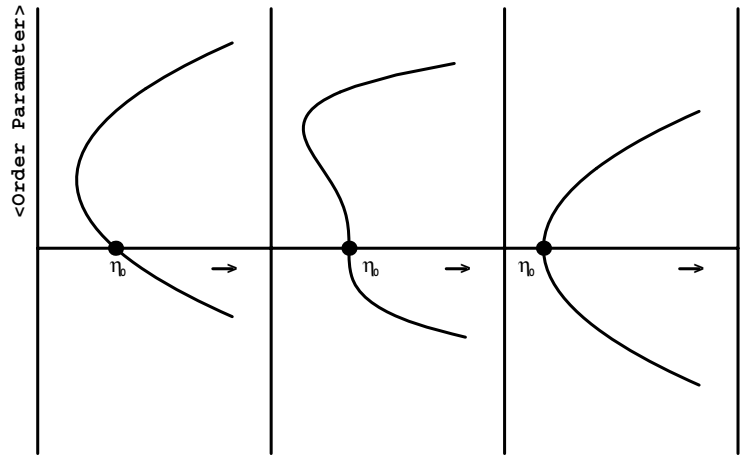

Figure 3.2: Three possible bifurcation schemes. The first and second show two scenarios for a first order transition and the last is of a continuous transition. The points with value η_0 can be found by means of a bifurcation analysis.

In figure 3.2 are three possible bifurcation schemes drawn. Some order parameter, e.g. the second Legendre polynomial (P_2) for nematic order, is sketched as function of the density. Since the isotropic phase has no structure, the order parameter is zero and the isotropic solution corresponds to the horizontal axis. At the points labeled with η_0

the isotropic phase becomes a locally unstable solution of the stationarity equation (3.21) and another solution branches of.

The first one represents a normal first order phase transition for which the first term in the density expansion η_1 is non-zero and as we will see later will be negative. The second diagram is also a first order transition. It branches of perpendicular to the horizontal axis ($\eta_1 = 0$) and bends back. In both cases the density at which the phase transition will occur is lower than the calculated value η_0. The last diagram corresponds to a continues phase transition. Again $\eta_1 = 0$ but now the solution does not bend back. Only in such a case the bifurcation density is the real density for the transition.

If we put the expansions (3.23) in the stationarity equation (3.21) we will obtain a bifurcation equation for every order of ε. The first and second order equations are given by

$$\frac{\psi_1}{\psi_0} + \eta_0 \mathcal{E}[\psi_1] = 0 \tag{3.24}$$

and

$$\frac{\psi_2}{\psi_0} - \frac{1}{2}\left(\frac{\psi_1}{\psi_0}\right)^2 + \eta_0 \mathcal{E}[\psi_2] + \eta_1 \mathcal{E}[\psi_1] = const. \tag{3.25}$$

All contributions which do not depend on Ω are contained in the Lagrange multiplier $\beta\mu$. This results for the first bifurcation in an eigenvalue problem. In the second equation remains a constant, though the ψ_i do not contain constant terms, powers and combinations of them usually do.

3.4.2 Eigenvalues and functions of the excluded volume

The first bifurcation equation (3.24) has taken the form of an eigenvalue problem. Therefore its wise to find out what there is to know about the eigenvalues and eigenfunctions of the excluded volume functional. At the end of section A.2 it is indicated that the functional has invariant subspaces $\mathcal{E}[\mathcal{S}^l_m] = \mathcal{S}^l_m$ which are spanned by the functions $\Delta^l_{m,n}$ and is represented by the matrix $E_{l,m,n}$ for fixed values of l.

This matrix is given by (3.15) and has a special form

$$(E_l)_{m,n} = \frac{8}{\pi}\mu_l E^l_m E^l_n \tag{3.26}$$

where

$$E^l_m = \sum_i l_i \Delta^l_{0,m}(q_i). \tag{3.27}$$

Notice that for odd values of l this means the matrix is zero. For even values of l it has exactly one non-zero eigenvalue which we will denote by λ_l and its eigenvector by χ^l_m,

$$\lambda_l = \sum_n E_{l,n,n} = \frac{8}{\pi}\mu_l \sum_n E^l_n E^l_n \tag{3.28}$$

$$\chi^l_m = \frac{\sum_n E^l_n \Delta^l_{m,n}}{\sqrt{\sum_n \left(E^l_n\right)^2}} \equiv \sum_n e_{l,n} \Delta^l_{m,n} \tag{3.29}$$

where we implicit have defined the coefficients $e_{l,n}$ of the eigenfunctions.

In general λ_l would be a function in three parameters l_1, l_2 and l_3. From equation (3.15) however we know that it is a second order homogeneous polynomial. It also should be invariant under permutations of the rods and the lengths add up to unity. Therefore it can be written in the form $\lambda_l = \mu_l(8/\pi)(ar^2 + b(l_1l_2 + l_2l_3 + l_3l_1))$ where a and b are constants and $r^2 = l_1^2 + l_2^2 + l_3^2$. From the definition (3.27) of E^l_n we see that l_3 can only appear in combination with $\Delta^l_{0,m}(q_3) = \Delta^l_{0,m}(0,0,0) = \delta_{0,m}$. From which we can evaluate $a = 1$ and $b = 2\Delta^l_{0,0}(q_1) = 2\kappa_l$. This gives us the general formula for non-zero eigenvalues

$$\begin{aligned} \lambda_l &= \tfrac{8}{\pi}\mu_l\left(\left(1-\kappa_l\right)r^2 + \kappa_l\right) \\ \kappa_l &= (-)^{l/2}\left(\tfrac{1}{2}\right)^l \begin{pmatrix} l \\ l/2 \end{pmatrix} \end{aligned} \tag{3.30}$$

Since $1/3 \leq r^2 \leq 1$ we find that all eigenvalues are negative or zero. As an example of the eigenfunctions we write χ^2_0 out

$$\chi^2_0 = \frac{(3l_3 - 1)\Delta^2_{0,0} + \sqrt{3}(l_1 - l_2)\Delta^2_{0,2}}{\sqrt{2(3r^2 - 1)}} \tag{3.31}$$

If we put $l_1 = l_2 = 0$ we have a particle that is a single long rod. In that case the eigenfunction is just $\Delta^2_{0,0}$, which coincides with the second order Legendre polynomial.

3.4.3 Solution

We are now ready to deal with the bifurcation equations. Starting with the first (3.24) we see that we have a simple eigenvalue problem. We have to find the lowest density η_0 at which the isotropic phase becomes unstable. If we take for ψ_1 any eigenfunction χ^l_m we obtain for the bifurcation density

$$\eta_0 = -\frac{1}{\psi_0 \lambda_l}. \tag{3.32}$$

So in order to find the lowest η_0 we actually have to find the absolutely largest but negative eigenvalue. If we now analyze expression (3.30) for the eigenvalues we find that there are two possibilities either λ_2 is the case or λ_4

$$\eta_0 = \begin{cases} -\frac{1}{\psi_0\lambda_2} = \frac{8}{3r^2-1} \text{ for } r^2 \geq 5/13 \\ -\frac{1}{\psi_0\lambda_4} = \frac{256}{5r^2+3} \text{ for } r^2 \leq 5/13 \end{cases} \tag{3.33}$$

We can distinguish two regions. For $r^2 > 5/13$ the bifurcation equations are dominated by terms coming from $l = 2$ which can be seen as nematic like and the for $r^2 < 5/13$ terms coming from $l = 4$ will dominate which are phases with less symmetry like cubatic.

The first part for the solution we obtain by putting $r^2 > 5/13$. We substitute for the general solution of the first bifurcation equation (3.24)

$$\psi_1 = c_0\chi_0^2 + c_2\chi_2^2 \tag{3.34}$$

were the coefficient c_0 and c_2 still have to be calculated. This can be done by filling this result in the next bifurcation equation. Before we do this however we first note that

$$< \chi_m^2|\frac{\psi_2}{\psi_0} >= \frac{1}{\psi_0\lambda_2} < \mathcal{E}[\chi_m^2]|\psi_2 >= -\eta_0 < \chi_m^2|\mathcal{E}[\psi_2] > \tag{3.35}$$

for $m = 0, 2$. Therefore if we take the inner product of the second bifurcation equation with χ_m^2 we obtain two equations

$$\frac{8\pi^2}{5}\lambda_2\eta_1 c_m = \frac{1}{2\psi_0^2} < \chi_m^2|(c_0\chi_0^2 + c_2\chi_2^2)^2 > \tag{3.36}$$

In order to evaluate the right-hand side of the above equations we use again a property of the $\Delta_{m,n}^l$-functions, which is in the appendix listed as (A.21)

$$\begin{aligned}\eta_1 c_0 &= \frac{1}{7}\lambda_2\eta_0^2\nu(\mathcal{E})(c_0^2 - c_2^2)\\ \eta_1 c_2 &= \frac{1}{7}\lambda_2\eta_0^2\nu(\mathcal{E})(-2c_0c_2)\end{aligned} \tag{3.37}$$

where the factor $\nu(\mathcal{E}) = e_{2,0}(e_{2,0}^2 - 3e_{2,2}^2)$ comes from the excluded volume interaction.

We now can eliminate the first order density deviation η_1 by combining the two. There remains an equation depending on the coefficients c_0 and c_2 and on $\nu(\mathcal{E})$

$$\nu(\mathcal{E})c_2(c_2^2 - 3c_0^2) = 0. \tag{3.38}$$

There are two cases to consider. The first one is that of $\nu(\mathcal{E}) \neq 0$. If we use as an arbitrary normalization that $c_0^2 + c_2^2 = 1$ we find three solutions for ψ_1 up to a sign

$$\begin{aligned}\psi_1^{(z)} &= \chi_0^2\\ \psi_1^{(y)} &= -\frac{1}{2}\chi_0^2 - \frac{1}{2}\sqrt{3}\chi_2^2\\ \psi_1^{(x)} &= -\frac{1}{2}\chi_0^2 + \frac{1}{2}\sqrt{3}\chi_2^2\end{aligned} \tag{3.39}$$

The first solution $\psi_1^{(z)}$ is invariant under rotations around the z-axis. Knowing this it is easy to check that the other two solutions are the same but with their symmetries around the y respectively x-axis. These three have all uniaxial symmetry and they represent the nematic phase which we will denote by N.

The second case we have to consider is that of $\nu(\mathcal{E}) = 0$. This leads according to equations (3.37) to $\eta_1 = 0$ and prevents us from calculating c_0 and c_2 at this level. It turns out that we need to solve the fourth order bifurcation equation to determine their

values. Surprisingly the solution for ψ_1 has the same form as before and is not a biaxial phase as seen by Mulder for spheroplatelets [13].

To determine the global sign of the solution we need to look at the consequences. For the first case we see from (3.37) that the sign of η_1 is determined by our choice

$$\eta_1 = \frac{1}{7}\lambda_2 \eta_0^2 \nu(\mathcal{E}) c_0 (c_0^2 - 3c_2^2) \tag{3.40}$$

We expect that the branch of the stable nematic solutions is connected via the back bending branch to the bifurcation point. Hence the sign of the solution follows from the necessity of negative η_1. Since $\lambda_2 < 0$ we have to choose the solution as shown in (3.39) if $\nu(\mathcal{E}) > 0$ and add a negative overall sign if $\nu(\mathcal{E}) < 0$.

In the second case where $\nu(\mathcal{E}) = 0$ we have something similar. Since $\eta_1 = 0$ we look at the next terms in the expansion of the density. It turns out that η_2 is independent of the sign of the solution, but η_3 is not. If we make the same assumption as before we have to take the solution as given in (3.39) to ensure that η_3 is negative.

To see for which particles $\nu(\mathcal{E}) = 0$ we have rewritten $\nu(\mathcal{E})$ in terms of l_1, l_2 and l_3, using the fact that they add up to unity

$$\nu(\mathcal{E}) = \frac{4(3l_1 - 1)(3l_2 - 1)(3l_3 - 1)}{(6r^2 - 2)^{(3/2)}}. \tag{3.41}$$

So of these particles one of their rods has length 1/3 and from the other two one is longer and the other is shorter.

The solution for $\nu(\mathcal{E}) > 0$ is invariant under rotations around the director. The main axis of these particles is the longest of the three rods. Since they include the single rod we will refer to this phase as a rod-like nematic phase N_+. On the other hand we have the particles with $\nu(\mathcal{E}) < 0$, which include a particle which consists of only two rods of the same length. Again this is a nematic phase but in this case the role of the main axis is played by the shortest rod which might even vanish. We will refer to this as a platelet-like nematic phase N_-. The boundary between these two regions is formed by the particles which have one rod of length 1/3 and form a N_+ as well.

For the second part of the solution for the bifurcation equations we have to put $r^2 < 5/13$. In this case the main contribution to the ODF comes from $l = 4$ terms. We now substitute as general solution

$$\psi_1 = d_0 \chi_0^4 + d_2 \chi_2^4 + d_4 \chi_4^4. \tag{3.42}$$

If we work this out in the same way as in the previous subsection we obtain three equations

$$\begin{aligned}
\eta_1 d_0 &= \frac{3}{\sqrt{4004}}\lambda_4\eta_0^2\mu(\mathcal{E})(18d_0^2 - 11d_2^2 + 14d_4^2) \\
\eta_1 d_2 &= \frac{3}{\sqrt{4004}}\lambda_4\eta_0^2\mu(\mathcal{E})(-22d_0 + 6\sqrt{35}d_4)d_2 \\
\eta_1 d_4 &= \frac{3}{\sqrt{4004}}\lambda_4\eta_0^2\mu(\mathcal{E})(28d_0d_4 + 3\sqrt{35}d_2^2)
\end{aligned} \tag{3.43}$$

where $\mu(\mathcal{E})$ is given by

$$\begin{aligned}
\mu(\mathcal{E}) &= 6e_{4,0}^3 - 11e_{4,0}e_{4,2}^2 + 3\sqrt{35}e_{4,2}^2e_{4,4} + 14e_{4,0}e_{4,4}^2 \\
&= \frac{2\sqrt{2}(200l_1l_2l_3 + 45r^2 + 3)}{(5r^2+3)^{(3/2)}}.
\end{aligned} \tag{3.44}$$

We can solve this set of equations with normalization $d_0^2 + d_2^2 + d_4^2 = 1$. Using the facts that $\mu(\mathcal{E})$ is positive and η_1 should be negative we obtain three sets of solutions. The first one is given by

$$\psi_1^{(z)} = \chi_0^4. \tag{3.45}$$

This solution has rotational symmetry around the z-axis of the reference frame. It is accompanied by the two solutions that are symmetrical around the x and y-axis. Together they represent the nematic phase. The second set of solutions is given by

$$\psi_1^{(z)} = \sqrt{\frac{7}{12}}\chi_0^4 - \sqrt{\frac{5}{12}}\chi_4^4. \tag{3.46}$$

This solution is symmetrical under rotations over $\pi/2$ about the z-axis. And is also accompanied by versions for the x and y-axis. The last solution is invariant under rotation over $\pi/2$ about the x, y and z-axis and hence corresponds to the cubic group which in group theory [23] is formally denoted by O

$$\psi_1 = \sqrt{\frac{7}{12}}\chi_0^4 + \sqrt{\frac{5}{12}}\chi_4^4. \tag{3.47}$$

This solution represents the cubatic phase in it simplest form. However on closer examination the second set is equivalent to the cubatic solution. For instance (3.46) has to be rotated over an angle of $\pi/4$ about the z-axis.

On the basis of a bifurcation analysis it is not possible to tell which of these two types of solution the correct one is.

For the third and final part of the solution of the bifurcation equations we set $r^2 = 5/13$. As a general solution we now take

$$\psi_1 = c_0\chi_0^2 + c_2\chi_2^2 + d_0\chi_0^4 + d_2\chi_2^4 + d_4\chi_4^4. \tag{3.48}$$

We have as a normalization $c_0^2 + c_2^2 + d_0^2 + d_2^2 + d_4^2 = 1$. If we follow the same procedure as before we end up with a set of five equations. But we cannot solve it analytical anymore. The solutions we obtained for the cubatic phase (3.46) and (3.47) still satisfy and there are three different nematic like solutions for which $c_2 = d_2 = d_4 = 0$.

There are also other combinations possible, which are independent of the above mentioned solutions (not a simple reference rotation). They can be seen as mixtures of the two and are less symmetric. Within our set of $\Delta^l_{m,n}$-functions there are only two possible symmetries left the D_4 phase, which has a 4-fold axis and the D_2 phase.

3.4.4 The phase diagram

At this moment we cannot tell which transition will occur for a certain particle. Only which possibilities there are. In fact as we will see later on it is possible to find outside the circle for instance a transition from isotropic to D_4 phase, which is not given by the bifurcation analysis. This is a consequence of the fact that a bifurcation analysis only studies the stability of the isotropic phase against small perturbations. Though it gives an upper limit for the transition to occur it is not necessary that the symmetry of the perturbation coincides with the actual phase we end up with.

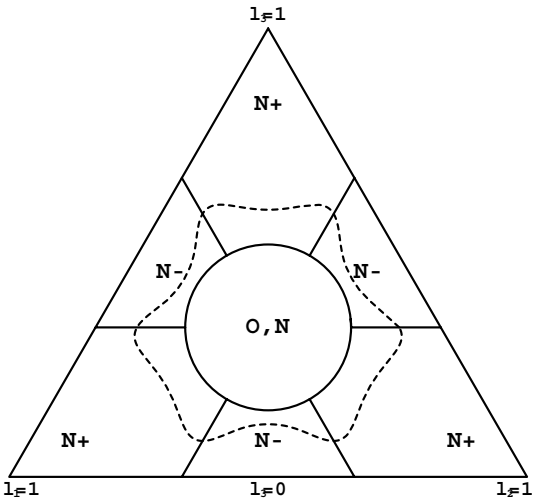

Figure 3.3: The phase diagram of the phase transition at lowest density according to the bifurcation analysis. The lines form the boundary between areas of different behavior. Points on the dashed line have $\eta_2 = 0$, outside and inside η_2 has negative respectively positive values.

We now know enough of the first phase transition to draw a qualitative phase diagram (figure 3.3). Our phase diagram is formed by a triangular base in which we can find all possible particles against the density. For simplicity we have drawn only constant density planes of the phase diagram. The triangular base is the projection of the plane definedf by $l_1 + l_2 + l_3 = 1$. The scales perpendicular to the edges are linear. For instance at the top of the triangle we have $l_3 = 1$ and $l_1 = l_2 = 0$. This points therefore represents the particle formed by a single rod. On the other hand, the base of the triangle is a line for which $l_3 = 0$ and represents, except for the edges, particles consisting of only two rods. All points inside the triangle correspond to particles with three rods.

The circle corresponds to $r^2 = 5/13$, i.e. all particles for which $\lambda_2 = \lambda_4$ and in which case we had to use (3.48). There are six straight lines connecting the edges of the triangle with the circle. These lines are formed by putting one of the l_i equal to $1/3$ and as we have seen the first order term in the density expansion $\eta_1 = 0$. They form the boundary between the areas for the two nematic phases which we denote by N_+ and N_-. They differ in the sense that in the first case the longest rods want to align and in the other case the shortest rods. The lines them selves belong to the N_+ phase.

Inside the circle we have $r^2 < 5/13$. There are two possibilities for the phase transition. It can go from isotropic-to-cubatic or nematic

From the fact that $\eta_1 \neq 0$ we may conclude that the transition will be first order. There is of course the exception for the straight lines in the diagram for which $\eta_1 = 0$. This can indicate that the transition is continuous. For that reason we plotted for particles outside the circle the curve (dashed line) for which the second term in the density expansion (η_2) is zero. Between this curve and the circle η_2 is negative. And outside the curve we have a positive value for η_2 and η_3 is the first negative term. From this we might expect that in the neighborhood of the lines and going from the inside to the edges the density at which the phase transition takes place approaches the bifurcation density.

3.5 Trial Functions

3.5.1 Method

We have seen that the bifurcation analysis gives us an idea of what might happen for the first phase transition. It shows possible symmetries of the phases and for which kind of particle we might expect them and also estimates the density at which is occurs by giving an upper limit. What it does not tell is whether the transitions we found also happen and if they do at which density. This is the problem which we are trying to solve in this section.

Density functional theory tells us that if we have found the ODF which gives the minimal free energy (3.1) it coincides with the equilibrium ODF and is the stable state of the system. So what we ought to do is make a trial function with some parameters in it and try to find those parameters which minimizes the free energy. Since the ODF is a probability distribution function it ought to be positive hence we take the following Ansatz

$$\psi(\Omega) = \exp\left(\sum_{l,m,n} \psi_{l,m,n} \chi^l_{m,n}(\Omega)\right) \tag{3.49}$$

where we have expanded in the complete set of orthogonal eigenfunctions of the excluded volume interaction. Now the $\psi_{l,m,n}$ can be seen as parameters of the function ψ. We can give them a starting value for fixed density and calculate its free energy. And from this point using an iterative process to optimize the coefficients to minimize the free energy. The normalization is maintained by adjusting $\psi_{0,0,0}$.

Instead of minimizing the free energy however we try to find solutions of the stationarity condition (3.21) and check afterwards whether it is a minimum for the free energy. If we use our trial function we obtain

$$\sum_{l,m,n} \psi_{l,m,n} \chi^l_{m,n}(\Omega) + \eta \mathcal{E}[\psi] = \beta\mu. \tag{3.50}$$

If we now multiply this equation with $\chi^l_{m,n}$, integrate over Ω and use (3.18) and the orthogonality of the eigenfunctions we obtain a set of equations

$$\frac{8\pi^2}{2l+1}\psi_{l,m,n} = -\eta < \chi^l_{m,n}|\mathcal{E}[\psi] >= -\eta < \psi|\mathcal{E}[\chi^l_{m,n}] > . \tag{3.51}$$

From this result we immediately may conclude that we only have to use those eigenfunctions of the excluded volume that have a non-zero eigenvalue. All of them have we already defined in (3.29). And we can write our trial function as

$$\psi(\Omega) = \exp\left(\sum_{l,m} \psi_{l,m} \chi^l_m(\Omega)\right) \tag{3.52}$$

where the coefficients ψ^l_m have to satisfy

$$\psi_{l,m} = -\frac{2l+1}{8\pi^2}\eta\lambda_l < \chi^l_m|\psi > \tag{3.53}$$

for even values of l and m where $0 \leq m \leq l$ and the coefficient ψ^0_0 is determined by the normalization condition $< 1|\psi >= 1$. From these equations the coefficients can in principle be calculated self-consistently.

The next thing we have to take care of is identifying each phase by means of an set order parameters for which we will take the $< \Delta^l_{m,n} >$. If there are non-zero $< \Delta^2_{m,n} >$ we first rotate our solution for the ODF in such a way that $< \Delta^2_{0,0} >$ has the absolute maximal value. This is done by rotating the reference frame as well as the initial orientation of the particle.

For the nematic phase we could now take for instance the usual second order Legendre polynomial as an order parameter

$$\mathcal{N} =< \Delta^2_{0,0}|\psi > . \tag{3.54}$$

The problem however is that a non-zero nematic order parameter does not tell us whether we actually have a nematic phase. So instead of looking whether a certain order parameter is non-zero we could better look for order parameters which are zero and give us better information.

For the isotropic phase we know that the ODF is a constant. This implies that all order parameters should be zero. Or if we say it the other way around if there is a non-zero order parameter it is not an isotropic phase.

For the nematic, the D_4 and the D_2 phase there is at least one of the rods of the particles which tend to align and hence $< \Delta^2_{0,0} >\neq 0$. But for the cubatic phase the ODF should be invariant under rotations over $\pi/2$ around any of the three frame axes. Which means that there cannot be any terms present with $l = 2$. Hence if $< \Delta^2_{m,n} >= 0$ and there are non-zero order parameters for $l = 4$ we have a cubatic phase.

If we find that $< \Delta^l_{m,n} > \propto \delta_{0,m}$ we have a solution which is invariant under rotations around the z-axis and hence a nematic phase. If we further more determine what the relevant rod in the particle is we know whether we have a rod-like or platelet-like nematic phase.

Finally if $< \Delta^2_{2,2} > \neq 0$ the ODF is not invariant under rotations over $\pi/2$ around the z-axis and we cannot have a D_4 phase. So it has to be the D_2 phase. Which leaves for the D_4 phase that $< \Delta^2_{2,2} >= 0$. In this case we can again determine the relevant rod and distinguish between D_{4+} and D_{4-}.

phase	$\Delta^2_{0,0}$	$\Delta^2_{2,2}$	$\Delta^4_{0,0}$	$\Delta^4_{4,4}$
Isotopic	0	0	0	0
Nematic		0		0
Cubatic	0	0		
D_4		0		
D_2				

Table 3.2: For each phase is indicated which of the order parameters is zero. The order parameter are determined by evaluating their integral with the ODF ψ.

We have summarized these results in table 3.2 where we indicated for each phase which order parameters should be zero. We have chosen to use $< \Delta^2_{2,2} >$ and $< \Delta^4_{4,4} >$ but these choices are arbitrary as long as they posses the right symmetry.

Given a solution we can calculate the free energy. As can be seen in (3.1) this involves a 6-dimensional integral, but this can be avoided. Since the ODF satisfies (3.50) and the right-hand side which is constant and equals $\psi_{0,0} + 2\eta$ we can write the free energy as

$$\beta f = \frac{1}{2} < \psi | \ln \psi > + \frac{1}{2}\psi_{0,0} + \eta + \beta \hat{f} \tag{3.55}$$

After having checked whether the solution is indeed the minimum of the free energy the pressure and chemical potential can easily be calculated by

$$\beta P = \rho + \rho^2 B_2(\psi) = \frac{\eta}{< B_2 >_I} \left(1 + \frac{1}{2}\eta < \psi | \mathcal{E}[\psi] > \right) \tag{3.56}$$

and

$$\frac{\beta G}{N} = \beta f + \frac{\beta P}{\rho} = 1 + \psi_{0,0} + 2\eta + \beta \hat{f} \tag{3.57}$$

where the last term up to a constant is given by $\beta \hat{f} = \ln \eta$. If now for different densities we find equal pressure and chemical potential we have coexistence of different phases.

3.5.2 Numerical Results

We solve the set of equations that we derived in the previous subsection self-consistently where we only use the functions with $l = 2$ and $l = 4$. By using several starting values

we obtain by means of an iterative process different numerical stable solutions. Given a stable solution we can calculate the free energy and check whether it is a minimum.

By taking more terms into account the coefficients change as well as the densities for which the transitions occurs. But since we are only interested in a qualitative picture this is of no real importance because the symmetry of the obtained phase remains the same. We used (3.55) to calculate the free-energy and in that way avoid the six-dimensional integral. But since we truncated the expansion of the ODF at $l = 4$ this means that we also truncate the free-energy. If we find solutions of the ODF with different symmetries we use this approximated value for the free-energy to determine which is the best of them. So we end up with only an estimate for the density at which the phase transition will take place but will find the right phase.

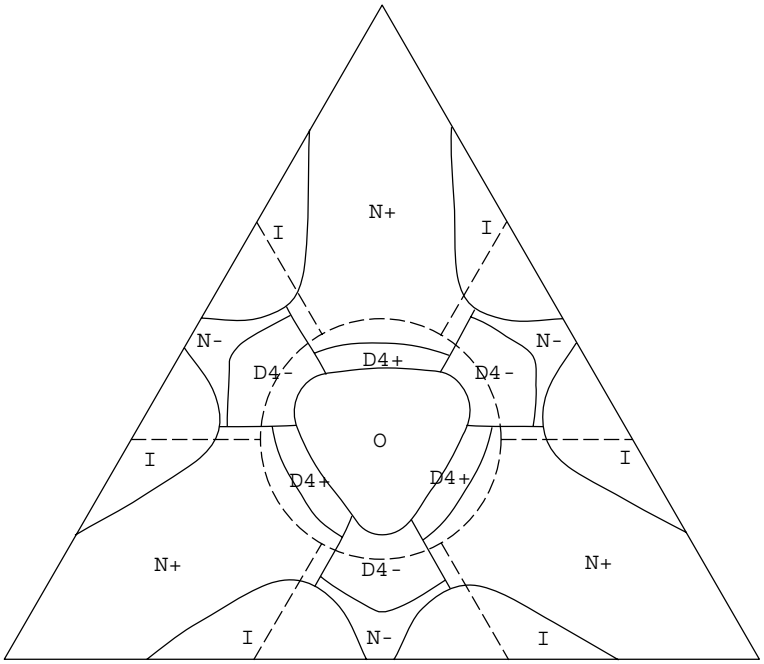

Figure 3.4: The phase diagram at a density below the bifurcation density($\eta/\eta_0 = 0.9$). The dashed lines denote the boundaries given by the bifurcation analysis of areas with different behavior.

In the figures 3.4 and 3.5 are two cross-sections of the phase diagrams sketched. They are drawn for rescaled densities $\eta = 0.9\eta_0$ respectively $\eta = 1.1\eta_0$. This is done in order to compare the behavior of all particles around their densities of interest. As can be seen from (3.33) this means that the real density in the middle is almost 14 times as high as at the vertices of the triangle. Analogous to the distinction we made between a rod-like nematic N_+ and platelet nematic phase N_- we can do this also for the D_4 phase.

The dashed lines represent the boundaries which we obtained from our bifurcation analysis and we see that they give a reasonable estimate of the real behavior. Around the points where a straight dashed line meets an edge we find at 90 percent of the bifurcation density still an isotropic phase. Though those regions become smaller when we approach the bifurcation density it remains quit stable and it is possible that for a

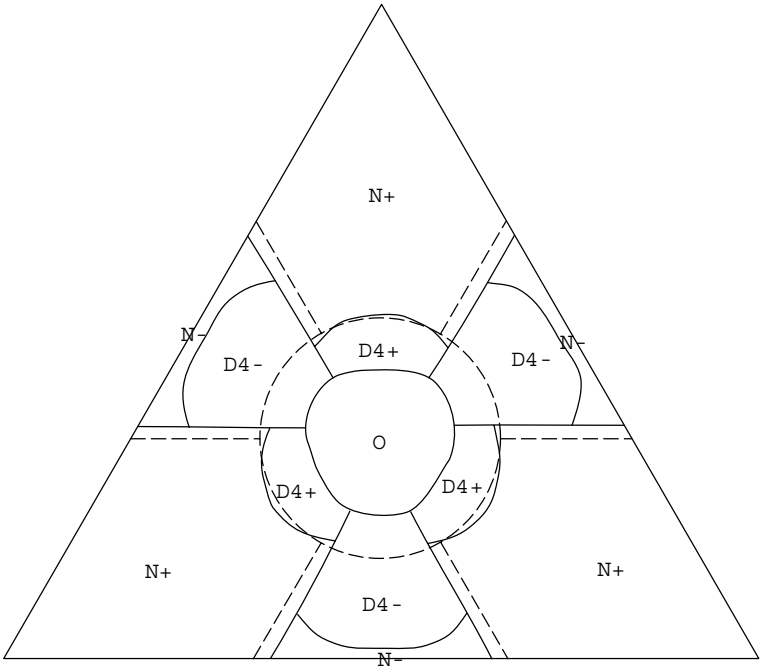

Figure 3.5: The phase diagram at a density above the bifurcation density($\eta/\eta_0 = 1.1$). The dashed lines denote the boundaries given by the bifurcation analysis of areas with different behavior.

very small region there is a continuous transition. Due to the approximation of taking only functions with $l \leq 4$ into account we cannot tell whether it is. As far as we know all other transitions are first order.

As we expected the nematic phase is found mainly outside the circle, there is however a part of the rod-like nematic phase which extends itself into the circle and also in the regions where we expected a platelet-like behavior. Apparently the longest rod has large influence on the system. The N_- phase is found only in small regions and since a platelet is a very crude approximation for these particles it is not surprisingly that it remains not stable for large densities. It disappears for $\eta \approx 1.3\eta_0$ by going to the phase D_{4-} where there is a discrete orientational symmetry around the z-axis.

Inside the circle we could expect the nematic, the cubatic and the D_4 phase. The cubatic phase is found in the middle for all particles which resemble the particle with three equal rods. It is surrounded by the D_4 phase.

If we increase the density the D_2 phase appears, along the boundaries between the phase for which the longest or shortest rod is ordered. It starts at a density of $\eta \approx 1.2\eta_0$ around the points where both D_4 phases and the N_+ phase meet each other which is near the points where the dashed lines touch the circle.

For very high densities all particles with no special symmetry end up in the D_2 phase in which rods with the same length are aligned. The particles for which two rods have the same length cannot go beyond the D_4 phase and they lay on the symmetry lines. The domains of the nematic and cubatic phase are merely points, the vertices respectively the middle of the triangle.

3.6 Gaussian Approximation

3.6.1 Nematics

We can obtain an approximate solution of the Onsager model describing the isotropic-nematic phase transition for long thin rods if we use the assumption that in the ordered phase the rods have a strongly peaked distribution around the z-axis which can be approximated by a Gaussian. The same approximation can be used for the isotropic-cubatic transition for the symmetrical particle with three rods (see Frenkel [20]).

It is possible to extend this approximation to our system for all phases. First we write down again the free energy

$$\beta f = \beta \hat{f} + \sigma(\alpha) + \eta\rho(\alpha) \tag{3.58}$$

where the first term is the ideal non-interacting system, given by $\beta\hat{f} = \ln\eta + const.$ The second part of the free energy describes the orientational entropy and is given by

$$\sigma(\alpha) = \int d\Omega\psi(\Omega)\ln(8\pi^2\psi(\Omega)). \tag{3.59}$$

The last term in the free energy is related to the translational entropy

$$\rho(\alpha) = \frac{4}{\pi}\int d\Omega \int d\Omega'\psi(\Omega)\psi(\Omega')\sum_{i,j} l_i l_j |\sin\gamma_{i,j}|. \tag{3.60}$$

In the isotropic phase the ODF is a constant, $\psi(\Omega) = 1/8\pi^2$ which gives the following exact results

$$\begin{aligned} \beta f_I &= \ln\eta + \eta \\ \beta P_I &= (\eta + \eta^2)/ < B_2 >_I \\ \beta\mu_I &= \ln\eta + 2\eta + 1 \end{aligned} \tag{3.61}$$

For a nematic where Ω is the direction of the ordering axis of particle the factor $8\pi^2$ reduces to 4π. The trial function in the original Onsager model is given by

$$\psi(\Omega) = \frac{\alpha}{4\pi\sinh\alpha}\cosh(\alpha\cos\theta). \tag{3.62}$$

For large values of α this is a sharply peaked distribution with its main contribution around $\theta \approx 0$ and $\theta \approx \pi$ which we can approximate by Gaussians

$$\begin{aligned} \psi(\Omega) &= \frac{\alpha}{4\pi}\exp\left(-\frac{\alpha\theta^2}{2}\right) \qquad (0 \le \theta \le \pi/2) \\ &= \frac{\alpha}{4\pi}\exp\left(-\frac{\alpha(\theta-\pi)^2}{2}\right) \qquad (\pi/2 \le \theta \le \pi) \end{aligned} \tag{3.63}$$

The orientational part of the entropy can easily be calculated in this approximation $\sigma(\alpha) \approx \ln(\alpha) - 1$. The translational part has three different type of contributions. The first is given by the interaction of the ordering rods which we label by l_3 and it is the

longest one in case of a rod-like nematic and the shortest one in case of a platelet-like nematic

$$\rho_{3,3}(\alpha) \approx \frac{4l_3^2}{\sqrt{\pi\alpha}}. \tag{3.64}$$

This term is important for rod-like particles and for platelet particles it is negligible. The second type is the interaction between one l_3 rod along the nematic axis and one that is perpendicular to it for instance l_1

$$\rho_{1,3}(\alpha) \approx \frac{4l_1 l_3}{\pi}. \tag{3.65}$$

And the last type consist of the interaction between two rods in the plane perpendicular to the nematic axis. Its main importance is for platelet-like particles. This contribution though is not proper described by the first term of the expansion if we use the Gaussian approximation which is due to the fact that a typical value for α in this region is 12, too small for a real Gaussian approximation. For that reason we use the original Onsager as a trial function to obtain a fit of this contribution which we will denote by $J(\alpha)$

$$\rho_{1,1}(\alpha) \approx \frac{4l_1^2}{\pi} J(\alpha) = \frac{4l_1^2}{\pi}(0.639 + \frac{1.45}{\alpha} - \frac{12.3}{\alpha^2} + \frac{75.0}{\alpha^3} - \frac{178}{\alpha^4}). \tag{3.66}$$

The total orientational entropy can now be written as

$$\rho(\alpha) = \frac{4l_3^2}{\sqrt{\pi\alpha}} + \frac{8}{\pi} l_3(1-l_3) + \frac{4}{\pi}(1-l_3)^2 J(\alpha) \tag{3.67}$$

and only depends on the length of the ordering rod. Since the proper value for α minimizes the free energy we differentiating the expression with respect to α and equate it to zero

$$\frac{d\beta f}{d\alpha} = \frac{1}{\alpha} - \eta \left(\frac{2l_3^2}{\alpha\sqrt{\alpha\pi}} - \frac{4}{\pi}(1-l_3)^2 J'(\alpha) \right) = 0. \tag{3.68}$$

After having solved this equation we can obtain finally the pressure and chemical potential of the nematic phase for any density.

3.6.2 Cubatics

In order to describe the cubatic phase by a Gaussian distribution we switch over to the xyz-convention of Eulerian axes. In this convention the general rotation is given by 3 subsequent rotations around three perpendicular axes

$$\mathcal{D}(\Omega) = e^{-\imath\phi J_x} e^{-\imath\theta J_y} e^{-\imath\psi J_z}. \tag{3.69}$$

So for the cubatic phase we can use as a Gaussian distribution

$$\psi(\Omega) = \frac{1}{24} \left(\frac{\alpha}{2\pi} \right)^{3/2} \exp\left(-\frac{\alpha}{2}(\phi^2 + \theta^2 + \psi^2) \right). \tag{3.70}$$

There are 24 such contributions corresponding to 24 possible orientations for the particle to align with the three axes of the system. The orientational part is again easy to calculate and given by

$$\sigma(\alpha) = \ln(\frac{8\pi^2}{24}) + \frac{3}{2}\ln(\frac{\alpha}{2\pi}) - \frac{3}{2} \tag{3.71}$$

For the translational contribution to the free energy we have to add for all possible orientations the excluded volumes for the aligned and perpendicular pairs of rods, which gives

$$\rho(\alpha) = \frac{4}{3\sqrt{\pi\alpha}} + \frac{8}{3\pi} \tag{3.72}$$

If we now minimize the expression for the free energy with respect to the parameter of the Gaussian α we obtain

$$\alpha = \frac{16\eta^2}{81\pi} \tag{3.73}$$

This gives us the free energy and hence the pressure and chemical potential of the cubatic phase in this approximation

$$\begin{aligned}
\beta f_O &= 4\ln\eta + \ln[\frac{\pi^2}{3}(\frac{2\sqrt{2}}{9\pi})^3] + \frac{3}{2} + \frac{8\eta}{3\pi} \\
\beta P_O &= (4\eta + \frac{8}{3\pi}\eta^2)/ < B_2 >_I \\
\beta \mu_O &= 4\ln\eta + \ln[\frac{\pi^2}{3}(\frac{2\sqrt{2}}{9\pi})^3] + \frac{11}{2} + \frac{16\eta}{3\pi}
\end{aligned} \tag{3.74}$$

If we combine these with the ones from the previous subsection for the isotropic phase we can find that there is a coexistence between the isotropic and cubatic phase for

$$\begin{aligned}
\eta_I &= 48.43 \\
\eta_O &= 50.80
\end{aligned} \tag{3.75}$$

in which case for the value for the parameter α of the Gaussian we obtain

$$\alpha = 162.3 \tag{3.76}$$

Because of this large value we can justify the Gaussian approximation.

3.6.3 The D_4 and D_2 phase

In the case of a D_4 phase there is one 4-fold degenerate axis which we assume along the z-axis. Our trial function has now two parameters, one α describes the strength of the ordering with respect to the z-axis and the other β describes the strength of the ordering with respect to the x and y-axis which are in this phase equivalent. The trial function has 8 contributions of the form

$$\psi(\Omega) = \frac{1}{8}\left(\frac{\alpha^2\beta}{8\pi^3}\right)^{1/2} \exp\left(-\frac{1}{2}(\alpha\phi^2 + \alpha^2\theta + \beta^2\psi^2)\right). \tag{3.77}$$

For σ we find again a simple equation

$$\sigma(\alpha,\beta) = \ln(\frac{8\pi^2}{8}) + \frac{1}{2}\ln(\frac{\alpha^2\beta}{8\pi^3}) - \frac{3}{2}. \tag{3.78}$$

For ρ however we get an expression containing an elliptical integral of the second kind

$$\rho(\alpha,\beta) = \frac{4l_3^2}{\sqrt{\pi\alpha}} + \frac{4(1-l_3)^2}{\sqrt{\pi^3\beta}}E(\sqrt{1-\beta/\alpha}) + \frac{2}{\pi}(1-l_3)(1+3l_3). \tag{3.79}$$

Minimizing the free energy with respect to α and β gives for $l_3 > 1/3$ that $\alpha > \beta$ which suggest a stronger ordering along the z direction, while for $l_3 < 1/3$ the opposite, $\beta > \alpha$, is found and therefore a stronger ordering along the x and y axes.

For the D_2 phase it is almost the same story as for the D_4 phase except that there are now only 4 possible orientations of the particle and we need 3 parameters in our trial function

$$\psi(\Omega) = \frac{1}{4}\left(\frac{\alpha\beta\gamma}{8\pi^3}\right)^{1/2} \exp\left(-\frac{1}{2}(\alpha\phi^2 + \beta^2\theta + \gamma^2\psi^2)\right). \tag{3.80}$$

There is the simple equation for σ but now of 3 parameters

$$\sigma(\alpha,\beta,\gamma) = \ln(\frac{8\pi^2}{4}) + \frac{1}{2}\ln(\frac{\alpha\beta\gamma}{8\pi^3}) - \frac{3}{2} \tag{3.81}$$

and the expression for ρ is somewhat more complex

$$\begin{aligned}\rho(\alpha,\beta,\gamma) = \frac{8}{\pi^{3/2}}\Bigg[&\frac{l_3^2}{\sqrt{\beta}}E(\sqrt{1-\beta/\alpha}) + \frac{l_2^2}{\sqrt{\gamma}}E(\sqrt{1-\gamma/\alpha}) \\ &+\frac{l_1^2}{\sqrt{\gamma}}E(\sqrt{1-\gamma/\beta})\Bigg] + \frac{4}{\pi}(1-r^2)\end{aligned} \tag{3.82}$$

3.6.4 Results

If we combine the Gaussian approximations of the different phases we can calculate the coexistence by equating pressure and chemical potential. In figure 3.6 the phase diagram at reduced density $\eta/\eta_0 = 1$ is drawn. At this density the isotropic phase is unstable but there are still isotropic areas. It is clear that the Gaussian approximation is cannot be valid there. Further more we find that the boundaries between the cubatic and D_4 phase are straight lines. This seems somewhat surprising but is merely a consequence of losing particle information in the approximation. This can be seen from the expression for the free energy which only depend on the length of one rod. Therefore if for two different particles with the same value for l_3 the same transition occurs the densities are

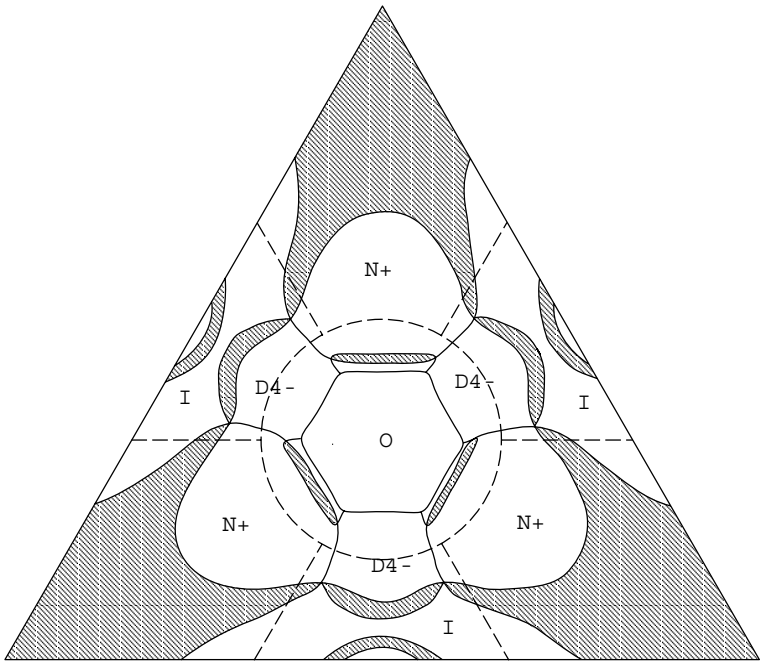

Figure 3.6: The phase diagram obtained by a Gaussian approximation at a density equal to the bifurcation density($\eta/\eta_0 = 1$). The dashed lines denote the boundaries given by the bifurcation analysis of areas with different behavior. The shaded regions correspond to particles which at this density have coexistence between two phases and therefore do not have a stable phase for this global density.

equal. Though the figure has a different density scale for both particles this is difference is in too small to make a visible difference in this figure.

The shaded areas in the figure correspond to particles which phase separate at this global density into two coexistence phases with different densities, the higher having less symmetry. There are three relatively large equivalent areas for the isotropic-nematic phase transition for the rod-like particles and smaller ones for the platelet-like particles. Some areas are very tiny and cannot be seen in the diagram at all. For instance between the cubatic and D_4 phases of both types there is a narrow strip of particles which have at this density coexistence between the cubatic and D_4 phase.

It is not observed and intuitive not expected that there are particles which go from rod-like to platelet-like behavior for instance via a transition from the N_- to a D_{4+} phase. Also a phase transition from cubatic phase to a nematic phase, so to a phase with higher symmetry, is not found. All data confirmed that phase transitions in this model can only go to lower symmetries.

If we take a cross-section of the diagram along the symmetry axis for which $l_1 = l_2$ and we plot now the real densities in units of B_2, the isotropic second virial coefficient which is equal for all particles, versus l_3 the length of one of the three rods. The result is shown in figure 3.7. Since the particles are 4-fold symmetric around this l_3 rod they cannot go beyond the D_4 phase in which they all will end up with only two exceptions, the cubatic particle and the single rod particle. As was explained before the N_- phase is very unstable and is only found in a very small region and will for somewhat higher

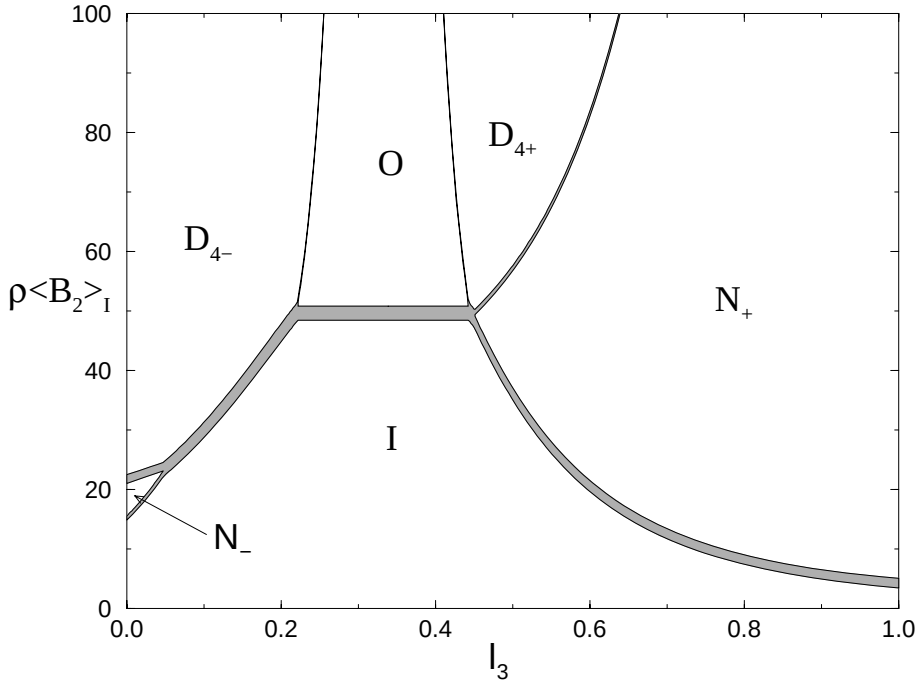

Figure 3.7: Cross section of the phase diagram along the symmetry line ($l_1 = l_2$) of the density versus the length of the remaining rod.

densities already form a D_4 phase. The N_+ phase is much more stable. The isotropic-cubatic phase transition takes place at a density which is almost 14 times as high as the isotropic-nematic phase transition for the single rod.

3.7 Discussion

We have investigated the orientational phase behavior of Onsager crosses, which are non-convex particles formed by rigidly joining three perpendicular elongated rods of different lengths in their centers. For this model we formulated the Helmholtz free energy as functional of the single particle orientational distribution function, by truncating the virial expansion after the second virial coefficient, assuming that higher order virial coefficients can be neglected.

We joined the rods of our Onsager crosses in their centers. But since we assumed that the rods contribute independently to the excluded volume interaction we effectively treat them as if they are only fixed to each other concerning their orientation. Hence our results are still valid if the rods are connected in any other way as long as their orientations are fixed and perpendicular to each other. For shorter rods however this is not valid anymore and one should use the real excluded volume which does depend on the way how the rods are connected. As well as that higher virial coefficients cannot be neglected anymore and should be taken into account.

We restricted ourselves to homogeneous orientationally ordered phases, of which there are for this kind of particles four possibilities. The uniaxial nematic phase (N), two biaxial nematic phases D_4 and D_2, and the cubatic phase (O) which is a three-axial nematic phase. It is obvious that there can also be phases with translational order like smectic and crystalline phases. We assumed that the densities at which these are stable

are well above the stable densities for the orientally ordered phases. For shorter rods the densities become of the same order and translational order should be taken into account.

We used three different methods to study the phase behavior of these systems, a bifurcation analysis, solving the stability equation of the free energy numerical and an Gaussian approximation.

To obtain a simple impression of the phase behavior we used a bifurcation analysis. It is an easy method which gives upper limits for the densities at which phase transitions take place by calculating the densities at which a phase becomes unstable and for which distortions this is the case. In order to use it one should therefore know the one particle distribution function of that phase and in general one doesn't, except for the isotropic phase. Furthermore the symmetry of the distortions give only an idea of what the symmetry of the phase will be, but are not conclusive. The bifurcation theory in our case gives that the distortions at the lowest density at which the isotropic phase becomes unstable have a nematic or cubatic symmetry, while the other methods we used also allowed an isotropic-to-D_4 transition. The numerical method of solving the stationarity equation is more reliable and gives all numerical stable solutions. By comparing the free energies of the solutions with different symmetries one finds the correct one, which has the lowest free energy. There are however a number of problems with this method. One has to choose an expansion of the one particle distribution function and is therefore limited in the accuracy. Because of the finite number of terms, the distribution function has to be smooth. Furthermore this method involves in iteration scheme with multiple integrations which makes it computationally more expensive.

The Gaussian approximation is a good alternative. It is computationally not expensive and gives the correct symmetries. It relies however on the assumption of peaked distribution functions and this is not always the case. But with the previous method, it forms a good combination which can deal over the whole range from low to high densities.

Depending on the shape of the particles we observe successive phase transitions. The isotropic phase undergoes a first order transition to the nematic, the cubatic or the D_4 phase. Which in their turn at higher densities have a transition via the D_4 phase to the D_2 phase. In some cases the D_4 phase is surpassed. These latter transitions are within our theory first order. According to Landau theory they can also be continuous, however we did not observe this. We did not find any evidence for a direct transition from the isotropic-to-D_2 phase.

Instead of the cross-like particles we used, a similar analysis can be done for particles related to other platonic solids. For instance the combination of four rods leading to a tetrahedral phase.

The question which remains is whether the cubatic phase can be observed in nature? To our knowledge so far it has not been seen. There is no direct candidate for cross-like particles such as tobacco mosaic virus for a long rod. Maybe it is possible in the future to make this kind of particles. Star like molecules are already produced with short flexible tails, but we need tails which are more rigid and longer.

Also computer simulations cannot yet deal with these large L/D ratios. It may be worthwhile to try simulations of these cross-like particles at smaller ratios. One of the problems we foresee is however the slow dynamics of the particles due to stereometric hindering which might make these systems rather glassy.

We do not necessarily have to restrict ourselves to cross-like particles in order to observe a cubatic phase. In 1992 Veerman and Frenkel [8] observed it in a totally different system. They were simulating a system of hard cut spheres. These disk-like particles are obtained by removing the parts of a sphere with diameter D which are more then a distance $L/2$ above or below the equatorial plane. For the ratio $L/D = 0.2$ this system formed stacks of particles which were ordered in a cubic symmetry.

4 Simulation of Crosses

In this chapter we report on simulations of cross-like particles. These particles have the potential of forming a cubatic phase in the limit of infinitely large aspect ratios. We discuss the validity of our approximations for finite aspect ratios and introduce a new simulation method for these glass-like systems.

4.1 Introduction

In the previous chapter we developed a simple theory, which showed that cross-like particles, formed by three perpendicular elongated rods, are able to form a cubatic phase. The results were obtained in the limit where the constituent rods of the particles had infinitely large aspect ratios.

In this chapter we will investigate the behavior of these particles when the aspect ratios are finite. As a consequence we need to describe the particles in more detail. For long particles the excluded volume is still proportional to $L^2D|\sin(\gamma)|$, but correction terms have to be taken into account. The theory, described in the previous chapter, is also independent of the way in which the rods are connected as long as this is done rigidly and perpendicular.

From the viewpoint of simulations it is more convenient to choose the particles to be spherocylinders rather than ellipsoids, because their overlap criterion is easier. Furthermore we assume the 3 rods to be identical and connected perpendicular to each other in their centers of mass, in order to obtain a fully symmetric particle.

The fact that these particles are non-convex makes it very difficult to describe the systems theoretically. For instance the second virial coefficient B_2 in the isotropic phase of two arbitrary convex particles A and B can be expressed in terms of properties of the single particles, the volume V, surface area S, and the integrals M and G over the mean respectively Gaussian curvature [24]

$$B_2(A,B) = \frac{1}{8\pi}\left(V(A)G(B) + S(A)M(B) + M(A)S(B) + G(A)V(B)\right) \quad (4.1)$$

For non-convex particles this is not possible anymore. The derivation of this relation is only possible because two convex overlapping particles have a convex volume in common [25]. Non-convex particles however can have several unconnected and possibly non-convex volumes in common. So far the only analytic results known for non-convex particles are for diatomics and linear symmetric triatomics [26].

Also in simulations these cross-like particles are complicated. In order to observe the cubatic phase large aspect ratios are needed. As the particles extend over a large part of space in all 3 directions, they interact with many other particles. As a consequence we can expect that it is extremely difficult for these particles to rotate or move around, and at higher densities these systems will probably show glass-like behavior.

4.2 Virial Coefficients

In obtaining our theoretical results on the Onsager crosses we made two basic assumptions. The first was that we assumed that the length over diameter ratio goes to infinity ($L/D \to \infty$). As a consequence we assumed that similar to the case of long rods, the third and higher virial coefficients can be neglected. What Onsager [4] showed in fact was that for the isotropic phase the third virial coefficient of long rods scales as

$$\frac{B_3}{B_2^2} = \mathcal{O}(D/L)\log(L/D) \tag{4.2}$$

which offers some justification for neglecting higher virial coefficients as well. This asymptotic behavior was later confirmed by numerical evaluation of the virial coefficients of spherocylinders and prolate ellipsoids by Frenkel [27–30]. We assumed that in our case a similar argument could be formulated, allowing us to neglect higher virial terms.

The second assumption we made was treating the different rods as being independent from each other. Since they are rigidly and perpendicular connected to one another this has to be corrected. Naively one would expect that corrections are of the order of the volume which the rods have in common and hence can be neglected as well.

To check the validity of both of these assumption we present here the results of numerical evaluation of the virial coefficients of Onsager crosses formed by three identical rods.

In 1964 Ree and Hoover [31] reported a Monte Carlo technique to calculate the virial coefficients of hard-core particles, based on trial configurations. In order to evaluate the second virial coefficient B_2 we put a particle with fixed orientation in the origin and generate randomly a position and orientation for the second particle in a volume, large enough to allow all possible overlaps. Since the maximum distance between two crosses which still touch is $L + D$, a cubic volume with sides $L + D$ will do. The value of B_2^{cross} will be given by

$$B_2^{\text{cross}} = \tfrac{1}{2}\frac{\text{Number of overlaps}}{\text{Number of trials}} \times \text{Volume} \tag{4.3}$$

However our particles are extremely non-spherical, therefore we do not use this brute force technique of counting the number of occurrences of overlap. Instead we follow a method similar to the one used by Frenkel to calculate the virial coefficients of long spherocylinders [27].

The Onsager crosses consist of three rods and therefore $3 \times 3 = 9$ pairs of rods can be formed from two particles. Each of these pairs might or might not overlap. This leads to $2^9 - 1 = 511$ combinations for which there is an overlap of the two particles. Some of them are identical and have just a different labeling. If we take this into account there remain 25 different overlap diagrams D_i as shown in figure 4.1. Each circle represents a

rod of a cross, and rods belonging to the same particle have the same color. The lines indicate which pairs of rods are overlapping.

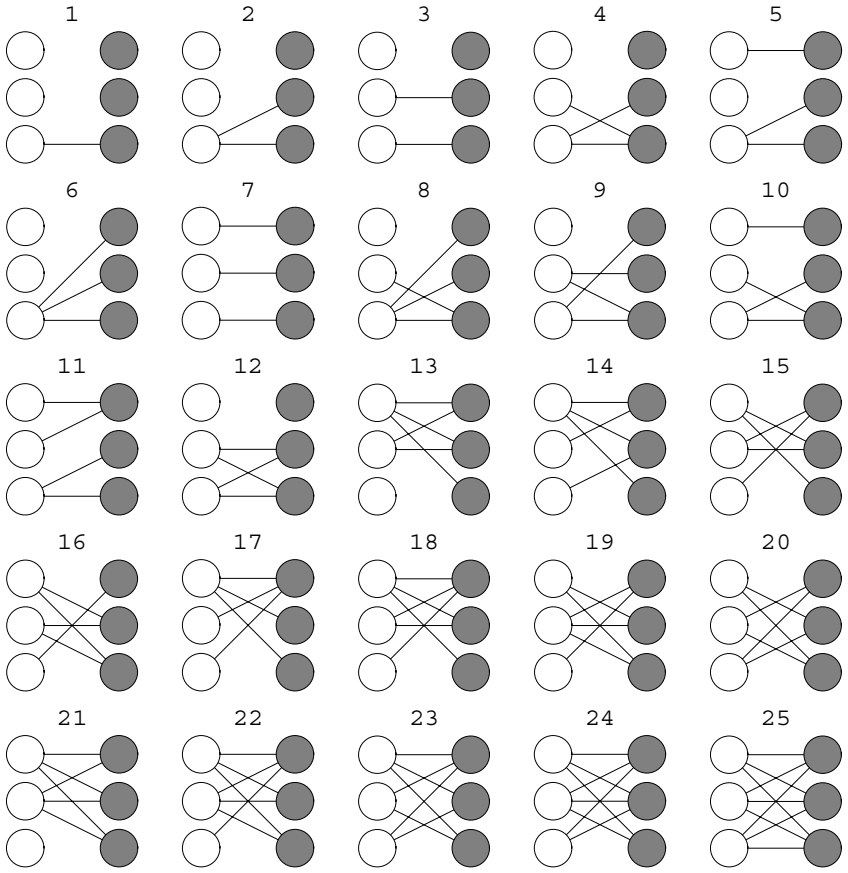

Figure 4.1: These are the 25 different overlapping configurations of 2 cross-like particles. Points of the same color correspond to the different spherocylinders of the same particle. Only the connected points overlap.

The number of overlaps in each diagram are listed in table 4.1, together with the number of realizations.

The value of each diagram can be obtained by analyzing the overlapping configurations and determine to which diagram it belongs, leading to

$$D_i = \frac{\text{Number of occurrences } D_i}{\text{Number of realizations}} \times \frac{\text{Volume}}{\text{Number of trials}} \tag{4.4}$$

The second virial coefficient B_2^{cross} of the crosses is given by half of the sum of all diagrams multiplied with the number of realizations.

We will now generate trial configurations, for which a chosen pair of rods, say the pair labeled with 1-1, is always overlapping. For each diagram D_i with k_i overlaps only $k_i/9$ times the total number of realizations is now allowed. This allows us to express the value of the diagram D_i under this constraint

diagram	overlaps	realizations
1	1	9
2,3	2	18
4,5	3	36
6,7	3	6
8,9,10	4	36
11,12	4	9
13,14,15	5	36
16,17	5	9
18,19	6	36
20,21	6	6
22,23	7	18
24	8	9
25	9	1

Table 4.1: The number of overlaps and realizations of the diagrams D_i.

$$D_i = \frac{\text{Number of occurrences } D_i}{\frac{k_i}{9} \times \text{Number of realizations} \times \text{Number of trials}} \times \text{Volume}|_{\text{1-1 overlap}} \tag{4.5}$$

The restricted volume leading to an overlap for the 1-1 pair is the volume averaged over all orientations leading to a spherocylinder overlap, and hence is twice the second virial coefficient B_2^{sphero}

$$B_2^{\text{sphero}} = \frac{\pi}{4}L^2D + \pi LD^2 + \frac{2}{3}\pi D^3 \tag{4.6}$$

For the second virial coefficient this leads to

$$\frac{B_2^{\text{cross}}}{B_2^{\text{sphero}}} = \frac{\sum_i \frac{9}{k_i}\text{Number of occurrence } D_i}{\text{Number of trials}} \tag{4.7}$$

The probability of finding an overlap for two spherocylinders is however dependent on the orientation. For given orientation we put the second particle in the excluded volume of the 1-1 pair. We can either generate the orientations randomly and give the configuration a weight proportional to the excluded volume, or generate the orientations proportional to the excluded volume

$$\mathcal{E}(\gamma) = 2L^2D|\sin(\gamma)| + 2\pi LD^2 + \frac{4}{3}\pi D^3 \tag{4.8}$$

where γ is the angle between the directors of the rods.

In summary we put one cross-like particle with fixed orientation in the origin and generate a random orientation for the second particle. We place the second particle

randomly in the excluded volume of the 1-1 pair to ensure overlap and give the configuration a weight proportional to the excluded volume, which will depend on the relative orientation of the 1-1 pair only.

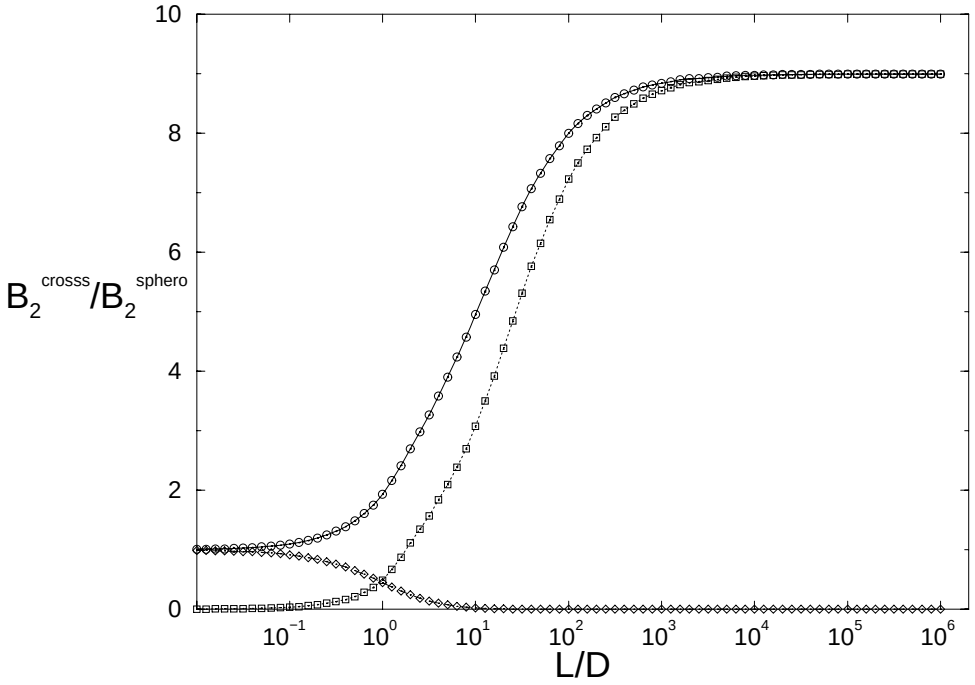

Figure 4.2: The second virial coefficient of Onsager crosses (○) as function of L/D in terms of the second virial coefficient of spherocylinders. The contributions of the diagrams, $\mathcal{D}_1$ (□) and $\mathcal{D}_{25}$ (◇) are shown as well.

The results for the second virial coefficient are given in figure 4.2, where we plotted their value in terms of B_2^{sphero}. Also the contributions of the two diagrams, $\mathcal{D}_1$ and $\mathcal{D}_{25}$ are shown. The first diagram corresponds to a single pair overlap and has the leading contribution for long aspect ratios. The second diagram corresponds to the overlap of all pairs of rods and will be the leading term for small values of the aspect ratios. For completeness we have listed the numerical values for the diagrams as well in table 4.2 as function of the aspect ratio L/D in powers of 10. This data is obtained by 100 blocks of each 10^6 trial configurations.

For small values of L/D the particles are almost spheres, hence all 9 pairs of rods are likely to overlap. The main contribution for the virial coefficient will therefore come from diagram $\mathcal{D}_{25}$. In this region the difference between the shape of a cross and a single spherocylinder will be marginal, because they both are almost spherical, and the virial coefficient of the first will be only slightly larger. For increasing value of L/D however, the particles becomes a very open cluster of rods for which it becomes very unlikely that there is more then 1 pair of rods which overlaps. The main contribution will therefore come from diagram $\mathcal{D}_1$ with only 1 overlapping pair of rods. But since there are 9 possible pairs of rods the virial coefficient of the crosses will be approximately 9 times as high as the one for spherocylinders. It is there where the rods which form the cross can be treated independent of each other and our assumption becomes valid. To satisfy this

L/D	$B_2^{\text{cross}}/B_2^{\text{sphero}}$	D_1/B_2^{sphero}	$D_{25}/B_2^{\text{sphero}}$
10^{-2}	1.00993(1)	0.00346(1)	0.991331(3)
10^{-1}	1.09928(2)	0.03597(2)	0.91679(1)
10^{0}	1.9512(1)	0.5084(1)	0.44919(1)
10^{1}	4.9713(1)	3.0939(1)	0.02506(1)
10^{2}	8.0053(1)	7.2292(1)	$3.44(1) \times 10^{-4}$
10^{3}	8.85512(3)	8.7265(1)	$3.5(1) \times 10^{-6}$
10^{4}	8.98188(1)	8.96522(2)	$4(1) \times 10^{-8}$
10^{5}	8.997832(3)	8.99582(1)	?
10^{6}	8.999731(1)	8.999494(2)	?

Table 4.2: The reduced values for second virial coefficients of crosses, as a function of length over diameter ratio. The estimated error in the last digit is indicated in parentheses.

requirement within one percent we need however a length over diameter ratio of about 2.0×10^3.

In order to calculate higher virial coefficients we evaluate the necessary diagrams [31] using the method of Frenkel [27] of growing a random chain of overlapping particles.

The first particle is put in the origin with fixed orientation. Using the brute force method of generating a random position and orientation until the new particle will overlap with the last particle in the chain would again have a poor efficiency for large aspect ratios.

Instead we select randomly one of the three rods of the last particle which will overlap with the new particle. Where as for the calculation of the second virial coefficient we could choose the 1-1 pair to overlap, for higher virial coefficients this is not longer allowed anymore, because only a restricted set of diagrams would be sampled. We also need to correct for the fact that we choose a specific pair of rods which will overlap. In order to do so we give each consecutive pair of overlapping particles a weight. This weight should be proportional to the contribution of this two particle configuration to the second virial coefficient, which as can be seen from (4.7), inversely proportional to number of overlapping pairs of rods.

The result of our calculations for the third, fourth and fifth virial coefficient are shown in figure 4.3 and table 4.3. This data is obtained by 100 blocks in which we have grown 10^6 independent chains of 5 particles. Note that there is a range of aspect ratio with negative value for the fifth virial coefficient, while for rod-like particles this remains positive [27, 29]. There is a region ($L/D \approx 15 - 35$) where both, the fourth and fifth virial coefficient, are negative. To our knowledge this is the first time such behavior is observed.

In order to observe the asymptotic behavior of the virial coefficients we can plot the scaled virial coefficients as is shown in figure 4.3. Each reduced virial coefficient is multiplied with L/D.

Unlike the behavior of the third viral coefficient of elongated particles, which for large aspect ratios scales as $(D/L)\log(L/D)$, for cross-like particles all three reduced virial coefficients scale proportional to D/L (see figure 4.4).

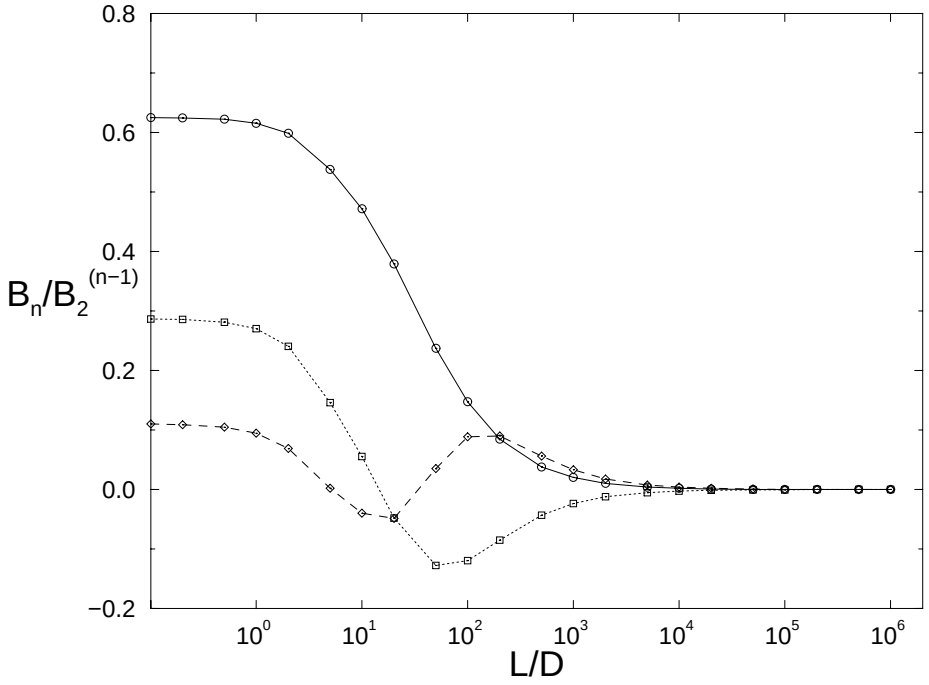

Figure 4.3: The third(○), fourth(□) and fifth(◇) virial coefficients of cross-like particles.

L/D	B_3/B_2^2	B_4/B_2^3	B_5/B_2^4
0	0.625	0.28695	0.11025
10^0	0.6157(1)	0.2704(2)	0.0945(3)
10^1	0.4716(1)	0.0554(1)	-0.0396(2)
10^2	0.14716(2)	-0.11923(4)	0.0887(1)
10^3	0.02012(1)	-0.02350(2)	0.0331(1)
10^4	0.002217(3)	-0.00257(1)	0.00389(2)
10^5	0.000236(1)	-0.000259(2)	0.00040(1)
10^6	0.0000247(3)	-0.000025(1)	0.000042(2)

Table 4.3: The reduced values for third, fourth and fifth virial coefficients of crosses. The estimated error in the last digit is indicated in parentheses.

It is clear that from these observations we have to conclude that the theory presented in the previous chapter is not able to give good predictions for the phase behavior of finite size particles. In order to ensure that the rods of the particle are independent we need to go to extremely large aspect ratios. Besides the fact that this assumption is not true for finite sized particles, we also should take into account the higher virial coefficients.

This does not necessarily mean that the general behavior of the system is predicted wrong as well, it only means that the description is not complete but strongly approximated. This is also the case for a system of elongated particles, as we make the aspect ratio smaller the higher virial coefficients should be taken into account, and the density for which the isotropic-to-nematic phase transition occurs is overestimated. Nevertheless this transition itself remains present up to aspect ratios of the order 5, depending on

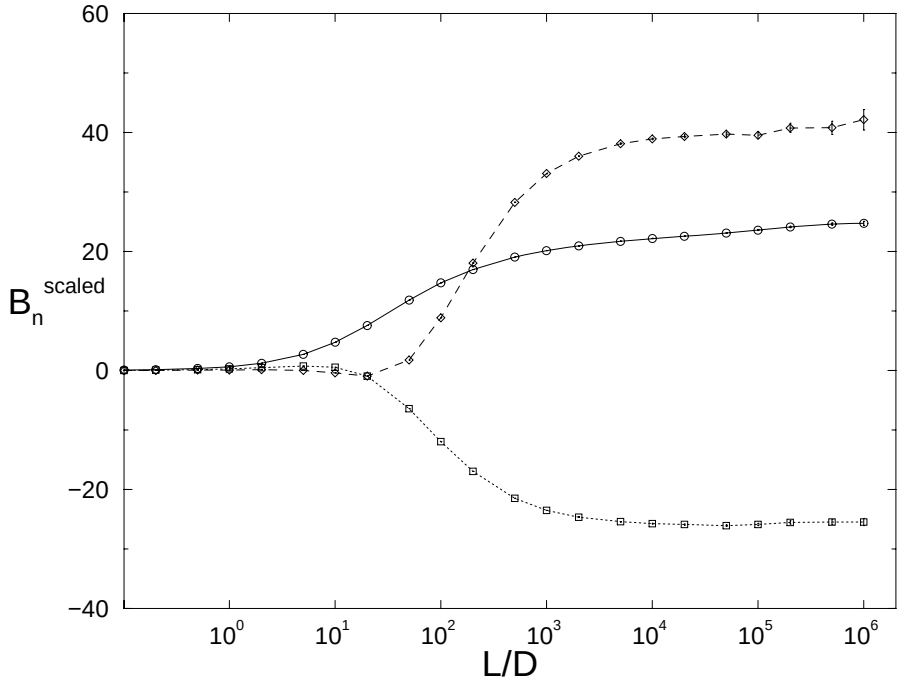

Figure 4.4: Asymptotic behavior of the scaled third (○), fourth (□) and fifth (◇) virial coefficients of cross-like particles scaled by $B_n^{scaled} = (L/D)B_n/B_2^{n-1}$.

the precise form of the particles. We therefore might expect similar effect to be true for systems of cross-like particles.

4.3 Parameter Hopping

As was mentioned before computer simulations on cross-like particles will be extremely difficult. In order to observe the cubatic phase we need large aspect ratios. This leads to particles extending over a large parts of space and therefore interacting with many neighboring particles. As a consequence particles will be confined to a relative small volume in which it will be very difficult to rotate as well. One can easily imagine that at higher densities this system will therefore might get trapped in a localized part of phase space, in the same way as a (spin) glass might get trapped in one of the many local minima in the free energy. A conventional simulation will therefore likely fail to characterize the system properly, and a different method is required.

In order to overcome this problem we introduce the simulation technique of parameter hopping. It is similar to the umbrella sampling technique as introduced by Torrie and Valleau [32]. The idea is to have a series of different Hamiltonians $\beta H_1, \beta H_2, \cdots, \beta H_n$, which for instance differ in temperature or interaction strength. A normal Monte Carlo simulation is performed on this system described by the usual configuration space and an extra variable taking care of the Hamiltonians. Sampling over the new variable is done by attempting to change the Hamiltonian and accepting with the appropriate weight. Unlike the normal umbrella sampling method, where by using an external force the system is biased and in an unphysical state, in this method the system is always sampled according to the real Boltzmann weight.

This method was used by several people mentioned by different names but in essence the same. Lyubartsev *et al* called it the method of expanded ensembles and used it to calculate the free energy in a single MC run on a model of electrolyte [33]. Marinari and Parisi called it simulated tempering, as it is closely related to simulated annealing, and used it on the Random Field Ising Model [34].

This method is also interesting for the study of the equilibrium behavior of glasses, because by increasing the temperature the system will expand making it easier to rearrange its configuration and come back to the original temperature. But instead of simulating only one system which can change it Hamiltonian, we will adopt the method described by Geyer [35] in which several systems with different Hamiltonians are simulated at the same time. Each system has its own Hamiltonian but there is an additional move in which Hamiltonians are swapped, maintaining one system per Hamiltonian. An advantage of this method is that for each Hamiltonian after accepting the swap a completely new configuration is used, leading to a better sampling of phase space.

In our case for simulating cross-like particles there is however no temperature involved. Instead we use the pressure as new variable. We perform a number of MC simulations for which the number of particles N is fixed to the same value, but for several different pressures $P_1, P_2, \cdots, P_n$. For these pressures we perform a normal NPT-simulation in which particles are displaced and rotated, and the volume is allowed to shrink or expand. After each sweep in which on average each particle has been attempted to move and rotate once, and also one volume move is tried, we do the extra move of swapping the pressures. Although we could select arbitrary pressures, it is best to take successive pressures in order to get a better acceptance.

Suppose we have two systems at pressures P_1 and P_2, with corresponding volumes V_1 and V_2. The configurations C_1 and C_2 are completely different. If we look at the swapping move from the point of view of the configurations, by attempting to swap the pressures P_1 and P_2 we continue the simulation for configuration C_1 at a new pressure P_2. If this new pressure is lower the configuration is allowed to expand and can therefore easier relax and possibly rearrange particles. If the new pressure is higher the configuration will increase its density, if possible.

If we look at the same move from the point of view of pressure P_1, the swap-move is in fact a large jump in phase space from a configuration C_1 and volume V_1 to a new configuration C_2 and volume V_2 and can be regarded as a combination of particle and volume moves. As far as the particle moves are concerned this is of no importance for the acceptance of this move, since both configurations are without any overlaps. The swapping move is therefore accepted by the same probability as for a normal volume move

$$P(C_1 \to C_2) = \min(1, \exp[-\beta P_1(V_2 - V_1)] \left(\frac{V_2}{V_1}\right)^N) \tag{4.9}$$

For pressure P_2 we have a similar acceptance,

$$P(C_2 \to C_1) = \min(1, \exp[-\beta P_2(V_1 - V_2)] \left(\frac{V_1}{V_2}\right)^N) \tag{4.10}$$

but as it is a combined move, the complete swap is accepted by the product of both acceptance probabilities which has the simple form

$$P(P_1 \leftrightarrow P_2) = \min(1, \exp[-\beta(P_1 - P_2)(V_2 - V_1)]) \tag{4.11}$$

These simulations require a parallel computer, but the communication between different systems is minimal. The only information which needs to be transferred is the information concerning pressure and volume to a master program, which will attempt the swapping moves, and return the outcome. The different systems can than continue the normal NPT-simulation but possibly for a different pressure. It is a simple matter of book keeping to extract the information at constant pressure.

4.4 Cubatic order

In order to make a distinction between different ordered phases we need to define order parameters. This can be done by using the orientations of the particles to measure the $\mathcal{D}^l_{m,n}$-functions. If we then take the appropriate combination we obtain a function with cubic symmetry

$$O = \tfrac{7}{12}\Delta^4_{0,0} + \tfrac{\sqrt{35}}{12}(\Delta^4_{4,0} + \Delta^4_{0,4}) + \tfrac{5}{12}\Delta^4_{4,4} \tag{4.12}$$

corresponding to the eigenfunction of the excluded volume of a symmetric cross (3.47). This order parameter however, measures the cubatic order in the reference frame, while the axes of a cubatic phase need not be along the axes of this frame.

Unlike the case of a nematic phase where a second rank nematic tensor can be used to calculate the nematic axis [36], for the cubatic phase such an analogous tensor is fourth rank. As a consequence the directions corresponding to the cubatic order cannot obtained in a simple way, but have to be evaluate numerically, by finding the frame in which the order parameter is maximal.

An alternative route is to use order parameters, which are invariant under rotations of the frame. They are formed by a combination of $\mathcal{D}^l_{m,n}$-functions

$$I_l = \left\langle \left(\sum_{m,n} \mathcal{D}^l_{m,n} \left(\mathcal{D}^l_{m,n}\right)^* \right)^{\frac{1}{2}} \right\rangle \tag{4.13}$$

and measure the total order related to the value of l. If there is nematic order present in the system this will in general be visible by a non-zero value for I_2, as it contains the function $\mathcal{D}^2_{0,0} = P_2(\cos\theta)$. But also I_4 will in general be non-zero in a nematic phase, because $\mathcal{D}^4_{0,0} = P_4(\cos\theta)$ will be non-zero. In order for cubatic order to be present, not only a non-zero value of I_4 is needed but also there should not be any nematic order, i.e. $I_2 = 0$.

The definition of the order parameters I_l however, is positive definite. As a consequence their values will, in a simulation, not be identical to zero but finite and of the order $1/\sqrt{N}$, where N is the number of particles used in the simulation.

The cubatic order parameter (4.12) can be used to define a two-particle cubatic correlation function $G_O(r)$. The reason is that for a correlation function the relative orientation between the particles is used. This function can be written as

$$g_O(r) =< \frac{5\sum_{i,j}(\vec{u}_i(0)\cdot\vec{u}_j(r))^4 - 9}{6} > \tag{4.14}$$

where $\vec{u_i}$ and $\vec{u_i'}$ are the directors of the rods of both particles.

4.5 High density phases

For high pressures normal systems will tend to crystallize in a neatly ordered phase, spheres for instance will crystallize to a face centered cubic crystal. This crystal phase will in general lead to higher densities than can be reached by a positional disordered phase. If particles are non-spherical this will have an influence on the crystalline behavior, and orientations have to be included. In the case of hard spherocylinders different crystalline structures can be observed. An good overview of this system as function of the aspect ratio has recently been published by Bolhuis and Frenkel [37], indicating three different crystal phases.

It is unknown what crystal phase, if any, will be the stable one for cross-like particles. The highest density for these systems with larger aspect ratio's will probably not be reached by a simple perfect positional and orientational ordered phase, because for such structures a maximum packing fraction can be derived.

Suppose that we have an ordered phase in which one of the three rods is along the z-axis. If we now consider the particles which have their center of mass in a slab with thickness D, the diameter of the particles, and try to arrange them in the highest possible density we need to order them as has been depicted in figure 4.5.

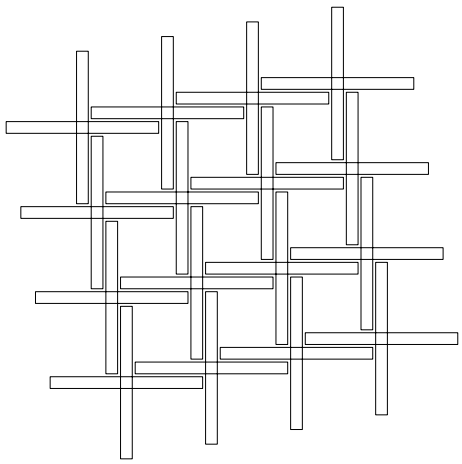

Figure 4.5: The most dense packing of cross-like particles, for which the centers of mass lie within the same plane, and one of the rods is oriented perpendicular to this plane.

The distance between the centers of mass is in first order $\frac{1}{2}L$. For a slab of thickness D and volume S this means that the number of particles within the slab is limited by $4S/(DL^2)$. The maximum packing fraction ϕ_{max} for this type of phase is therefore

$$\phi_{max} = \frac{N v_0}{V} \approx \frac{4}{DL^2} \frac{3}{4} \pi L D^2 = 3\pi (D/L) \tag{4.15}$$

where v_0 is the volume of a cross-like particle. It is therefore likely that the most stable high density phase is not a regular crystal or ordered phase. It might even be possible that no thermodynamically stable crystalline phase does exist.

In order to obtain high density starting configurations for large aspect ratios we form a crystal phase with perfect orientational order. It is formed by an FCC crystal arrangement. On the vertices and midpoints of a cubic unit cell the particles are oriented such that the rods are along the sides of the cube. This 'frame work' is than copied and translated to several points within the unit cell, ensuring that no overlaps occur.

4.6 Simulation results

We will only discuss here the results for a system for which the crosses have an aspect ratio of 25. The simulations are performed on a parallel machine using 15 simulation boxes at a time using 512 particles. Starting at low densities in an configuration made by random insertion we slowly increase the pressure. In this initial phase of the simulation the pressure move is very useful. Since all boxes start with more or less the same volumes the pressure move can be accepted easily.

In figure 4.6 the equation of state for this system is shown. For low pressures the system behaves like normal isotropic fluids. For higher densities the results from compression and the ones starting from an crystal are both indicated. For comparison the equation of state obtained via a virial series is shown using up to the fourth virial coefficient. But already at packing fractions of the order 0.05 they start to deviate significantly. Moreover the curve using the fourth virial coefficients becomes negative as a consequence of the negative fourth virial coefficient. For the fifth virial coefficient it would be even worse.

The equation of state is formed by 5 overlapping windows of the pressure, each window consisting of 15 pressures which are chosen equidistant. On the compression branch there is a good acceptance of the move, on average between 10 and 20 %, except near the borders of a patch where configurations at both end get isolated. This is due to configurations which are able to compress easier or more difficult.

In case of the crystal branch this is even worse. The large differences in densities are caused by different crystal structures, since the crystal we used are FCC lattices which are randomly copied in the unit cell.

The volume of the cross-like particles v_0 needs a small correction for the fact that the spherocylinders intersect. This correction with respect to the sum of the volumes of the rods is small but becomes relevant for short aspect ratio's

$$v_0 = \frac{3\pi}{4} D^2 L + \left(\frac{\pi}{2} - \sqrt{2} \right) D^3 \tag{4.16}$$

this formula only holds for $L \geq D$.

Two snapshots 4.7 give an impression of what these systems look like on both branches. They are about the same packing fraction of $\phi = 0.1$. One can easily imagine that these systems behave glassy.

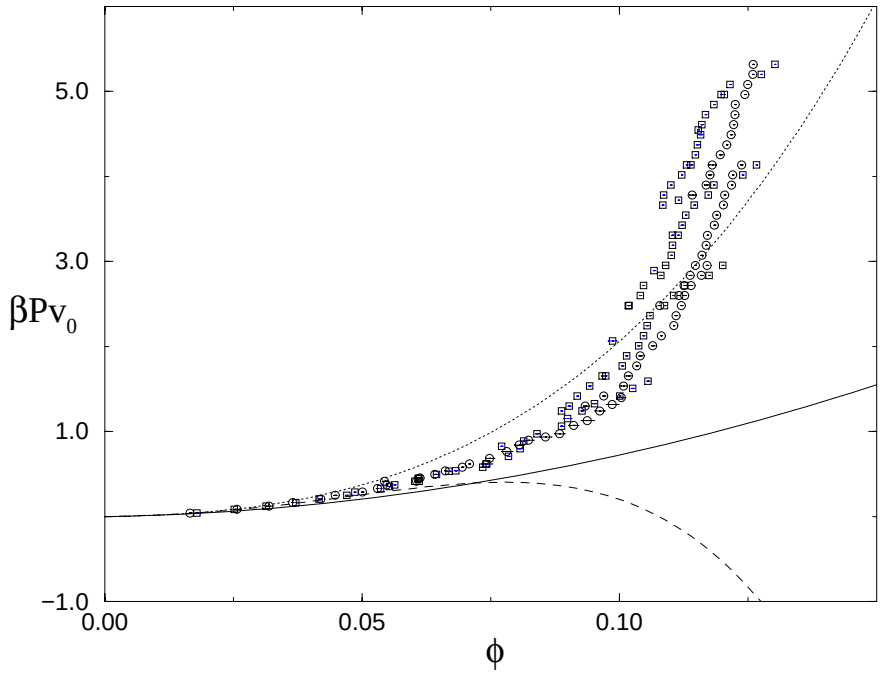

Figure 4.6: The equation of state for crosses with an aspect ratio $L/D = 25$ for compression (○) and crystal (□), the latter obtained via expansion or compression from a generated FCC-like crystal. The curves correspond to the virial equation of state using second (solid), third (dotted) and fourth (dashed) virial coefficient.

If we try to compress the system further, this becomes increasingly difficult, and it seems impossible to compress the system beyond a packing fraction of 0.15. In figure 4.8 the radial distribution $g(r)$ of the system for several densities is shown, indicating that there is no real structure present. It is obtained by following a configuration rather than sampling at a given pressure.

For completeness we plotted also the cubatic correlation function $g_O(r)$ defined by (4.14) in figure 4.9. It only shows a small peak for short length scales, long distance correlations are absent.

The order parameter used to detect cubatic order is denoted by I_4 and is a member of a class of invariants defined by (4.13). The results for this order parameter for compression are given in figure 4.10. Since by definition this order parameter is positive definite the resulting value will be non-zero. The obtained value is of the order $\sqrt{1/N}$ meaning that this value is not significantly different from the isotropic phase. The large error bars for the lower densities are due to large rotations of the particles causing the order parameter to fluctuate . For the higher densities there seems to be a significant cubatic order, this is however merely a consequence of the glass-like behavior which makes large fluctuations impossible, leading to deceptive order parameters.

From these figures we can only conclude that there is no detectable order in the system, obtained by compression and can be at most considered to be an disordered solid or glass. Even the new technique of parameter hopping is in this case not enough to overcome the problem of 'glass'-formation.

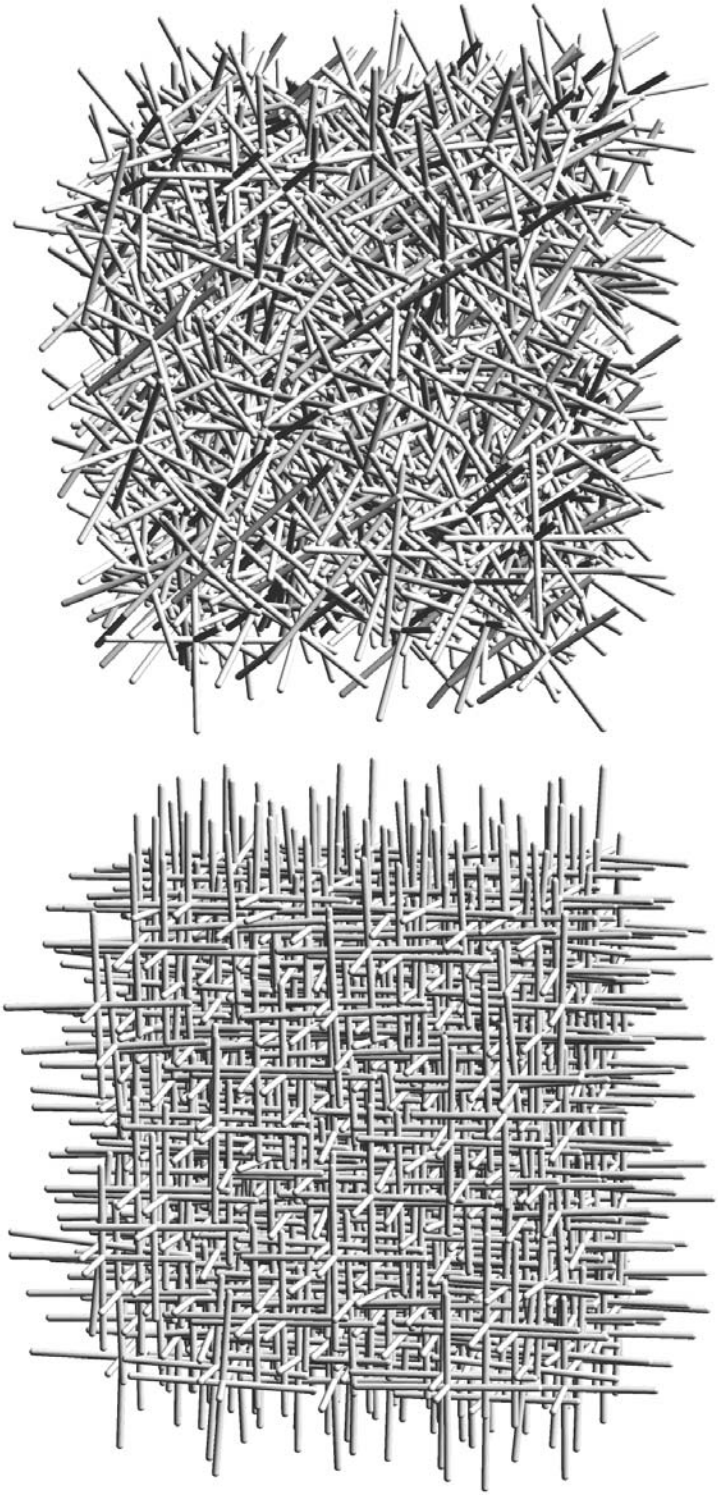

Figure 4.7: Two snap shots from the simulation, both at the same packing fraction $\phi = 0.10$. The upper one is obtained via compression from an low density isotropic configuration. The lower one is obtained starting from a FCC-like crystal.

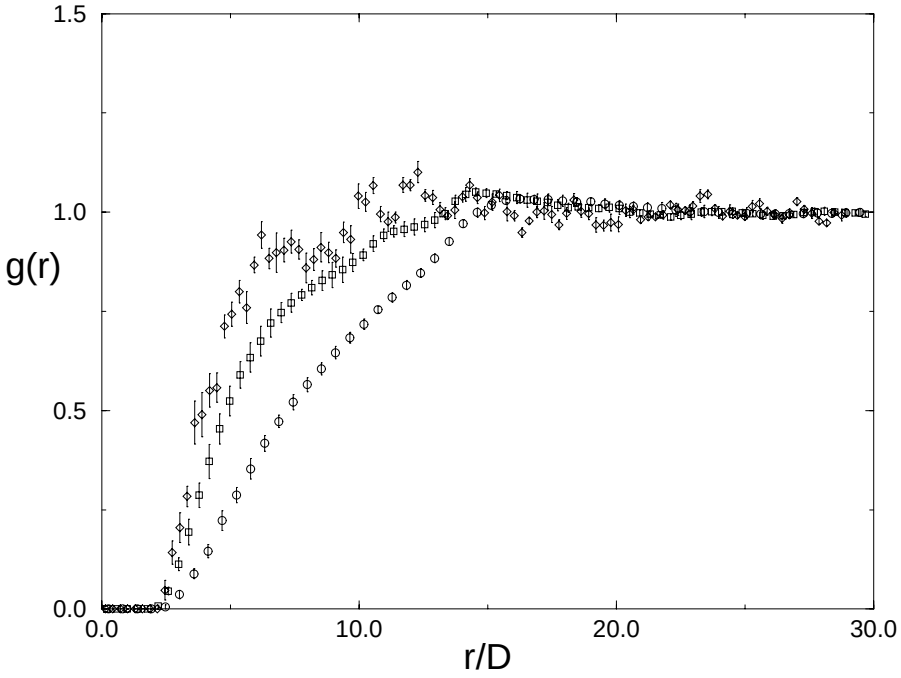

Figure 4.8: The radial distribution for packing fractions 0.017 (○), 0.055 (□) and 0.121 (◇) on the compression branch.

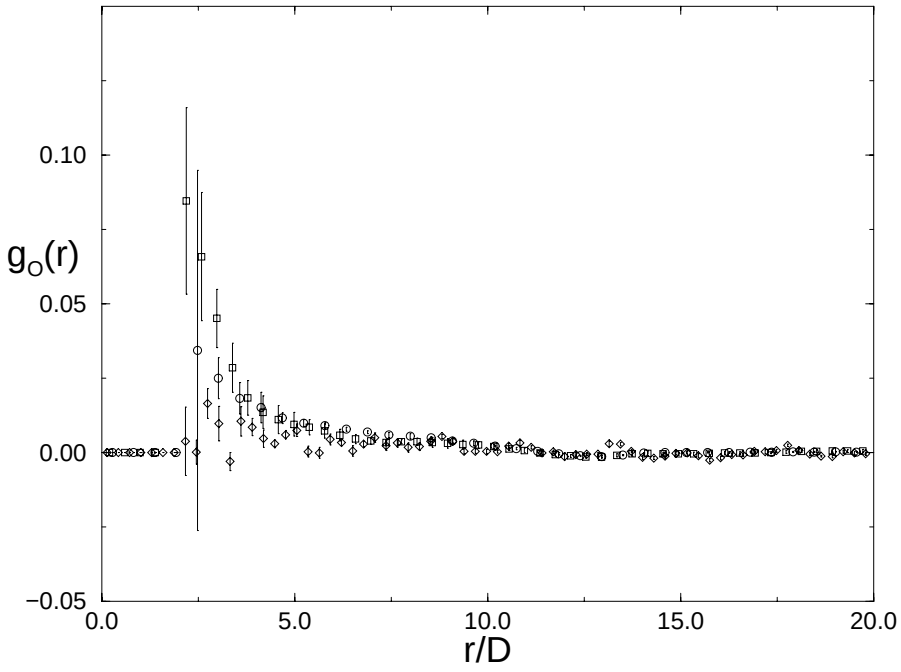

Figure 4.9: The cubatic correlation function for packing fractions 0.017 (○), 0.055 (□) and 0.121 (◇) on the compression branch.

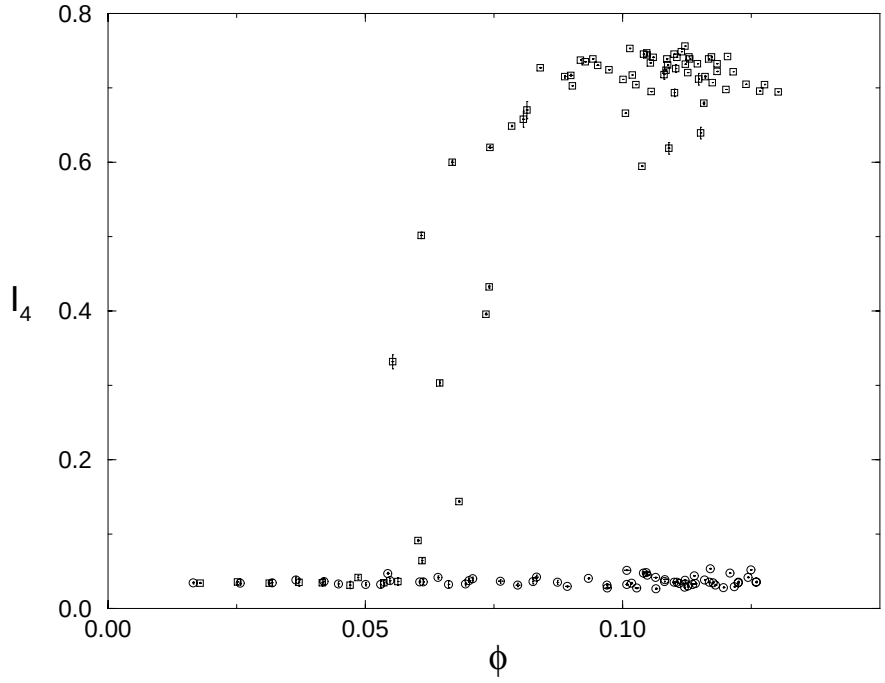

Figure 4.10: The cubatic order parameter on the compression (○) and crystal branch (□).

We can also start with a perfect aligned system, of the type described in the previous section. By rotating the particles the system can even increase its density. The radial distribution $g(r)$ and cubatic correlation function for one density are shown in figure 4.11. The peak near $r/D = 22$ is due to the

nearest neighbors in the FCC-lattice, and remains present in all crystals. The cubatic order parameter for this branch is plotted in figure 4.10, together with the values for the compression branch.

The intermediate values for this order parameter indicate that the crystal is melting, but has not reached equilibrium yet. Its exact position depends on the chosen form of crystal.

Since on average the crystal branch has a lower density than the compression branch the first is probably not thermodynamically stable but only mechanical. This probably means that simulations are just not long enough to reach relax to an disordered structure as obtained via compression.

The fact that no crystallization or orientational ordering is observed, does not necessarily mean that it is impossible. It only means that if it is possible even the technique of parameter hopping is not able to overcome the glass behavior of these systems and to find such phase.

Similar behavior is observed for other aspect ratio's. Larger aspect ratio's can be considered but will increase the simulation time needed rapidly, since the interaction extend over a larger range. Further more the box-lengths in the simulations for $L/D = 25$ are for the most dense system with $\phi \approx 0.13$ of the order 60. Larger aspect ratios have to be considered therefore more carefully, because if the simulation box becomes smaller that twice the maximal length scale of the simulated particles we cannot use anymore

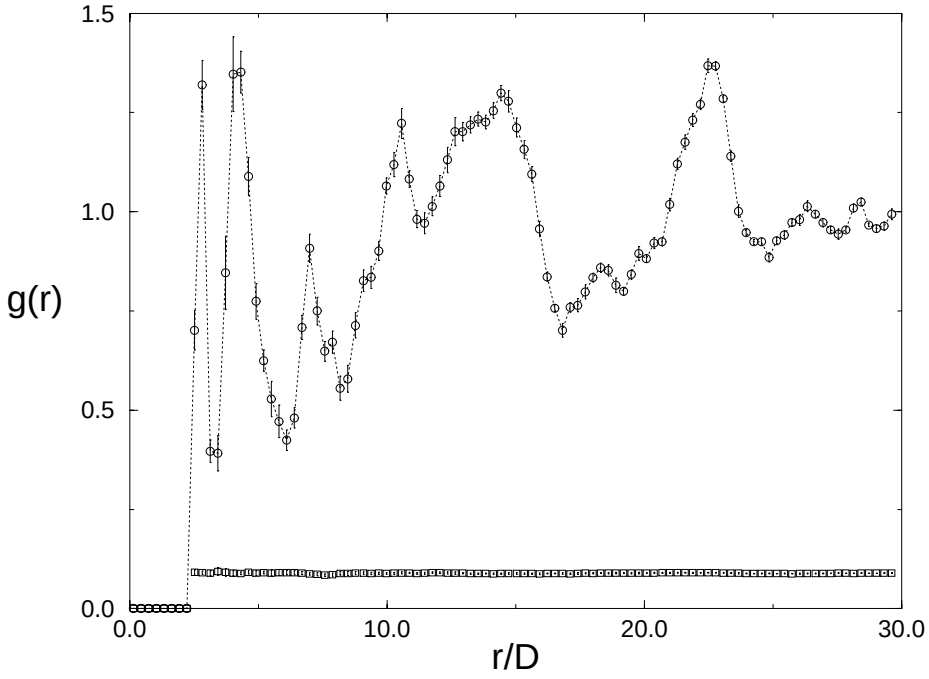

Figure 4.11: The radial distribution (○) and cubatic correlation function (□) for $\phi = 0.12$ on the 'crystal' branch.

the closest distance between two particles, to decide whether they interact we will need to take into account other periodic images as well [37]. The alternative is to use more particles, but both methods will require substantially more computing time.

4.7 Discussion

In this chapter we have investigated the phase behavior of cross-like particles with a finite size and checked the validity of approximations made in the previous chapter on infinitely large particles.

We first calculated the virial coefficients of these particles in the isotropic phase. In the Onsager theory of chapter 3 we assumed that the rods forming the crosses can be treated independent from each other and that the interaction between two particles can be approximated by the sum over all pair interactions. However in order to make this assumption valid within 1% we need to go to extremely large aspect ratio of 2000 or larger.

We also assumed that virial coefficients beyond the second can be neglected. We found that the reduced third, fourth and fifth virial coefficients all scale proportional to the inverse aspect ratio D/L. For the latter two a similar behavior is observed in the case of spherocylinders and ellipsoids by Frenkel. For the third virial coefficients these particles scale however proportional to $(D/L)\log(L/D)$.

As could be expected these systems are extremely hard to simulate. Due to their shape these particles will get entangled leading to a glass-like behavior. In order to attempt to overcome this problem we introduced the parameter hopping method. And although this method might be helpful in other glass-like systems, it is not able to

overcome the glass-formation in these systems as was illustrated by simulation of a system of cross-like particles with an aspect ratio $L/D = 25$.

The simulations on this system showed no indication of the presence of a cubatic phase. There exists a crystal phase which is at least mechanically stable, but no other types of ordering are observed.

In order to observe a cubatic phase one needs to go to even larger systems and aspect ratios. Confirmation of the existence of a cubatic phase in systems of cross-like particles will therefore not be an easy task.

It might be interesting to look at other cross-like particles, for instance the combination of only two rods with different lengths. According to the theory these particle change from rod-like to plate-like behavior. Since these particles are only 2-dimensional, they probably will be easier to simulate than the full crosses.

5 Monodisperse Cylinders

In this chapter we develop a simple theory for hard cylinders. For relatively small aspect ratios of order unity these particles have an interesting property which might lead to cubatic behavior.

5.1 Introduction

One of the most studied and by now well understood monodisperse hard particle systems is that consisting of the spherocylinders. Spherocylinders are cylindrical bodies with hemispherical caps on either end. The excluded volume of two spherocylinders is a smooth function of the mutual angle with a clear minimum and maximum at parallel, respectively perpendicular orientations. From the point of view of Monte Carlo simulations where a test is needed to tell whether particles overlap, these particles are relatively simple, because the test only involves the calculation of the distance between two line segments.

However, if we would take only the body without caps, i.e. the cylinder, then things are different. For large aspect ratios the low-density behavior of cylinders and spherocylinders is similar. But at higher density, the difference in the structure of the caps results in different phase behavior. For low aspect ratios there is of course an obvious distinction between the smooth, almost sphere-like, spherocylinder and the cylinder itself.

Also the excluded volume behaves differently, because, except for both extreme aspect ratios, the maximum in the excluded volume is not found anymore for perpendicular orientations. In spite of the fact that the overlap criterion was known in principle, no simulations of cylinders have been reported in the literature.

An incentive for studying hard cylinders is the observation of a cubatic phase in simulations of cut-spheres by Veerman and Frenkel [8]. They looked at spherical particles with diameter D of which the parts that lie more than $\frac{1}{2}L$ above or below the equatorial plane are removed. As a function of L/D this particle can change from a sphere to a disk-like object. Veerman and Frenkel used these particles as a model for plate-like particles , which unlike the infinitely thin disks of [38], have a non-zero excluded volume for parallel orientations. For the case of $L/D = 0.2$ they found that this system showed an isotropic-to-cubatic phase transition. Snapshots of the simulations seem to indicate that these disk-like particles tend to form stacks of typically 4 - 6 particles, yielding approximately a cylindrical shape. Particles within these stacks have the same orientation.

In this chapter we will try to explain the existence of this cubatic phase for the cut-spheres on the level of the stacks that are formed. We assume that the stacks are perfect monodisperse cylinders and explore their behavior. Since we are interested in the cubatic phase, which is positionally disordered, we focus on the orientationally ordered phases only and neglect the possibility of forming crystal or glass phases.

5.2 Excluded Volume

The excluded volume of two cylinders was already derived in Onsager's original paper of 1949 [4]. For two cylinders of lengths L_1 and L_2 and diameters D_1 and D_2 respectively it is given by

$$\begin{aligned}\mathcal{E}(\gamma) =& \frac{\pi}{4} D_1 D_2 (D_1 + D_2) \sin\gamma + L_1 L_2 (D_1 + D_2) \sin\gamma + \\ & L_1 \left(\frac{\pi}{4} D_1^2 + D_1 D_2 E(\sin\gamma) + \frac{\pi}{4} D_2^2 |\cos\gamma| \right) + \\ & L_2 \left(\frac{\pi}{4} D_2^2 + D_1 D_2 E(\sin\gamma) + \frac{\pi}{4} D_1^2 |\cos\gamma| \right)\end{aligned} \tag{5.1}$$

where γ is the angle between the two cylinders and $E(x)$ is the complete elliptical integral of the second kind [22]. In this chapter we focus on a system of monodisperse cylinders with length L and diameter D, which reduces this formula to

$$\begin{aligned}\mathcal{E}(\gamma) =& \frac{\pi}{2} D^3 \sin\gamma + 2L^2 D \sin\gamma + \\ & LD^2 \left(\frac{\pi}{2} + 2E(\sin\gamma) + \frac{\pi}{2} |\cos\gamma| \right)\end{aligned} \tag{5.2}$$

In both extreme limits where the aspect ratio L/D goes to infinity or to zero this excluded volume is dominated by a term proportional to $\sin(\gamma)$. Hence the excluded volume will be minimal for parallel orientations and maximal near perpendicular orientations.

In the first limit we have a system of long rod-like particles, which will have an isotropic-to-nematic phase transition as was explained by Onsager [4].

In the second limit we have a system of thin disks, which also will have an isotropic-to-nematic phase transition as was shown by Eppenga and Frenkel by means of Monte Carlo simulations [38].

There is however an intermediate region of aspect ratios where the behavior of the excluded volume is different. In figure 5.1 the excluded volume as function of the angle between the directors is plotted for several values of the aspect ratio L/D. For comparison they are normalized to unity for perpendicular orientations.

Surprisingly the maximum excluded volume of two cylinders is not found for perpendicular orientations, but at a smaller angle. In fact for all aspect ratios, with the exception only of $L/D = 0$ the excluded volume shows a local minimum for perpendicular orientations. This can be found directly from (5.2) by noticing that its derivative with respect to γ at $\gamma = \frac{1}{2}\pi$ is negative. The location of the maximum of the excluded volume shifts as function of the aspect ratio to smaller angles. The smallest angle at which the maximum occurs is reached for an aspect ratio of $\frac{1}{2}\sqrt{\pi} \approx 0.886$ where $\gamma \approx 1.339$ or 76.70 degrees. The maximum excluded volume is 1.055 times that of the perpendicular orientation. For larger aspect ratios the angle shifts back to $\frac{1}{2}\pi$.

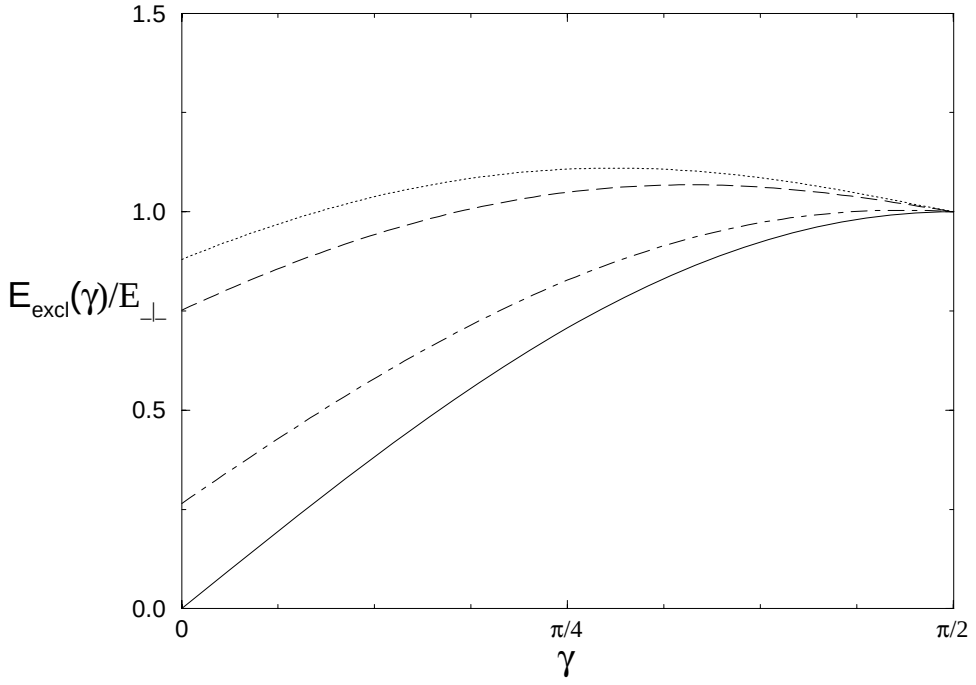

Figure 5.1: The excluded volume of two identical cylinders as function of the mutual angle γ for different aspect ratios $L/D = 0$ and ∞ (solid), 1 (dotted), 2 (dashed) and 10 (dotted-dashed). The excluded volume is normalized to unity for perpendicular orientations.

Another striking feature is that, for an aspect ratio of about one the excluded volumes for parallel and perpendicular orientations are almost the same. This can be seen more clearly from figure 5.2 where the ratio of the perpendicular and parallel excluded volume versus the aspect ratio L/D is plotted.

The minimum of this curve is found at $L/D = \frac{1}{2}\sqrt{\pi}$, at which point the excluded volume for the perpendicular orientation is 1.133 times that of the parallel orientation. Near this aspect ratio interesting things might occur, because the excluded volume of these particles and therefore their mutual interaction has two nearly equivalent preferred orientations. One of them is the parallel orientation, which as far as orientationally ordered phases are concerned, gives rise to a nematic phase while the other one is a perpendicular orientation. This might lead to a phase in which the particles have an orientational distribution which is not uni-axial, but might exhibit peaks for both parallel and perpendicular orientations. One could imagine that in such a phase some particles would be oriented along the z-axis of a suitable chosen system while other particles would lie in the xy-plane. Within that plane particles could be distributed isotropically, in which case it would still be a uniaxial phase or there could also be an additional preferred direction in the plane, in which case it would be a biaxial phase. If one continues the argument for perpendicular orientations of the particles, they could be oriented along two perpendicular directions, the x- and y-axis in which case there would be an overall cubic symmetry. Assuming that this could be realized in the absence of any translational order, this would then be a cubatic phase.

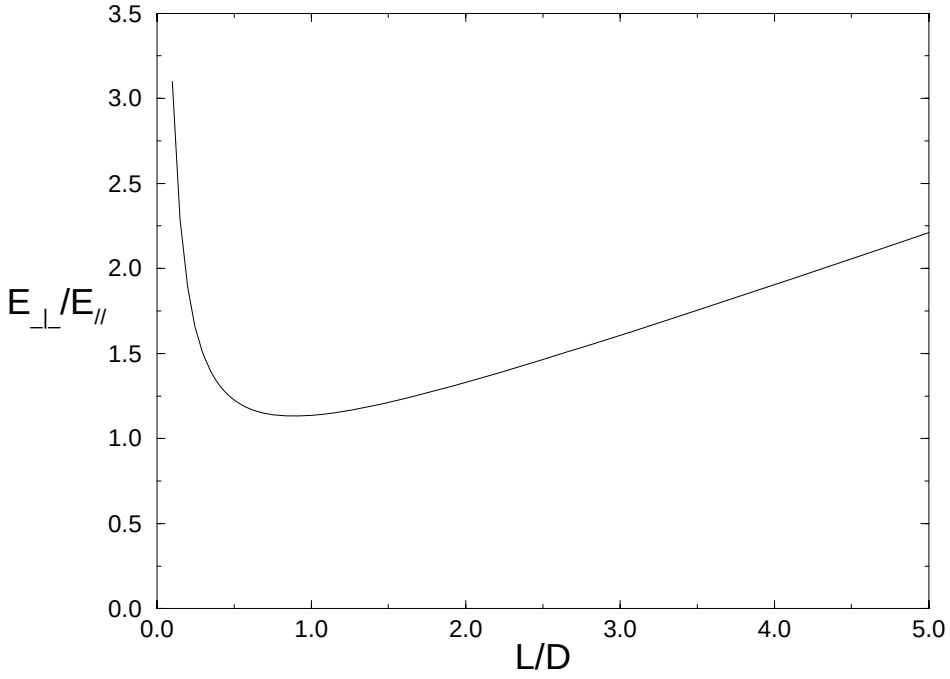

Figure 5.2: The ratio of perpendicular and parallel excluded volume of cylinders as function of the aspect ratio.

5.3 Series Expansion

In order to proceed with the excluded volume it is sometimes convenient to expand it in a series of suitable chosen functions instead of using its normal form. Since it only depends on the mutual angle between the two directors of the particles an expansion in Legendre polynomials will do.

For the three functions of (5.1) we have the following expansions

$$\begin{aligned} |\cos\gamma| &= \sum_{i=0}^{\infty} c_{2i} P_{2i}(\cos\gamma) \\ \sin\gamma &= \sum_{i=0}^{\infty} s_{2i} P_{2i}(\cos\gamma) \\ E(\sin\gamma) &= \sum_{i=0}^{\infty} e_{2i} P_{2i}(\cos\gamma) \end{aligned} \tag{5.3}$$

where P_{2i} are the Legendre polynomials. Since all functions are symmetric with respect to $\gamma = \frac{1}{2}\pi$ all coefficients with odd indices are zero. Using 7.231.1, 8.922.5 and 8.928.2 from Gradshteyn and Ryzhik [22], we find for the coefficients

$$
\begin{aligned}
c_{2i} &= -\frac{(4i+1)}{(2i-1)(2i+2)} P_{2i}(0) \\
s_{2i} &= -\frac{\pi}{2}\frac{(4i+1)}{(2i-1)(2i+2)} P_{2i}(0)^2 \\
e_{2i} &= -\frac{\pi^2}{4}\frac{(4i+1)}{(2i-1)(2i+2)} P_{2i}(0)^3
\end{aligned}
\tag{5.4}
$$

Using these results in (5.1) we can expand the excluded volume of two arbitrary cylinders in Legendre polynomials,

$$
\mathcal{E}(\gamma) = \sum_i E_{2i} P_{2i}(\cos\gamma) \tag{5.5}
$$

Furthermore the first expansion coefficient E_0 is the average excluded volume and hence twice the value of the second virial coefficient in the isotropic phase

$$
\begin{aligned}
B_2^{iso} =& \frac{\pi^2}{32} D_1 D_2 (D_1 + D_2) + \frac{\pi}{8} L_1 L_2 (D_1 + D_2) + \\
& \frac{\pi}{16} L_1 (2D_1^2 + D_2^2 + D_1 D_2 \pi) + \frac{\pi}{16} L_2 (2D_2^2 + D_1^2 + D_1 D_2 \pi)
\end{aligned}
\tag{5.6}
$$

5.4 Free Energy

The simplest way to treat this kind of hard particle systems at low densities, is to make use of the Helmholtz Free Energy functional. This free energy consists of a part related to the orientational entropy and a part which is related to the translational entropy. The latter can be expanded in terms with an increasing number of interacting particles. The simplest way to proceed would be by truncating this expansion after the two-body interaction. Such a second virial approach has been very successful in describing the isotropic-nematic phase transition in systems of elongated particles, in which case it can be shown explicitly that higher order contributions can be neglected. For smaller aspect ratios however this is no longer true and higher order terms become more important. Surprisingly this approach still describes the phase behavior itself in a qualitatively correct way, but it leads to an overestimate of the densities at which the transition occurs.

Since we are only interested in orientationally ordered phases, the position dependence can be integrated out and the Helmholtz Free Energy functional per particle can be written as

$$
\frac{\beta\mathcal{F}}{N}[\psi] = \log(n\mathcal{V}_T) - 1 + \int d\hat{\omega}\psi(\hat{\omega}) \log(4\pi\psi(\hat{\omega})) + \frac{\beta\mathcal{F}^{ex}}{N}[\psi] \tag{5.7}
$$

where ψ is the orientational distribution function of a single particle, which measures the fraction of particles with an orientation $\hat{\omega} = (\sin\theta\cos\varphi, \sin\theta\sin\varphi, \cos\theta)$, and is normalized to unity. Since these particles are uniaxial their orientation is defined completely by the two polar angles (θ, φ). n is the number density and $\mathcal{V}_T$ the thermal volume.

The first term on the right-hand side is the ideal gas contribution, the integral is the orientational entropy of the system and the last term is the excess free energy which takes care of the interaction between the particles.

The part of the free energy which is related to the orientational entropy will be denoted by σ

$$\sigma[\psi] = \int d\hat{\omega}\psi(\hat{\omega})\log(4\pi\psi(\hat{\omega})) \tag{5.8}$$

In case of an isotropic phase where $\psi = \frac{1}{4\pi}$ this term is identical zero. For all other normalized distribution functions this integral will be positive. Since the equilibrium phase corresponds to the minimal free energy, this term favors an isotropic phase.

The excess free energy is an infinite expansion in the density, involving all virial coefficients of the particles. For sufficiently low densities, the virial coefficients beyond the second can be neglected and this excess term is the integral of the excluded volume of two cylinders with orientations $\hat{\omega}$ and $\hat{\omega}'$ respectively and given distribution ψ

$$\frac{\beta\mathcal{F}^{ex}}{N}[\psi] = \tfrac{1}{2}n\int d\hat{\omega}d\hat{\omega}'\mathcal{E}(\hat{\omega},\hat{\omega}')\psi(\hat{\omega})\psi(\hat{\omega}') \tag{5.9}$$

In case of the isotropic phase, where $\psi = \frac{1}{4\pi}$ this leads to second virial approximation

$$\frac{\beta\mathcal{F}}{N}[\psi] = \log(n\mathcal{V}_T) - 1 + nB_2^{iso} \tag{5.10}$$

On increasing densities, higher order corrections have to be taken into account. One of the ways in which this can be done is by using Parsons approach [39] which was applied by Lee to a nematic liquid crystal [40]. The basis for this approach is the Carnahan-Starling equation of state of hard spheres, where the excess free energy is given by

$$\frac{\beta\mathcal{F}_{CS}^{ex}}{N} = \frac{\phi(4-3\phi)}{(1-\phi)^2} \tag{5.11}$$

where ϕ is the volume fraction of the particles. For the hard sphere system the expansion of this function reproduces the third virial coefficient exactly and agrees very well with the exact results, even up to packing fractions of 0.5. Lee generalized this excess free energy in order to apply it on elongated particles by multiplying it with the average excluded volume

$$\frac{\beta\mathcal{F}^{ex}}{N} = \frac{\phi(4-3\phi)}{(1-\phi)^2}\frac{<\psi|\mathcal{E}|\psi>}{8v_0} \tag{5.12}$$

which is normalized with v_0 the volume of the particles and where we have introduced the shorthand notation

$$<\psi|\mathcal{E}|\psi'> \equiv \int d\hat{\omega}d\hat{\omega}'\psi(\hat{\omega})\mathcal{E}(\hat{\omega},\hat{\omega}')\psi'(\hat{\omega}') \tag{5.13}$$

Note that in the case of hard spheres the factor (5.12) is unity and hence the Carnahan-Starling equation of state is recovered.

It is convenient to write one of the integrals in the form of a functional defined by

$$\mathcal{E}[\psi](\hat{\omega}) \equiv \int d\hat{\omega}' \mathcal{E}(\hat{\omega}, \hat{\omega}')\psi(\hat{\omega}') \tag{5.14}$$

Using the expansion of the excluded volume found in (5.5) this can be rewritten as an infinite summation over functionals of the Legendre polynomials

$$\mathcal{E}[\psi](\hat{\omega}) = \sum_{l=0}^{\infty} E_{2i} P_{2i}[\psi](\hat{\omega}) \tag{5.15}$$

These functionals possess a number of important and useful properties that we shall exploit. In the appendix we briefly discuss the most relevant properties of these functionals.

5.5 Bifurcation Analysis

A bifurcation analysis can be used to get a general impression of the In a stable phase, the orientation distribution function corresponds to a minimum in the free energy. This means that a small change in this function would give rise to an increase of the free energy. In other words, the derivative of (5.7) with respect to ψ should be zero while the second derivative should be positive. There is, however, an additional constraint on the system: the function ψ should remain normalized to unity. To take care of this we need to add an additional term to the free energy

$$-\mu \int d\hat{\omega}\psi(\hat{\omega}) \tag{5.16}$$

where μ is a Lagrange multiplier. The distribution function ψ is now implicitly defined as that function which leads to the lowest value of the free energy (5.7). This means that a small variation in the distribution function, under the condition that the normalization is conserved, will not change the value of the free energy. Taking the functional derivative of the free energy (5.7) with respect to the distribution function ψ leads to the stability or stationarity equation

$$\log(4\pi\psi(\hat{\omega})) + \frac{\phi(4-3\phi)}{4v_0(1-\phi)^2}\mathcal{E}[\psi](\hat{\omega}) = \mu \tag{5.17}$$

where the excluded volume is now written as a functional of ψ. The stability of the homogeneous, isotropic phase can be determined by expanding ψ and ϕ in the small parameter ε about the bifurcation density ϕ_0 and isotropic distribution function ψ_0

$$\begin{aligned} \psi &= \psi_0 + \varepsilon\psi_1 + \varepsilon^2\psi_2 + \cdots \\ \phi &= \phi_0 + \varepsilon\phi_1 + \varepsilon^2\phi_2 + \cdots \end{aligned} \tag{5.18}$$

Expanding the stationarity equation in ε leads to a coupled set of bifurcation equations. The lowest order has the simple form of an eigenvalue problem

$$\frac{\psi_1}{\psi_0} + \frac{\phi_0(4-3\phi_0)}{4v_0(1-\phi_0)^2}\mathcal{E}[\psi_1] = 0 \tag{5.19}$$

In order to solve this equation, all eigenvalues of the excluded volume functional need to be calculated. Since all functions can be expressed as a linear combination of modified spherical harmonics $C_{l,m}$, the most general Ansatz for the eigenfunction χ is

$$\chi = \sum_l \sum_{m=-l}^{l} c_{l,m} C_{l,m} \tag{5.20}$$

If this expression is inserted in the functional of the excluded volume (5.15) and its properties are used (see appendix), we obtain

$$\mathcal{E}[\chi] = \sum_{l',l,m} c_{l,m} E_{l'} C_{l',0}[C_{l,m}] = \sum_{l,m} \left(\frac{4\pi}{2l+1} E_l\right) c_{l,m} C_{l,m} \tag{5.21}$$

From equation (5.21) it is clear that the eigenvalues can be expressed in terms of the expansion coefficients of the excluded volume

$$\lambda_l = \frac{4\pi}{2l+1} E_l \tag{5.22}$$

Moreover the complete set of spherical harmonics is automatically divided into sub classes labeled by the index l, which all have the same eigenvalue λ_l. The spherical harmonics themselves are therefore a logical basis for the eigenfunctions of the excluded volume.

The first four eigenvalues are plotted in figure 5.3 as function of the aspect ratio L/D. Eigenvalues corresponding to higher values of l are not relevant as far as the bifurcation behavior is concerned.

To each eigenfunction corresponds a specific bifurcation density at which the isotropic phase becomes unstable with respect to a distortion with that symmetry. This density can be obtained by applying (5.19),

$$\frac{1}{\psi_0 \lambda_l} + \frac{\phi(4-3\phi)}{4v_0(1-\phi)^2} = 0 \tag{5.23}$$

The relevant bifurcation density ϕ_0 is the lowest density at which the isotropic phase becomes locally unstable with respect to some kind of ordering. And since the second fraction in (5.23) is positive, the eigenvalue has to be negative in order to lead to physical solutions. Moreover in order to make ϕ_0 as small as possible the eigenvalue also needs to be the largest in absolute value. For both small and large aspect ratios this is the eigenvalue with $l = 2$.

But from the figure we see that there is a region where the eigenvalue with $l = 4$ takes over. At the aspect ratios $L/D = 0.412892$ and $L/D = 1.902919$ the eigenvalues

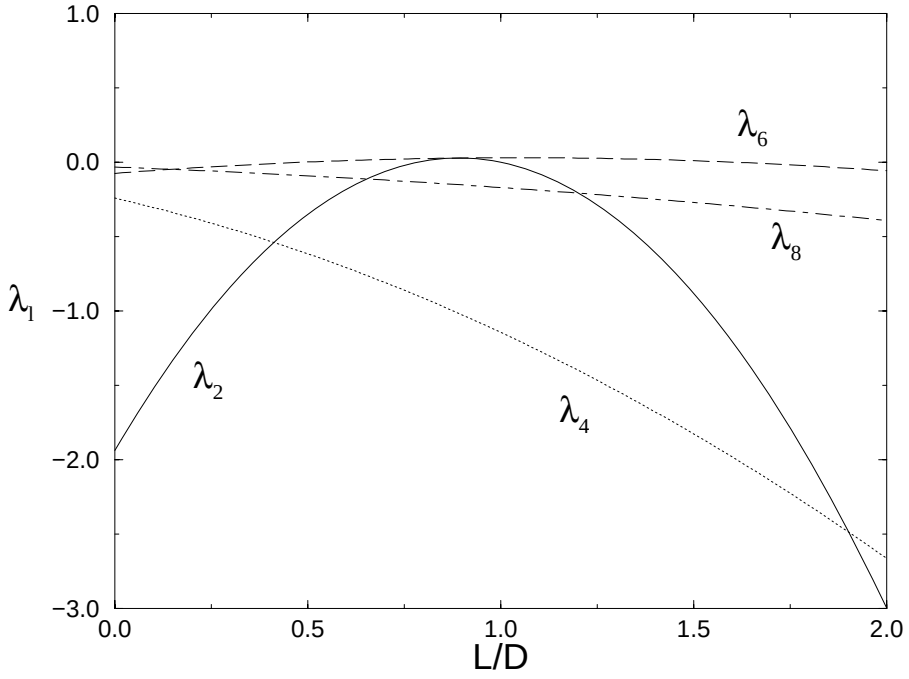

Figure 5.3: The first 4 eigenvalues of the excluded volume functional for cylinders as function of the aspect ratio.

of $l = 2$ and $l = 4$ have the same value. In between the eigenvalue of $l = 4$ is smaller and hence will lead to a lower bifurcation density. This means that there is a range of densities at which the isotropic phase becomes unstable with respect to fluctuations corresponding to those $l = 4$ eigenfunctions, while it is still stable with respect to $l = 2$ eigenfunctions.

The most important eigenvalues are therefore are those with index $l = 2$ and $l = 4$, and are given by respectively

$$\begin{aligned} \lambda_2 &= -\frac{\pi^2}{16} D(4L - \pi D)(L - D) \\ \lambda_4 &= -\frac{\pi^2}{1536} D(16L + 3\pi D)(3L + 4D) \end{aligned} \tag{5.24}$$

Although λ_4 remains negative for all aspect ratios, λ_2 does not. For aspect ratios between $L/D = \pi/4$ and $L/D = 1$, λ_2 becomes positive. Hence the corresponding bifurcation density becomes negative. This means that the isotropic phase is linearly stable with respect to $l = 2$ perturbations of the orientational distribution function.

The next step is to calculate the eigenfunctions corresponding to the eigenvalues λ_l in order to determine the symmetry of the new phase. Since all spherical harmonics with subscript l have the same eigenvalue, any linear combination

$$\psi_1 = \sum_{m=-l}^{l} c_{l,m} C_{l,m}(\theta, \phi) \tag{5.25}$$

where C_{lm} are the modified spherical harmonics, can be used. Since the first order bifurcation equation cannot give any additional information the second order bifurcation equation is needed.

$$\frac{\psi_2}{\psi_0} - \tfrac{1}{2}\left(\frac{\psi_1}{\psi_0}\right)^2 + \frac{\phi_0(4-3\phi_0)}{4v_0(1-\phi_0)^2}\mathcal{E}[\psi_2] + + \frac{\phi_1(2-\phi_0)}{2v_0(1-\phi_0)^3}\mathcal{E}[\psi_1] = cst \tag{5.26}$$

The function ψ_2 can be expanded in spherical harmonics with coefficients that remain to be determined. Furthermore, it can be assumed to be orthogonal to ψ_1. If that is not the case it is possible to redefine ε in order to achieve this. In fact, the same argument holds for all other ψ_n.

The left-hand side of (5.26) can be expressed as a sum which is linear in spherical harmonics, which means that it is really a set of coupled equations in c_m. Moreover since the equation includes the square of ψ_1 it is non-linear. There are l relevant equations related to the functions in ψ_1, the other equations will determine most of ψ_2. These equations only depend on the coefficients $c_{l,m}$ of ψ_1 and on ϕ_1.

In this case, since $l = 2$ or $l = 4$, these equations can be solved completely. The solutions of ψ_1 always consist of solution families, because any rotation of a solution will automatically also be a solution. For the case of $l = 2$ this solution is

$$\psi_1 = C_{2,0}(\theta,\varphi) = \tfrac{1}{2}(3\omega_z^2 - 1) \tag{5.27}$$

where we expressed the function in terms of the unit vector $\hat{\omega}$ described by the polar coordinates θ and φ.

This solution has a single rotational axis of symmetry, and hence is related to the nematic phase. For the case of $l = 4$ there are two families of solutions. The first one is given by the fourth Legendre polynomial, the second solution is a more interesting solution and is a combination of spherical harmonics

$$\psi_1 = \begin{cases} C_{4,0} & = \tfrac{1}{8}(35\omega_z^4 - 30\omega_z^2 + 3) \\ \sqrt{\frac{7}{12}}C_{4,0} + \sqrt{\frac{5}{24}}(C_{4,4} + C_{4,-4}) & = \sqrt{\frac{7}{48}}(5(\omega_x^4 + \omega_y^4 + \omega_z^4) - 3) \end{cases} \tag{5.28}$$

The first solution is again uniaxial symmetric and corresponds to a nematic phase. However, the second solution has a different character. It is only invariant under discrete rotations over $\pi/2$ about any of the x-, y- or z-axis. It has a cubic symmetry and hence is related to the cubatic phase.

Hence, for small and large aspect ratios the isotropic phase first becomes unstable with respect to fluctuations with a symmetry of the second Legendre polynomial. This suggests that there is a transition form the isotropic phase to a phase with nematic phase symmetry.

For the intermediate range of aspect ratios there are two different eigenfunctions. The first will also lead to a isotropic-to-nematic phase transition. The second however suggests the possibility of an isotropic-to-cubatic phase transition.

In figure 5.4 the bifurcation packing fractions are drawn as function of the aspect ratio, where Parsons approach is used. Note that without the Parsons approach the packing fractions might be larger than unity, which is unphysical.

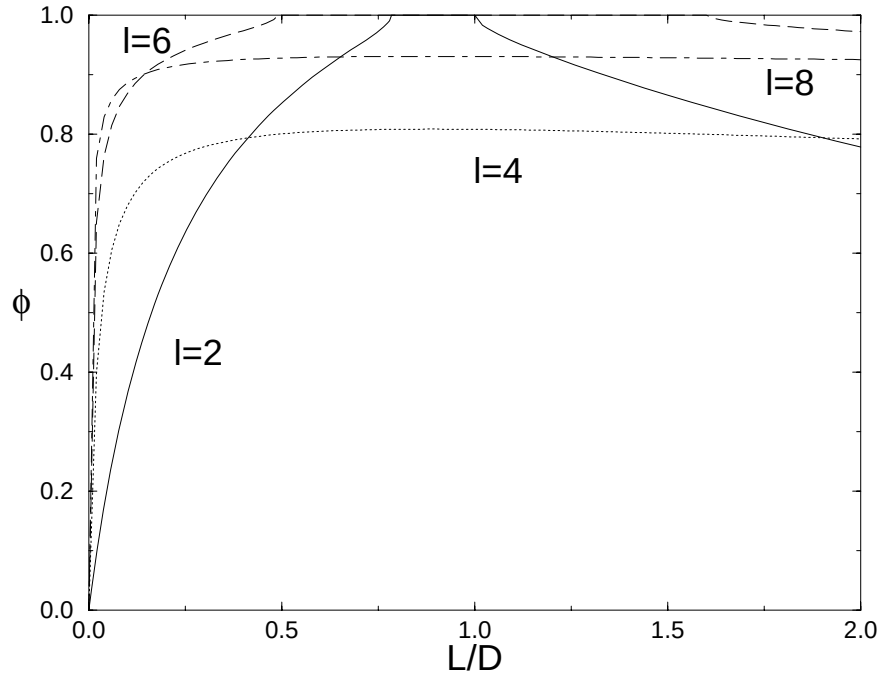

Figure 5.4: The packing fractions at which the isotropic phase becomes unstable, with respect to spherical harmonics of order l, as function of the aspect ratio using Parsons approach.

The bifurcation analysis is, of course, only indicative of the phase behavior. First of all, it is not at all sure that the cubatic phase is more stable than the nematic phase. But more important is the fact that the possibility of crystallization is left out and this might well happen before any orientational ordering takes place, especially given the relatively high packing fractions involved

5.6 Trial Functions

As the bifurcation analysis is not able to predict whether a phase transition, that is possible in principle, occurs in practice, we need a more direct approach. Since the real equilibrium particle distribution function is that function which minimizes the free energy we can try to minimize the free energy (5.7) directly.

Determination of the real distribution function is however a time consuming and messy task that would involve an iterative scheme for which at all steps a 4 dimensional integral should be evaluated. If the distribution function would be smooth and not to strongly peaked this would in principle still be possible. However, as it will turn out this is not case. So instead of doing the complete calculation we will make use of trial functions.

Trial functions are a way to reduce the infinite dimensional function space for the distribution function to a finite dimensional, preferably single parameter space. In this

parameter space we then minimize the free energy. The resulting free energy will be higher than the true free energy. But by choosing proper trial functions, we obtain a good estimate. There is a considerable degree of freedom in the choice of the trial functions. Since we know from the bifurcation analysis what different phases might appear, we can make a reasonable assumption about the symmetry of the trial functions. For instance we could choose the trial function to be a linear combination of a finite number of modified spherical harmonics

$$\psi = \sum_{l \leq 4} \sum_{m=-l}^{l} c_{l,m} C_{l,m}(\theta, \varphi) \tag{5.29}$$

This would mean that we have to minimize the free energy in the space of coefficients $c_{l,m}$. There are two problems with this expansion. First of all, it is not suited to describe strongly peaked distribution functions. Secondly, since the distribution function should be positive for all orientations there is a restriction on the set of coefficients. From the point of view of numerics this is not convenient.

It is therefore better to use a trial function which already takes care of both of these problems. An attractive option is to use is the trial function, that was used by Onsager in his study of the isotropic-to-nematic phase transition for rod-like particles [4]

$$\psi_z = \frac{\alpha}{4\pi \sinh \alpha} \cosh(\alpha \omega_z) \tag{5.30}$$

This function is already normalized to unity and only depends on a single parameter α and the relative angle of the orientation $\hat{\omega}$ and the direction of the nematic direction, which is chosen along the z-axis. For small values of $\alpha = 0$ the function is constant. For large α becomes strongly peaked around $|\omega_z| = 1$.

Another advantage of this trial function is that it allows us to evaluate one of the integrals in the free energy function analytically. This is the integral related to the orientational entropy σ (5.8)

$$\sigma[\psi_z] = \log(\frac{\alpha}{\tanh \alpha}) - 1 + \frac{\arctan \sinh \alpha}{\sinh \alpha} \tag{5.31}$$

Although the distribution function does not depend on φ, the excluded volume interaction does. This means that the complete evaluation of the second integral of the free energy would lead to a four dimensional integral. Only one integral over φ can be done directly. But there still remains a three dimensional integral. It is however possible to reduce the integral into 1-dimensional integrals only. This can be seen as follows.

We already found a way to expand the excluded volume in terms of Legendre polynomials (5.5) depending on the relative orientation of the particles. For a single Legendre polynomial there exists a closure relation (A.24) which allows us to separate the orientational dependencies.

$$P_l(\cos \gamma) = \sum_{m=-l}^{l} C^*_{l,m}(\hat{\omega}) C_{l,m}(\hat{\omega}') \tag{5.32}$$

Hence the average excluded volume can be written as

$$\begin{aligned} < \psi_z|\mathcal{E}|\psi_z > &= \sum_l E_l < \psi_z|P_l|\psi_z > \\ &= \sum_{l,m} E_l < \psi_z|C^*_{l,m}(\hat{\omega})C_{l,m}(\hat{\omega}')|\psi_z > \\ &= \sum_{l,m} E_l < C^*_{l,m} >_{\psi_z} < C_{l,m} >_{\psi_z} \\ &= \sum_l E_l < P_l >^2_{\psi_z} \end{aligned} \tag{5.33}$$

where we in the last line made use of the fact that the distribution function ψ does not depend on φ and hence the integrals for $m \neq 0$ would be zero. We also introduced a shorthand notation for the average over the distribution function

$$< f >_\psi = \int d\hat{\omega}\psi(\hat{\omega})f(\hat{\omega}) \tag{5.34}$$

The 1-dimensional integrals which we are left can now also be evaluated analytically.

$$\begin{aligned} < P_2 >_{\psi_z} &= 1 - \frac{3}{\alpha \tanh \alpha} + \frac{3}{\alpha^2} \\ < P_4 >_{\psi_z} &= 1 - \frac{10}{\alpha \tanh \alpha} - \frac{105}{\alpha^3 \tanh \alpha} + \frac{45}{\alpha^2} + \frac{105}{\alpha^4} \end{aligned} \tag{5.35}$$

Effectively we replaced the 3-dimensional integral by an infinite sum, of known functions.

We are, however, not only interested in the nematic phase but also in the cubatic phase. So we also need a trial function with the cubatic symmetry. Guided by the results for the nematic phase we can try to do something similar. Hence as a trial function we take a linear combinations of Onsager trial functions along the x-, y- and z-axes.

$$\psi_O = \tfrac{1}{3}(\psi_x + \psi_y + \psi_z) = \frac{\alpha}{12\pi \sinh \alpha} \left(\cosh(\alpha\omega_x) + \cosh(\alpha\omega_y) + \cosh(\alpha\omega_z)\right) \tag{5.36}$$

The subscript O of the distribution refers to common symbol for the cubic symmetry group [23]. This distribution is also normalized to unity and reduces for $\alpha = 0$ to the isotropic distribution function. Unfortunately the integral (5.8) can no longer not be evaluated analytically. However for small values of α it can be expanded in α and for large values of α its behavior is very similar to (5.31)

$$\begin{aligned} \sigma[\psi_O] &= \int \tfrac{1}{3}(\psi_x + \psi_y + \psi_z) \log(4\pi \tfrac{1}{3}(\psi_x + \psi_y + \psi_z)) \\ &= \int \psi_z(\log(4\pi(\psi_x + \psi_y + \psi_z)) - \log 3 \\ &\approx \sigma[\psi_z] - \log 3 \end{aligned} \tag{5.37}$$

where the distribution function is separated in the parts along the different axes. The first step is a consequence of the symmetry. The second step is true only for large values of α when the main contribution, to the integral is coming from ψ_z. But since it is a 1-dimensional integral, it can also easily be evaluated numerically.

For the average excluded volume we can perform for this cubatic trial function a similar trick as we did for the nematic case. For symmetry reasons, we can split the average excluded volume into two parts

$$< \psi_O|\mathcal{E}|\psi_O >= \tfrac{1}{3} < \psi_z|\mathcal{E}|\psi_z > + \tfrac{2}{3} < \psi_x|\mathcal{E}|\psi_z > \tag{5.38}$$

The first part is identical to that of the nematic case. For the second part we have to take the average over two distribution functions along different axes. For ψ_x we have the following identity

$$\psi_x(\hat{\omega}) = \psi_z(R^{-1}\hat{\omega}) \tag{5.39}$$

where R is a rotation about the y-axis over $\frac{1}{2}\pi$, which gives for the second term in the average excluded volume

$$\begin{aligned} < \psi_x|\mathcal{E}|\psi_z > &= \sum_{l,m} E_l < \psi_z(R^{-1}\hat{\omega})|C_{l,m}(R(R^{-1}\hat{\omega}))C_{l,m}(\hat{\omega}')|\psi_z(\hat{\omega}') > \\ &= \sum_{l,m,p} E_l < \psi_z(R^{-1}\hat{\omega})|\mathcal{D}^l_{m,p}(R)C_{l,p}(R^{-1}\hat{\omega}))C_{l,m}(\hat{\omega}')|\psi_z(\hat{\omega}') > \\ &= \sum_{l,m,p} E_l < C_{l,p} >_{\psi_z} < C_{l,m} >_{\psi_z} \mathcal{D}^l_{m,p}(R) \\ &= \sum_{l} E_l < P_l >^2 P_l(0) \end{aligned} \tag{5.40}$$

where we used that the Euler angles for the rotation R are $(0, \frac{1}{2}\pi, 0)$ and the relation (A.5). So for the average excluded volume with our cubatic trial function we obtain

$$< \mathcal{E} >_{\psi_O} = \sum_l E_l \tfrac{1}{3}(1 + 2P_l(0)) < P_l >_{\psi_z} \tag{5.41}$$

With the two trial functions and the expressions we obtained for the free energy we are now able to calculate the phase coexistence between both phases and the isotropic phase in order to determine whether an isotropic-to-cubatic phase transition is possible. For a given aspect ratio and density we need to minimize the free energy with respect to the parameter α. Using the free energy as function of the density we now can calculate the pressure and chemical potential per particle from

$$\beta P = n^2 \frac{d\beta F/N}{dn} \tag{5.42}$$

$$\frac{G}{N} = \frac{F}{N} + \frac{P}{n} \tag{5.43}$$

In figure 5.5 we have plotted the packing fraction of the isotropic phase at coexistence with the nematic phase as function of the aspect ratio. We truncated the expansion of the excluded volume interaction after respectively the fourth, eighth and sixteenth term. The difference between the latter two is small enough to assume that, we have essentially converged to the untruncated solution.

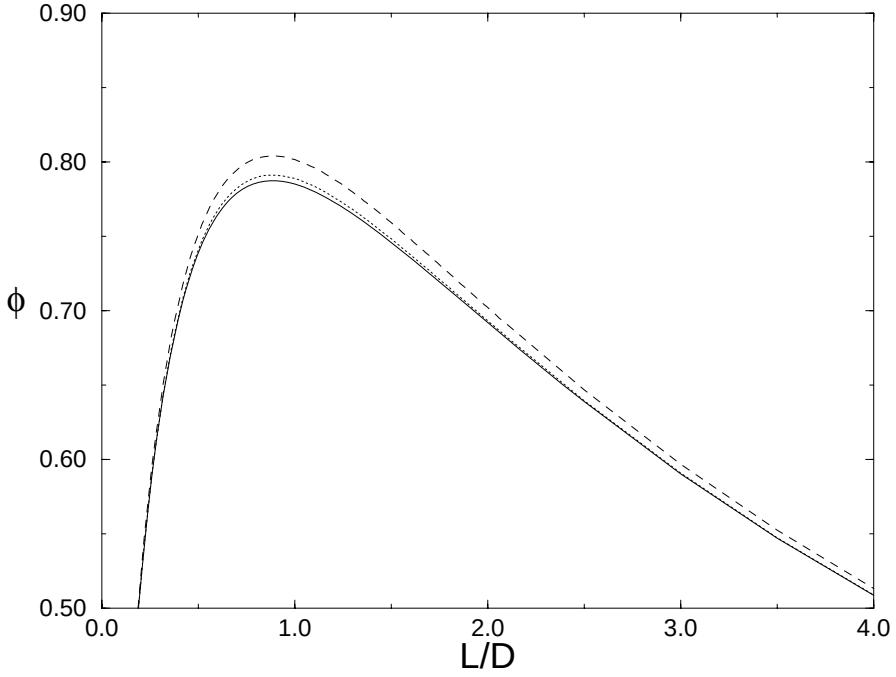

Figure 5.5: The packing fraction of the isotropic phase at coexistence with the nematic phase as function of the aspect ratio. The different curves correspond to taking up to the fourth (dashed), eighth (dotted) and sixteenth (solid) order Legendre polynomial in the excluded volume.

The same thing is observed for the cubatic phase, for which the successive approximations lie even closer together.

The final results of this calculation, based upon an expansion up to order $l = 16$, are plotted in figure 5.6.

The isotropic-to-nematic transition precedes the isotropic-to-cubatic transition for all aspect ratios, even in the range of L/D where the isotropic phase was stable with respect to the second Legendre polynomial for all densities. This seems a contradiction but the reason lies somewhat deeper in the bifurcation analysis. This analysis deals only with a linear stability but more importantly the bifurcation density corresponding to $l = 4$ leads to two possible symmetries one of which has the nematic, and the other the cubatic symmetry. Apparently the first is preferred.

In figure 5.7 the values of the parameter α in the trial functions (5.30) and (5.36) in the nematic and cubatic phase, are plotted as function of the aspect ratio. The points correspond to densities at which the ordered phase coexists with the isotropic phase. For aspect ratios of order unity α shows a strong peak for the nematic phase. Its value

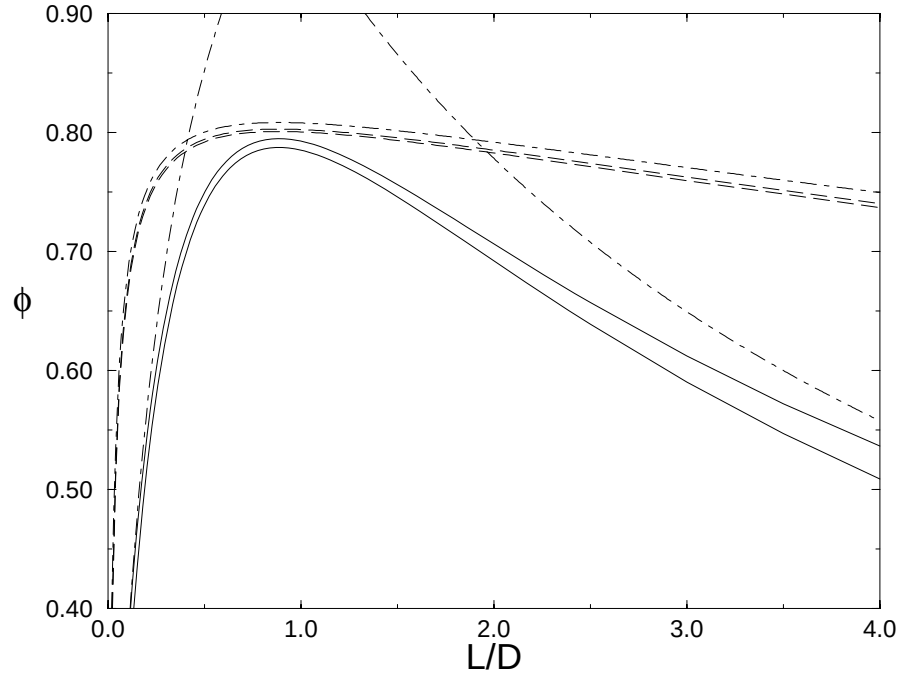

Figure 5.6: The phase diagram of short cylinders as function of the aspect ratio. The isotropic-nematic transition (solid lines) occurs before the isotropic-cubatic transition (dashed lines). The dotted dashed lines are the bifurcation results

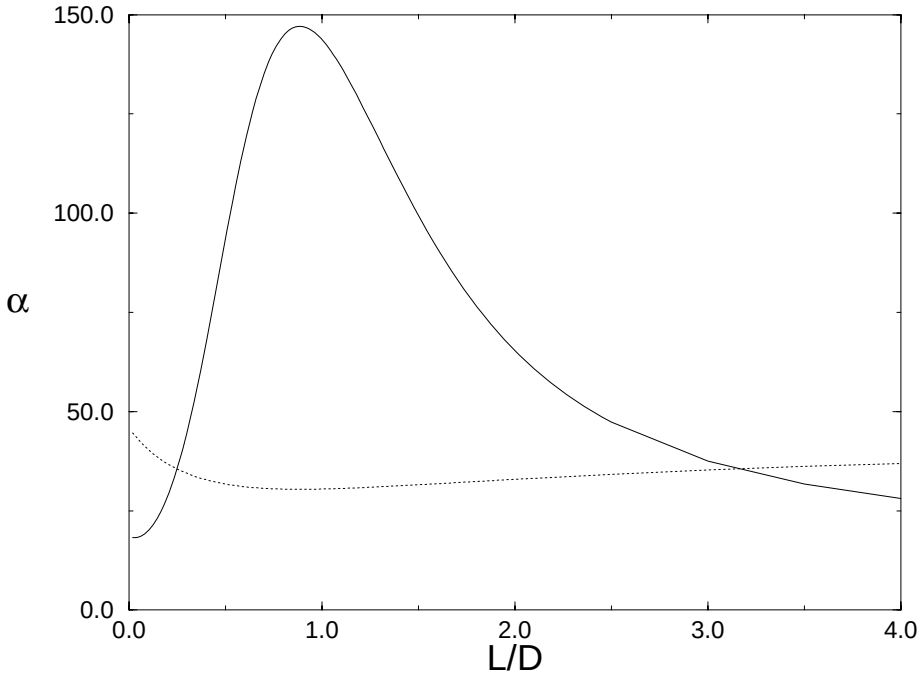

Figure 5.7: The α parameters corresponding to the nematic (solid) and cubatic (dotted) phase at coexistence with the isotropic phase.

of about 150 corresponds to a value of 0.98 for the nematic order parameter. For this strength 99% of the distribution function is contained in a cone with a maximum angle of 14 degrees.

The peaks in the orientational distribution of the cubatic phase are much weaker and α reaches a minimum for aspect ratios of order unity. The loss in orientational entropy, caused by ordering, with respect to the isotropic phase, will be therefore larger in the case of the nematic phase. This is in favor of the cubatic phase, but this effect is not enough to compensate for the contribution to the free energy due to the excluded volume.

Moreover, even at higher densities we do not observe coexistence between the nematic and cubatic phase.

5.7 Discussion

In this chapter we developed a simple theory for the phase behavior of cylinders. We mainly focused on particles with an aspect ratio of order unity. These specific particles have two preferred directions with respect to each other. Both for parallel and perpendicular orientations the excluded volume has a (relative) minimum would make it possible for these particles to form a cubatic phase.

To investigate these systems we developed a simple theory, in which we only looked at orientations and assumed that there is no positional order. Since the cylinders have a small aspect ratio, we had to take more-particle effects into account. We did this, by using the Parsons approach.

This gave us an expression for the free energy which we investigated in two ways. First we used a bifurcation analysis and determined the stability of the isotropic phase. This analysis showed that for aspect ratios between 0.4 and 1.9 the isotropic phase becomes first unstable with respect to two different symmetries, one nematic the other cubatic, which allows for the possibility of an isotropic-cubatic phase transition.

The second (variational) method we used was to minimize the Helmholtz free energy using an Onsager style trial functions, that have nematic symmetry, and a similar trial function with the cubatic symmetry. These calculations showed that the nematic phase precedes the cubatic phase for all aspect ratios, and coexistence between the nematic and cubatic phase could not be found.

Hence, according to this theory, the cubatic phase cannot be found in a system of monodisperse cylinders. In order to explain the existence of the cubatic phase in a system of cut-spheres we need to go beyond the simple idea of uniform cylindrical stacks.

As a final remark, we mention that we made two important assumptions. The first was that we neglected the possibility of crystallization and the second that we used Parsons approach. It is not obvious that this approach describes correlations in an effective way. In fact there are reasons to doubt it. The packing fractions we obtained for the isotropic-to-nematic transition at aspect ratios of order unity are about 0.8. In the case of hard spheres the same approximation already breaks down at packing fractions of about 0.5 where crystallization occurs. The high values we obtain therefore make it likely that we are close to, or even beyond, the point of crystallization and an orientationally ordered liquid might not be stable at all. Moreover for the ordered phases

we used the same scaling relation of the virial coefficient as for the isotropic phase and this is in general not true.

Although our theory does not yield an isotropic-to-cubatic phase transition, it does not rule out the possibility altogether. The trial functions of section 5.6 show that in the interesting range of aspect ratios the isotropic-to-cubatic transition takes place at a density which is less than 2% higher than the isotropic-to-nematic transition. And since we made several approximations only a small correction might be enough to turn the balance in favor of the cubatic phase.

6 Assembly and Polydispersity of Cylinders

In this chapter we extend our model for monodisperse cylinders to include aggregation, in order to explain stack formation observed in the cut-sphere system, the driving force behind the cubatic phase. We also allow for polydispersity, which tends to destabilize crystalline behavior.

6.1 Introduction

In the previous chapter we saw that cylinders with an aspect ratio of order unity are close to forming a stable cubatic phase. An original approach was to model the cubatic phase as observed in the systems of cut-spheres in terms of the formation of perfect cylindrical stacks. In reality however these stacks are neither perfect cylinders nor do they all have the same shape. As a consequence there is an amount of free energy related to the internal configuration of the stacks that was completely ignored.

Furthermore we obtained extremely high packing fractions at which the isotropic-to-nematic phase transition occurs, and it is likely that crystallization, which possibly already occurs at lower densities, will play an important role.

In order to investigate both these possibilities we extend the theory developed in the previous chapter in two ways. First, we replace the description of perfect cylinders by clusters of disk-like objects which have an effective cylindrical shape. The number of units in a given cluster however may vary.

The second way in which we will extend our theory is by including polydispersity in the lengths but not of the diameters of the cylinders. As it will turn out, this polydispersity will not only make perpendicular orientations of particles more favorable, but also has the tendency to destabilize any crystalline structure.

6.2 Aggregation

Consider a system consisting of N identical particles or monomers, in our case are thin cylinders, all having their own position and orientation. Assume that these monomers can aggregate into small clusters of dimers, trimers, etc., or in general s-mers. These clusters will have their own average position and orientation, and of course internal configuration. These two descriptions, one on the level of the monomers the other on the level of s-mers, are closely related.

At fixed volume V, and temperature T, the partition function of the system of N monomers is given by (2.6)

$$Z(N,V,T) = \frac{1}{N!\mathcal{V}^N}\int dq^N \exp(-\beta U_N(q^N)) \tag{6.1}$$

where $\mathcal{V}$ is the thermal volume of a monomer. It depends on the mass and moments of inertia of the single particle. The generalized coordinates of a single particle ($\vec{r}$ and orientation $\hat{\omega}$) are denoted by q.

In order to describe the same system at the different level of clusters we need to describe the clusters in more detail. We will assume that clusters with the same number of particles are all similar and therefore behave as if they are a new type of indistinguishable particles.

The first observation is that clusters will contain different numbers of particles. We assume that the system contains N_1 single particles, N_2 dimers, N_3 trimers and in general N_s s-mers. The total number of particles however is constrained to N, leading to the following normalization

$$N = \sum_s sN_s \tag{6.2}$$

Furthermore we need to correct for the fact that the monomers are indistinguishable. The total number of monomers N is distributed over the different sized clusters, which can be done

$$\frac{N!}{\prod_s (s!)^{N_s} N_s!} \tag{6.3}$$

different ways. The factor $N_s!$ has to be included, because clusters of the same size s are assumed to be indistinguishable.

If we assume for the moment that clusters of size s behave as a new type of particle which can be described by the positions and orientations q_s of all the monomers by which it is formed, the total interaction energy can be separated into intra-cluster interactions U_s and inter-cluster interaction $W_{s,s'}$. We can thus write the total energy of the system as

$$U_N(q^N) = \sum_s \sum_{i_s} U_s((q_s)_{i_s}) + \tfrac{1}{2}\sum_{s,s'}\sum_{i_s,i_{s'}} W_{s,s'}((q_s)_{i_s},(q_{s'})_{i_{s'}}) \tag{6.4}$$

where we used the index i_s to sum over clusters of size s. Our goal is not to describe the interactions between the clusters in great detail.

Rather, we use an effective interaction that depends only on the average position of the center of mass and the average orientation only, denoted by R_s. This allows us to rewrite the partition function as

$$Z(N,V,T) = \prod_s \frac{1}{N_s!}\left(\frac{\int dq_s \exp(-\beta U_s(q_s))}{s!\mathcal{V}^s \int dR_s}\right)^{N_s} \int d\{R\} \exp(-\beta W(\{R\})) \tag{6.5}$$

where we abbreviated the set of all average positions and orientations of the clusters by $\{R\}$. If we would have described the system as a mixture of different components labeled by s, we would have obtained the following expression for the partition function

$$Z(N,V,T) = \prod_s \frac{1}{N_s! \mathcal{V}_s^{N_s}} \int d\{R\} \exp(-\beta W(\{R\})) \tag{6.6}$$

where N_s is the number of particles of type s and $\mathcal{V}_s$ is the thermal volume of a particle of this species. Comparing equations (6.5) and (6.6) we can interpret $\mathcal{V}_s$ as the thermal volume of a cluster of s monomers defined by

$$\mathcal{V}_s = \frac{\mathcal{V}^s V_0}{Q_s} \tag{6.7}$$

where $V_0 = \int dR_s$ and Q_s denotes the internal configuration integral of an s-mer

$$Q_s = \frac{1}{s!} \int dq_s \exp(-\beta U_s(q_s)) \tag{6.8}$$

The value of V_0 depends on the way the clusters are described. If we describe clusters as spherical objects they do not have an orientation and $V_0 = V$ the proper volume. If the clusters are not spherical, their orientation should be taken into account for the description. In that case $V_0 = 8\pi^2 V$. Extension to more complicated descriptions of the clusters is straightforward.

The thermal volume of a cluster or assembly of particles is not only dependent on the total mass and moment of inertia but also on the interaction of the monomers within the cluster. For instance the monomers could be chemically bonded to each other.

By taking the logarithm of the partition function we obtain the Helmholtz free energy of the system. For the isotropic mixture we can write this in the form of a virial series, similar to the one for a one-component system (2.14)

$$\frac{\beta F}{V} = \sum_s \rho_s \left(\log(\rho_s \mathcal{V}_s) - 1\right) + \sum_{s,t} \rho_s \rho_t B_2^{s,t} + \cdots \tag{6.9}$$

where we introduced the number density $\rho_s = N_s/V$ of an s-mer. The two particle interaction of an s- and t-mer is put in the effective second virial coefficient $B_2^{s,t}$. The first term can be written in a more convenient form by using (6.7)

$$\sum_s \rho_s \log(\rho_s \mathcal{V}_s) = \log(\rho\mathcal{V}) \sum_s s\rho_s + \sum_s \rho_s \log(\frac{\rho_s}{\rho}) - \sum_s \rho_s \log(\frac{\rho^{s-1} Q_s}{V_0}) \tag{6.10}$$

where we used the monomer density $\rho = N/V$. The first summation is identical to ρ due to the normalization. If we now introduce $x_s = \rho_s/\rho$, i.e. the fraction of s-mers present in the system, the Helmholtz free energy per monomer can be written as

$$\frac{\beta F}{N} = \log(\rho\mathcal{V}) + \sum_s x_s(\log(x_s) - 1) - \sum_s x_s \log(\frac{\rho^{s-1}Q_s}{V_0}) + \rho \sum_{s,t} x_s x_t B_2^{s,t} \tag{6.11}$$

where we truncated the expansion after the second virial coefficient. Note that the dependence on mass and moments of inertia is completely contained in the first term, and only adds a constant to the free energy. As a consequence these values will never have any influence on any of the observables. The second summation is the entropy of mixing of multi component system. The third terms contains the interaction of the particles within a single cluster and the last term is the interaction between different clusters.

All clusters are in dynamical equilibrium. These clusters themselves are continuously breaking into smaller clusters and re-assembling into larger clusters, hence this process can described as a set of chemical reactions. For a stable phase these reactions ought to be in chemical equilibrium , leading to relations in the chemical potentials of all cluster sizes. The equilibrium condition of s-mers and t-mers, is given by

$$t\mu_s = s\mu_t \tag{6.12}$$

where μ_s and μ_t are the chemical potentials of an s- respectively t-mer, which are related to the total Helmholtz free energy by

$$\mu_s = \left(\frac{\partial F}{\partial N_s}\right)_{V,T,N_i} \tag{6.13}$$

where the volume V, temperature T and the number of clusters of all different clusters N_i remain fixed. Is is easily verified that this set of equations is solved by

$$\mu_s = s\mu \tag{6.14}$$

where μ is the chemical potential of a single monomer.

The goal is to obtain the distribution function $\{x_s\}$ which determines the distribution of monomers over the clusters. Instead of equating the chemical potentials of each cluster size by (6.14) we can also minimize the total free energy per particle (6.9) with respect to x_s. By adding the term

$$-\mu \sum_s s x_s \tag{6.15}$$

we ensure the equality of chemical pressures, where μ is now a Lagrange multiplier.

6.3 The Isotropic Phase

We will apply the theory described in the previous section to a system of cylinders. We take monomers with an aspect ratio of L/D as our monomers, typically of the order 0.2. For that aspect ratio the cut-spheres form stacks and are able to form a cubatic phase. In order to compare with results obtained in the previous chapter we use

again Parsons approach to effectively take into account higher virial coefficients. This modifies the Helmholtz free energy to

$$\begin{aligned}\frac{\beta F}{N} =& \log(\rho\mathcal{V}) + \sum_s x_s(\log(x_s) - 1) - \sum_s x_s \log(\frac{\rho^{s-1}Q_s}{V_0}) + \\ & \frac{\rho(4-\phi)}{4(1-\phi)^2}\sum_{s,t} x_s x_t B_2^{s,t} - \mu\sum_s s x_s\end{aligned} \tag{6.16}$$

where ϕ is the packing fraction. In order to find the distribution of different clusters we have to minimize this free energy expression with respect to the fractions x_s, leading to a set of coupled equations. Furthermore we have to make some assumptions about the shape of clusters and hence the internal configurational integral Q_s.

We assume that particles in a s-mer are stacked close together with almost identical orientations. Effectively an s-mer can then be described by a cylinder with length L_s and constant diameter D along the length. Along the direction of the stacks successive particles are able to move freely such that the maximum distance will not exceed a certain limit $2l_s$. The average distance is l_s, leading to an average length of the stack $L_s = sL + (s-1)l_s$. The distance of the center of mass of a sub-unit with respect to the axis of the stack will be limited by a small value d and the orientation is confined to the solid angle Ω, which for all s-mers for simplicity we take to be the same. Since s particles can be stacked in $s!$ different ways the internal configuration integral is given by

$$Q_s = V_0(\frac{\pi}{2}d^2 l_s \Omega)^{s-1} \tag{6.17}$$

where $V_0 = 4\pi V($ 4π instead of $8\pi^2$ because we assume the s-mers to be effectively uniaxial).

Since s-mers have an effective volume that is larger than the sum of the volumes of its sub-units, also the packing fraction has to modified to an effective packing fraction

$$\phi = \rho\sum_s x_s \frac{\pi}{4}D^2 L_s \tag{6.18}$$

In addition to minimizing the free energy with respect to x_s we now also need to minimize with respect to l_s. But before we proceed, we first introduce some shorthand notations. We define

$$\eta = \rho\frac{4-3\phi}{4(1-\phi)^2} \tag{6.19}$$

which is the factor from the Parsons approach. The second virial coefficient for two arbitrary cylinders (5.6) can be written as

$$B_2^{s,t} = b_0 + b_1(L_s + L_t) + b_2 L_s L_t \tag{6.20}$$

where we used the fact that they have equal diameters D. The coefficients b_0, b_1 and b_2 are defined by

$$\begin{aligned} b_0 &= \frac{\pi^2}{16} D^3 \\ b_1 &= \frac{\pi}{16}(3+\pi) D^2 \\ b_2 &= \frac{\pi}{4} D \end{aligned} \tag{6.21}$$

If we now take the derivative of the free energy with respect to l_s, we obtain the first set of coupled equations,

$$\frac{1}{l_s} = 2\eta \sum_t x_t (b_1 + b_2 L_t) + \eta' \sum_{s,t} x_s x_t B_2^{s,t} \tag{6.22}$$

where $\eta' = (\partial\eta/\partial l_s)/(x_s(s-1))$ is independent of s or x_s and the common factor $(s-1)x_s$ is divided out. We see that our choice leads to an equation which determines the length scale l_s and that it is independent of s. Therefore $l_s = l$ is the same for all s-mers. This can be understood by realizing that the derivative of the free energy with respect to the length scale l_s is comparable to the internal pressure of an s-mer.

The second set of equations for which we take the derivative of the Helmholtz free energy with respect to x_s is given by

$$\log x_s - \log\left(\frac{\rho^{s-1} Q_s}{V_0}\right) + 2\eta \sum_t x_t B_2^{s,t} + \eta' L_s \sum_{s,t} x_s x_t B_2^{s,t} - s\mu = 0 \tag{6.23}$$

Using this equation with $s = 1$ enables us to eliminate μ. Combining the result with equation (6.22) we can express x_s in terms of x_1 and l

$$x_s = x_1^s \frac{\rho^{s-1} Q_s}{V_0} \left\{ \exp\left[2\eta \sum_t x_t (b_0 + b_1 L_t) - 1 \right] \right\}^{s-1} \tag{6.24}$$

The final expression for the distribution x_s in the isotropic phase therefore has a simple form $x_s = x_1 q^{s-1}$. Using the normalization $\sum_s s x_s = 1$ we find that x_s can be expressed in terms of x_1 only

$$x_s = x_1 (1 - \sqrt{x_1})^{s-1} \tag{6.25}$$

The combination of this equation with (6.24) and (6.22) can now be solved self consistently to yield the numerical value of x_1 and the length scale l for any given value of the number density, monomer shape and Q_s. The main result is that in the isotropic phase the distribution of s-mers shows a simple behavior.

Note that all summations over s and/or t can now be expressed in terms of x_1 only by

$$\begin{aligned}\Sigma^0 &\equiv \sum_s x_s = \sqrt{x_1} \\ \Sigma^1 &\equiv \sum_s x_s s = 1 \\ \Sigma^2 &\equiv \sum_s x_s s^2 = \frac{2}{\sqrt{x_1}} - 1\end{aligned} \tag{6.26}$$

The last summation will be needed in the next section.

6.4 Bifurcation Analysis

What we have done so far is to determine the distribution x_s for the isotropic phase. What we are after however is the possible existence of ordered phases. To this end we perform a bifurcation analysis. First we need to extend the Helmholtz free energy to include orientational ordering in the system

$$\begin{aligned}\frac{\beta\mathcal{F}}{N}[\{\psi^{(s)}\}] = &\log(\rho\mathcal{V}) + \sum_s x_s(\log(x_s) - 1) - \sum_s x_s \log(\frac{\rho^{s-1}Q_s}{V_0}) + \\ &\sum_s x_s \sigma[\psi^{(s)}] + \tfrac{1}{2}\eta \sum_{s,t} x_s x_t < \psi^{(s)}|\mathcal{E}^{s,t}|\psi^{(t)} > - \\ &\mu \sum_s s x_s - \sum_s \mu_s \int d\hat{\omega}\psi^{(s)}(\hat{\omega})\end{aligned} \tag{6.27}$$

This is a functional of the set of $\psi^{(s)}$ describing the ordering of the s-mers. The degree of order, though coupled , for the aggregates of different size will in general not be equal. We abbreviated the orientational entropy by σ, defined similar to (5.8). The second virial coefficient is replaced by half the average excluded volume $\mathcal{E}^{s,t}$ of an s- and t-mer. The last summation involves a set of Lagrange multipliers μ_s, that are fixed by the normalization of the different ODF's $\psi^{(s)}$. Note that for the isotropic phase, where $\psi^{(s)} = \frac{1}{4\pi}$, equation (6.27) reduces to (6.16).

We now need to minimize the free energy not only with respect to x_s and l_s but also with respect to the ODF's ψ_s. Taking the derivative with respect to l_s a set of equations similar to (6.22) is obtained, leading to the same conclusion that $l_s = l$ for all s-mers.

Taking the functional derivatives with respect to the ODF's $\psi^{(s)}$ gives a set of coupled stationarity equations

$$\log(4\pi\psi^{(s)}) + \eta \sum_t x_t \mathcal{E}^{s,t}[\psi^{(t)}] = \mu_s \tag{6.28}$$

In the same fashion as we did for $B_2^{s,t}$ in (6.20) we can split the functional of the excluded volume $\mathcal{E}^{s,t}$ in

$$\mathcal{E}^{s,t} = \mathcal{E}^{(0)} + (s+t)\mathcal{E}^{(1)} + st\mathcal{E}^{(2)} \tag{6.29}$$

where the exact form of the functionals $\mathcal{E}^{(0)}$, $\mathcal{E}^{(1)}$ and $\mathcal{E}^{(2)}$ can be obtained by substitution of $L_s = s(L+l) - s$ into $\mathcal{E}^{s,t}$. This reveals an interesting property of the stationarity equations, because they can now be written as

$$\psi^{(s)} \propto \exp\left[\eta\left(\mathcal{E}^{(0)}[X] + \mathcal{E}^{(1)}[Y]\right)\right] \times \exp\left[s\eta\left(\mathcal{E}^{(1)}[X] + \mathcal{E}^{(2)}[Y]\right)\right] \tag{6.30}$$

where we introduced the abbreviations X and Y for the summations

$$\begin{aligned} X &= \sum_t x_t \psi^{(t)} \\ Y &= \sum_t x_t t \psi^{(t)} \end{aligned} \tag{6.31}$$

The relevance of this observation is that the equilibrium ODF's of all cluster sizes are proportional to those of the monomers and dimers. Instead of solving a complete set of coupled stationarity equations only two of these equations in X and Y remain, but even now it is still difficult task to solve these equations. Similar behavior is observed for polydispersity in long rods [41].

We will only determine the influence of cluster formation on the bifurcation density. The problem is now more complicated than in the monodisperse case because one should take into account that the isotropic phase is described not only by the packing fraction ϕ, but also by the internal length l and distribution x_s.

If the expansions are performed as in to the monodisperse case, and the first order bifurcations equations are written in the terms X_1 and Y_1 we find

$$\begin{aligned} X_1 + \eta_0\psi_0\left(\Sigma^0\mathcal{E}^{(0)}[X_1] + \Sigma^1\mathcal{E}^{(1)}[X_1] + \Sigma^0\mathcal{E}^{(1)}[X_1] + \Sigma^1\mathcal{E}^{(2)}[X_1]\right) &= 0 \\ Y_1 + \eta_0\psi_0\left(\Sigma^1\mathcal{E}^{(0)}[X_1] + \Sigma^2\mathcal{E}^{(1)}[X_1] + \Sigma^1\mathcal{E}^{(1)}[X_1] + \Sigma^2\mathcal{E}^{(2)}[X_1]\right) &= 0 \end{aligned} \tag{6.32}$$

where η_0 refers to (6.19) at the bifurcation density. For this set of first bifurcation equations the values which can be used for l and x_s are still the equilibrium values of the isotropic phase.

We can now substitute a combination of modified spherical harmonics for both X_1 and Y_1, similar to (5.20). Since we can expand all the functionals in term of Legendre polynomials and then make use of the property (A.26) this reduces to solving, for each combination of l and m, a set of two linear equations. Since we want to determine the stability of the isotropic phase we need a non-trivial solution, which requires that the determinant of (6.32) is zero. This gives us a polynomial equation in l, ϕ and x_1. If we combine this equation with (6.22) and (6.24) these equations can be solved simultaneously.

Figure 6.1 shows the solutions of (6.22), (6.24) and (6.32) for several ratios of l and L. The value Q_s (6.17), which can be interpreted as a type of binding energy, is along these lines not constant.

The bifurcation densities are plotted versus the aspect ratio. Instead of the solutions of x_1 we indicated the average length of the cluster which, due to (6.26), is just $1/\sqrt{x_1}$. For the limit of the distance $l \to 0$ the results of the monodisperse case are recovered.

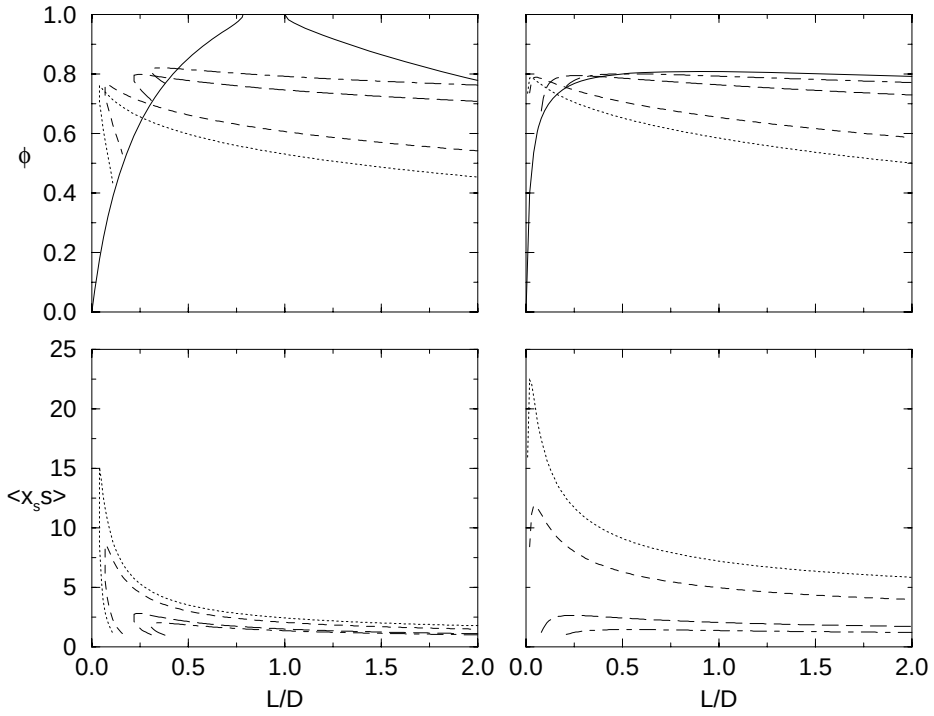

Figure 6.1: Bifurcation solutions for $l/L = 0.1$ (dotted), $l/L = 0.05$ (dashed), $l/L = 0.01$ (long dashed) and $l/L = 0.005$ (dotted dashed). The solid curves are the results of the monodisperse bifurcation equations. The left figures represent the $l = 2$ or Nematic bifurcation, the right two figures the $l = 4$ bifurcation.

If we look at the $l = 2$ bifurcation we observe that the stability region which was obtained in the monodisperse case, has disappeared. This can be easily understood, because if the ratio l/L is finite this will lead to a few clusters, that for the particles in this range of aspect ratios, are more rod-like and will drive the instability. Since in the monodisperse case the bifurcation density for increasing aspect ratios shifts to lower values, the same can be observed in this case. This in contrast with thin cylinders, where clusters of several particles enter the region of aspect ratios of order unity. We recall that for these aspect ratios in the monodisperse case the stability is enhanced, leading to a higher bifurcation density, as is also observed in the present case.

Different solutions for the same aspect ratio are made possible by different values of the parameters in (6.17). The solutions for lower densities correspond to larger values of Q_s, hence weaker coupling. The $l = 4$ bifurcation of the isotropic shows similar results. If the distance l between the monomers increases however the order in which both instabilities occur changes.

These results are interesting, not in the sense that they explain the formation of a cubatic phase as observed in the cut-sphere system, but because they show that it is possible, by forming stacks of particles, to decrease the value of bifurcation density and to destabilize the isotropic phase. On the other hand, it is also possible, for thin discs, to increase the stability of the isotropic phase. As a consequence the difference in the bifurcation densities for $l = 2$ and $l = 4$ becomes smaller, which is in favor of the cubatic phase.

6.5 Polydispersity

In this section we will investigate the behavior of a polydisperse mixture of cylinders. As we have seen in the previous chapter the isotropic-to-nematic phase transition occurred at a packing fraction of about 0.8. Although the exact number might be different because of the highly approximative way in which the effect of higher virial coefficients is modeled, there is a clear trend of increasing transition densities in the interesting region of aspect ratios of order unity. As a consequence crystallization should be considered as well. It is known that the presence of polydispersity in a system can destroy the crystalline order. Therefore by allowing for polydispersity the problem of crystallization might be overcome.

We will assume that we have a system of cylinders with identical diameters, and polydispersity is only present as a distribution over different lengths of the cylinders. Apart from the fact that polydispersity will destabilize crystalline phases, there is another reason why it is interesting. The excluded volume (5.2) for monodisperse cylinders is minimal for parallel orientations, but it has a local minimum for perpendicular orientations. According to the results obtained by the trial function in the case of monodisperse cylinders (section 5.6), the cubatic phase is nowhere stable In order words the difference in excluded volume between the parallel and perpendicular orientation of particles is still large enough to stabilize the nematic phase. If we allow for polydispersity however and look again at the ratio of the perpendicular and parallel excluded volume for two cylinders with different lengths, we find

$$\frac{\mathcal{E}_\perp}{\mathcal{E}_\parallel} = \frac{(2D + (L_1 + L_2))(\pi D + 2(L_1 + L_2))}{4\pi D(L_1 + L_2)} - \frac{(L_1 - L_2)^2}{4\pi D(L_1 + L_2)} \tag{6.33}$$

This indicates that for given value of $L_1 + L_2$ the ratio becomes smaller if $L_1 \neq L_2$. In figure 6.2 the ratio of the perpendicular and parallel excluded volume is plotted. The minimum found in the monodisperse case is in fact a saddle point in the polydisperse case. This suggests that the cubatic phase might be stabilized by polydispersity.

We assumed a given distribution function $f(l)$ for the polydispersity which denotes the fraction of total particles with a given length $(1+l)L$, where L is a reference length, and diameter D. This function is normalized to unity and has an average value of zero

$$\begin{aligned} \int dl\, f(l) &= 1 \\ \int dl\, f(l) l &= 0 \end{aligned} \tag{6.34}$$

The second constraint leads to an average length of L for the particles. And since the particles have fixed lengths the packing fraction of the system is therefore $(\pi/4)\rho D^2 L$. We also wish to consider order in the system. For this purpose we label the ODF's of a given length by ψ_l. The Helmholtz free energy of this system is given by

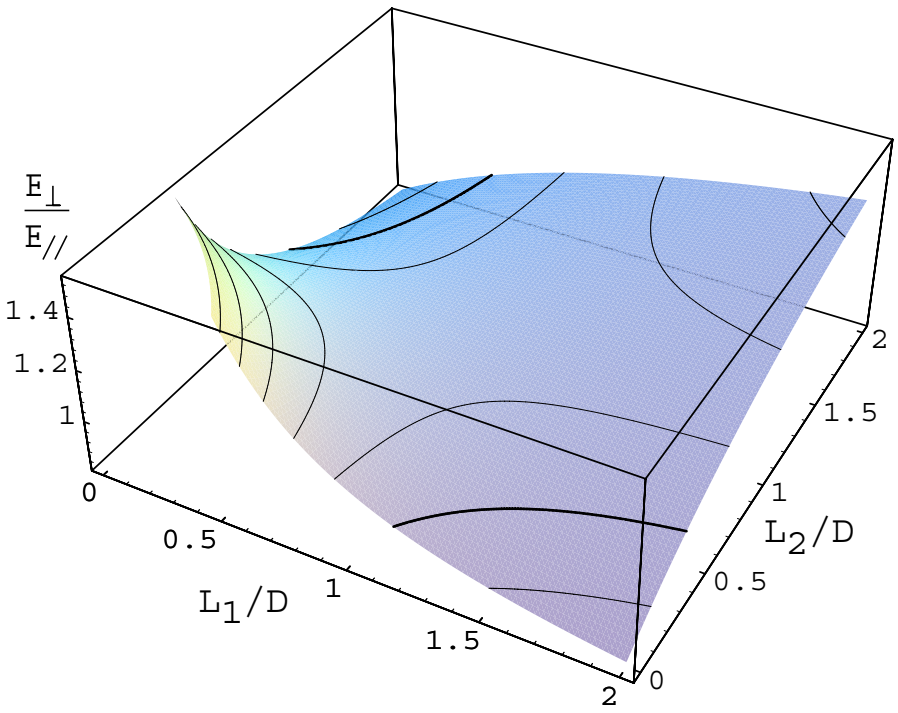

Figure 6.2: The ratio of perpendicular and parallel excluded volume of two cylinders with identical diameters and aspect ratios between 0 and 2. The thick, solid lines denotes the plane in which the perpendicular and parallel excluded volume are the same.

$$\frac{\beta F}{N} = \log(\rho \mathcal{V}_0) - 1 + \int dl f(l) \log(f(l)\mathcal{V}_l/\mathcal{V}_0) + \int dl f(l)\sigma[\psi_l] + \tfrac{1}{2}\eta \int dl f(l) \int dl' f(l') < \psi_l | \mathcal{E}^{l,l'} | \psi_{l'} > \tag{6.35}$$

which is similar to (6.27), but the summations over x_s are replaced by integrals over l. Terms involving Lagrange multipliers have been left out, but are easily implemented. $\mathcal{V}_l$ it the thermal volume of cylinder with length $(1+l)L$. If we consider the system for given composition $f(l)$ the second term is constant and will not have any effect on the system, and will therefore be left out. Taking the functional derivative of this free energy with respect to ψ_l leads to a stationarity equation similar to (6.28)

$$\log(4\pi\psi_l) + \eta_0 \int dl' f(l') \left(\mathcal{E}^{(0)}[\psi_{l'}] + l' \mathcal{E}^{(1)}[\psi_{l'}] + l \mathcal{E}^{(1)}[\psi_{l'}] + l l' \mathcal{E}^{(2)}[\psi_{l'}] \right) = cst. \tag{6.36}$$

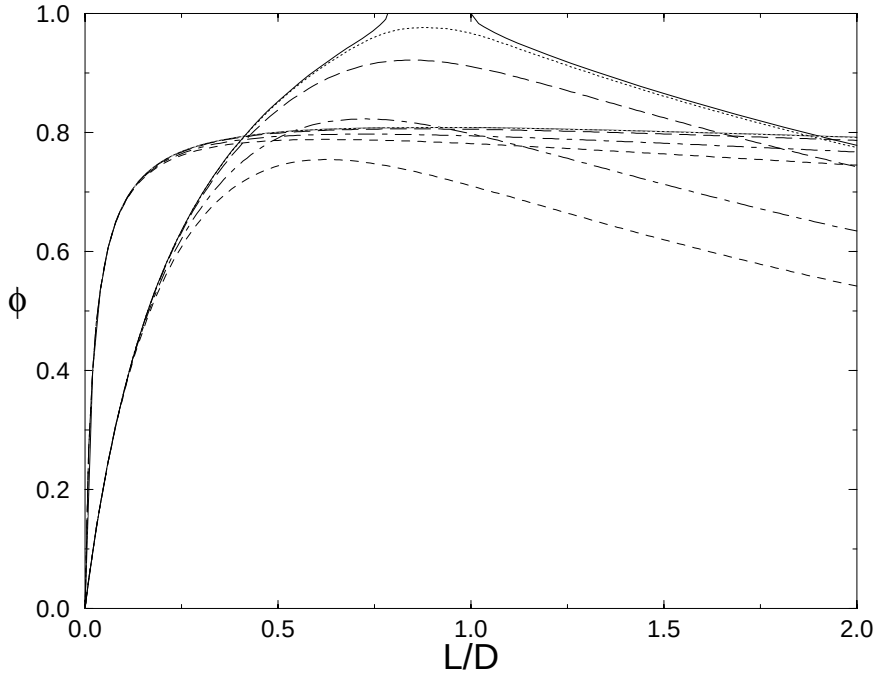

Figure 6.3: The bifurcation densities for $l = 2$ and $l = 4$ for $< l^2 >_f = 0$ (solid), 0.01 (dotted), 0.1 (long dashed), 0.5 (dotted-dashed) and 1 (dashed).

where we used the same trick as in (6.29) and expanded the excluded volume in a part independent of l and linear in l. The result is that the ODF ψ_l can be written as

$$\psi_l \propto \chi_1 \chi_2^l \tag{6.37}$$

where χ_1 and χ_2 are two, yet undetermined ODF's.

If we perform a bifurcation analysis for this system, the first bifurcation equation has the form

$$\frac{(\psi_l)_1}{\psi_0} + \eta_0 \left(\mathcal{E}^{(0)}[X_1] + \mathcal{E}^{(1)}[Y_1] + l\mathcal{E}^{(1)}[X_1] + l\mathcal{E}^{(2)}[Y_1] \right) = 0 \tag{6.38}$$

for all l. Using the linear property of the excluded volume functionals and performing the integrations over l' on the right-hand side, leads to the two relevant ODF's, $X = \int f(l)\psi_l$ and $Y = \int f(l) l \psi_l$. If we multiply both sides with $f(l)$ respectively $f(l)l$, and perform the integration over l making use of (6.34), we obtain two simple coupled equations

$$\begin{aligned} X_1 + \eta_0 \psi_0 \left(\mathcal{E}^{(0)}[X_1] + \mathcal{E}^{(1)}[Y_1] \right) &= 0 \\ Y_1 + \eta_0 \psi_0 \left(\mathcal{E}^{(1)}[X_1] + \mathcal{E}^{(2)}[Y_1] \right) &< l^2 >_f = 0 \end{aligned} \tag{6.39}$$

Note that these two equations only depend on $f(l)$ through the average value of l^2 in the second equation. If this average is zero equation (5.19) for the monodisperse system is recovered.

Since we are interested in non-trivial solutions the determinant of these equation has to be zero. The results are shown in figure 6.3 for several values of $< l^2 >_f$.

The vanishing of the $l = 2$ bifurcation density which in the monodisperse case was obtained, is only true for the case where the average squared distance between monomers $< l^2 >= 0$. The effect of increasing the polydispersity (via this parameter $< l^2 >$) is to shift the instabilities of the isotropic phase to lower densities. The effect on the $l = 4$ line is only small, and a sufficient amount of polydispersity in this system will therefore likely prefer an isotropic-nematic rather than an isotropic-cubatic phase transition.

6.6 Discussion

In this chapter we developed two simple extensions of the theory for monodisperse cylinders. In the first part we tried to model in a simple fashion the formation of stacks of cylindrical particles. By combining the description on the level of monomers and on the level of independent clusters we were able to obtain an expression for the free energy including the internal configuration of the clusters.

A bifurcation analysis of this system showed that stack formation can have two effects, it decreases the stability of long particles but for thin particles it has the opposite effect. If the 'binding' in the cluster becomes too weak however, the $l = 2$ bifurcation precedes the one of $l = 4$, which might make the cubatic phase impossible.

In the second part we examined the effects of polydispersity in a system of cylinders. The first observation we made is that for cylinders with different lengths, the excluded volume of perpendicular orientations can be less than for parallel cylinders. This might help to form a cubatic phase. In order to check this we performed a bifurcation analysis which revealed that introducing polydispersity lowers the maximum density of stability in the isotropic phase. The effect on the $l = 2$ bifurcation, however, is much larger and seems to indicate that too much polydispersity will exclude the possibility of a cubatic phase.

In both cases we found that the orientational order in the system of particles with different aspect ratios, due to the special form of the interaction, are closely related. The problem, which in principle involves different ODF's for different particle shapes, reduces to the calculation of only two of these functions, determining all others up to a normalization constant.

It is not obvious what will be the effect of polydispersity on the true transition; the bifurcation analysis yields merely an indication. Both theories indicate that the nematic phase is affected more than the cubatic phase. In order to check this, the free energy expressions have to analyzed more carefully, for example by using a Gaussian approximation.

7 Simulation of Cylinders

In this chapter we report about simulation of hard cylinders. Several different simulation techniques are used in order to see whether cylinders with relative short aspect ratio can form a cubatic phase and if not what phase they do form. We consider both monodisperse and polydisperse systems.

7.1 Introduction

There have been done already a lot of simulations on the relative simple type of hard particle systems. The first simulations were those on hard spheres systems by Alder and Wainwright [1], which at that time unexpectedly, crystallized. Since then several different kind of particles have been studied, ellipsoids [6, 7], spherocylinders [37], cut-spheres [8], infinitely thin rods [42, 43] and plates [38, 5]. The phase behavior of most of these particles is now well understood from simulations and theory. Some of these systems are now also experimentally accessible and confirm the obtained results.

What these particles all have in common is that their shapes are very easy to describe. This is necessary for a single reason. Hard particles in a simulation are not supposed to overlap. This means that given two particles with known size, position and orientation, we should be able to determine whether they overlap or not.

For spheres this is very easy because the only thing which is needed is the distance between the centers and both radii. Only when the distance is less than the sum of the radii do the particles overlap. It is not difficult to imagine that if we change the shape of the particles this calculation becomes more difficult. More difficult means longer calculation and hence the simulation time needed goes up with increasing complexity of the particles.

In this chapter we report the results of simulations done on hard cylinders. So far only approximate simulations of freely rotating, hard cylinders have been reported in the literature [44]. The reason for looking at these particles was already explained in chapter 5, and was related to an attempt to explain the cubatic phase in a system of cut-spheres. The theory we developed did not allow the existence of a cubatic phase, but on the way we made several assumptions, which in this chapter will be checked by means of computer simulations.

As it turns out, the overlap criterion for cylinders is too time consuming at present to make use of molecular dynamics. We therefore will restrict ourselves to Monte Carlo simulations in the NPT-ensemble, constant number of particles, pressure and temperature.

Since we are interested in the possible existence of the cubatic phase we do not attempt to map out the complete phase diagram as function of the aspect ratio. We restrict our selves to only one relevant aspect ratio. Based upon the theory of chapter 5 we focus on systems with $L/D = 0.9$, which is close to the aspect ratio for which the ratio of the perpendicular and parallel excluded volume is minimal. If cylinders have any cubatic behavior it should be close to this aspect ratio. Larger aspect ratios resemble real rod-like particles like shorter ratios will behave more like disc-like particles which both have a normal isotropic-to-nematic phase transition.

7.2 Overlap Criterion

As was already mentioned in the introduction, the most important ingredient for doing computer simulations of hard particles is an overlap criterion. For given sizes of particles, relative positions and orientations it should be able to tell whether particles overlap or not. The second requirement is that it should be as simple as possible to minimize the use of computer time.

In [45] an overview is given of the most widely used overlap criteria. The one for cylinders is only outlined. It consists out of three steps.

1. *spherocylinder overlap*: For the first step we replace the cylinders by spherocylinders by adding hemispheres on both sides of the cylinders. We then compute the closest distance between the spherocylinders. If the spherocylinders do not overlap the cylinders will not either. If the spherocylinders do overlap we can only conclude that the cylinders overlap if and only if the vector of shortest distance intersects both cylindrical parts.
2. *disk-disk overlap*: If the last condition is not satisfied we need to continue with the second step. In this step we check whether there is an overlap of the flat faces of the cylinders.
3. *disk-cylinder overlap*: If no overlap is found in of second step, and the spherocylinders in the first step did overlap we need to proceed with the third step, which is the most time consuming one. We have to check whether one of the flat faces of a cylinder overlaps with the cylindrical part of the other cylinder.

According to [45] this last problem reduces to calculating overlaps between two planar ellipses, and hence is a special case of the overlap between two ellipsoids.

Suppose we now look in the plane defined by the flat face of the first cylinder. If it does not intersect the other cylinder there is no overlap. If there is an intersection however it is an ellipse or a truncated ellipse if a flat face of the second cylinder also intersects the same plane (see figure 7.1) . If we proceed along this line we need to check therefore whether the overlap between the ellipses lies on the allowed parts and we therefore actually need to calculate a point of intersection.

For ellipsoids there exist two different criteria to determine whether there exists an overlap or not. The first is due to Vieillard-Baron [46] and the second due to Perram and Wertheim [47]. Both criteria determine whether there exists an overlap without calculating any points which both particles have in common. And this is precisely what has to be established for the overlap of the two planar ellipses, because one of them need not be complete.

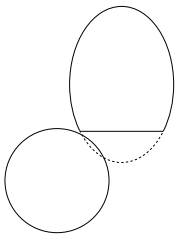

Figure 7.1: Projection of non-overlapping cylinders due to truncation of the ellipse.

The alternative route is to look at the problem as the overlap between a flat face of one cylinder with a sequence of circles of the second particle. This results in a fourth order polynomial equation and can in principle be solved analytically. The main problem with this approach is that during simulations it will result in severe problems, and not always find the correct outcome. The reason for this is that the coefficients of the polynomial equation are inversely proportional to the sine of the angle between the particles. Therefore the coefficients can differ orders of magnitudes, which makes it hard to solve and not always accurate.

The method we applied for the last step in the overlap criterion therefore is a direct minimization of the distance between a point on the edge of the first cylinder and a point on the axis of the second cylinder. Although it is slower is has proven to be very reliable.

7.3 Virial coefficients

Using the overlap criterion for cylinders as obtained in the previous section we can calculate the third and fourth virial coefficients as function of the aspect ratios. The results are plotted in figure 7.2. In section 4.2 we already explained the way in which virial coefficients can be calculated by growing chains of particles and analyzing to which diagrams the configurations belong.

In chapter 5 we used the Parsons approach, in which we approximated the higher virial coefficients leading to the excess free energy (5.12), which can be expanded for low densities. This excess free energy should approximate the real expansion in term of virial coefficients

$$\frac{\beta \mathcal{F}^{ex}}{N} = B_2\rho + \tfrac{1}{2}B_3\rho^2 + \tfrac{1}{3}B_4\rho^3 + \cdots \tag{7.1}$$

Comparison of these two series give us the approximated values for the virial coefficients

$$\begin{aligned} B_3 &= \tfrac{5}{2}v_0 B_2 \\ B_4 &= \tfrac{9}{2}v_0^2 B_2 \\ B_5 &= \tfrac{14}{2}v_0^3 B_2 \end{aligned} \tag{7.2}$$

These estimated values are for comparison also plotted in figure 7.2. What we observe is that the general behavior is very similar, but the actual values differ. The third virial coefficient is underestimated and according to the Parsons approach the fourth virial

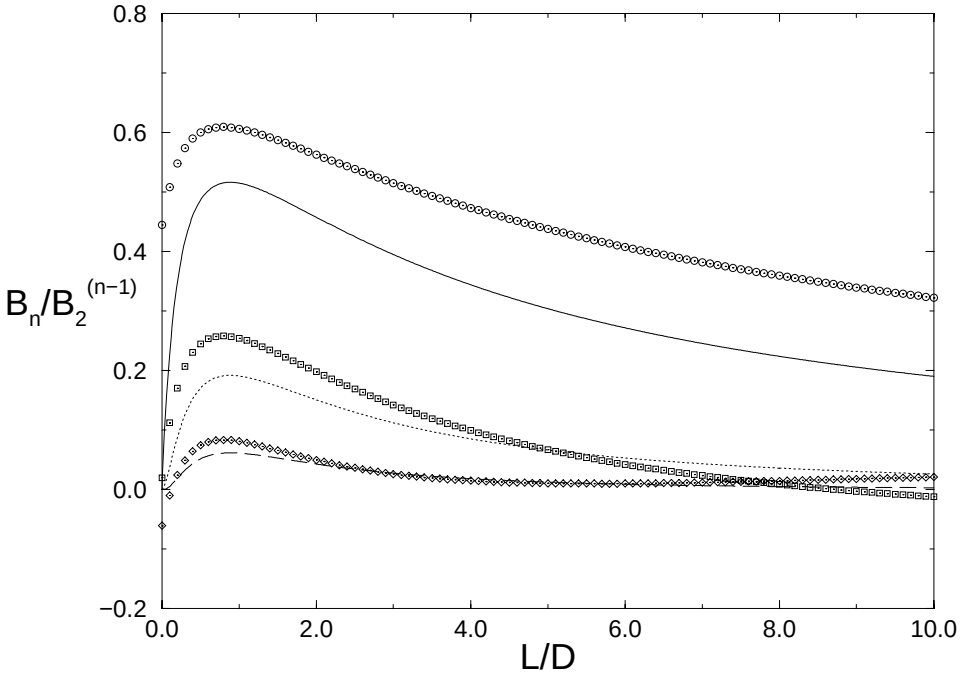

Figure 7.2: The reduced virial coefficients B_3/B_2^2, B_4/B_2^3 and B_5/B_2^4 for the isotropic phase as estimated by the Parsons approach (solid, dotted resp. dashed curve) and their true values (circles, squares resp. diamonds).

coefficient is always positive, while for rod-like particles, and hence increasing aspect ratios, it should become negative [27].

This disagreement might have some effects on the calculated coexistence, but it is not obvious whether this enough to prefer a cubatic over the nematic phase for aspect ratios of order unity.

7.4 The Flip-move

In Monte Carlo simulations we try to sample the complete phase-space in an effective way. It is however possible that a simulation gets stuck in a restricted part of the phase space. If this is the case we need to broaden the repertoire of possible MC-moves. In the case of short cylinders such a move exists and is surprisingly simple and effective.

From the normal simulation we already have the move of position and orientation of the particles, and we change the volume anisotropically. One can imagine that in dens systems the particles are close together and it becomes hard for the particles to move or rotate. In order to get an acceptance of 35-50% of the moves this means that we have a small value for the maximum rotation, with a maximum of about 5-10 degrees, depending on aspect ratio and density.

The projections of a short cylinder with diameter D and length L in the direction parallel and perpendicular to its orientation are a circle with diameter D respectively a rectangle with sides L and D. These projections have almost the same dimensions if L and D are of the same magnitude, which is the case for the systems that we are interested in. Hence it is possible to rotate a short cylinder directly over 90 degrees to a perpendicular orientation without causing an overlap in the system. This 'flip' however

is much harder to establish via the normal path of rotations, as can be seen in figure 7.3. The reason is simple, the maximum dimension of a cylinder in term of its length and diameter is $\sqrt{L^2 + D^2}$ which can be up to 50% higher than the length or diameter. And therefore in denser systems there is just not enough room for these rotations to happen, unless all particles in the neighborhood move away to create the necessary space.

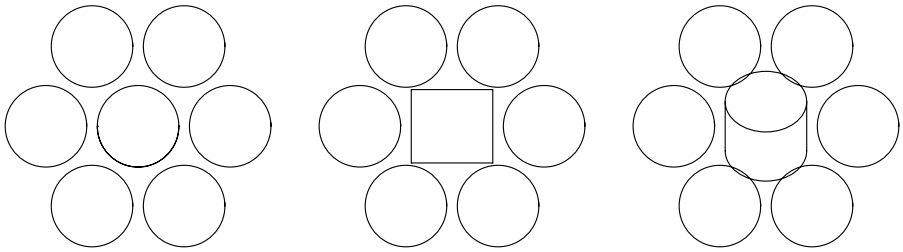

Figure 7.3: Top view of a hexagonal structure for cylinders with aspect ratio of order unity. From left to right the angle of the particle in the middle goes from 0 to $\pi/2$ and somewhere in between, The last causing overlap.

During our simulations on average 1 out of every 10 rotations will be the attempt to flip a particle. Here to we select at random an orientation in the plane perpendicular to the direction of the particle. And accept if there is no overlap in the new situation. The acceptance of this move depends of course strongly on the aspect ratio and density, but can be as large as 5 %, even in a crystalline phase.

7.5 Crystal Phases

There are several relevant crystalline structures to study for a system of cylinders with an aspect ratio of order unity. The highest possible density in a system of cylinders is reached when all cylinders are perfectly aligned in a closed packed structure with packing fraction $\phi = \pi/\sqrt{12}$.

The relevant closed packed structure is formed if the particles are packed in an hexagonally ordered layers. These layers can be stacked in an 'AAA' fashion, such that particles in different layers are exactly on top of each other. It is in principle also possible to order layers in another fashion for instance 'ABC' of shifted randomly with respect of each other. As it will turn out however these variants are are not stable and will relax to the AAA-crystal.

This highest packing fraction can also be obtained by a columnar phase. In the AAA-crystal phase the particles are stacked in perfect columns perpendicular to the layers. These columns can therefore slide along each other to form a columnar phase. Although this shifting of the columns is observed in the simulation this is probably a finite size effect.

In the phases described above the particles are aligned. There is one crystal that exhibits cubic like orientational order, namely the simple cubic crystal. Therefore we also use this crystal in which all particles get randomly an orientation along one of the three crystal axes assigned.

In order to allow for structural relaxation, the box shape was allowed to change, as is depicted in figure 7.4. This extension was first used by Parrinello and Rahman [48–50]

in MD simulations and later by Najafabadi and Yip in MC simulations [51]. Allowing for shape changes is only useful in crystalline structures, because then the presence of the crystal structure acts as a restoring force and will ensure that the box shape cannot become extremely anisotropic in contrast, in the liquid phase, such extreme deformations might occur.

Figure 7.4: Changing the box shape.

The position of a particle $\vec{r}$ in a non rectangular box is

$$\vec{r} = H\vec{s} \tag{7.3}$$

where $\vec{s}$ are scaled coordinates inside a unit cube. $H = (\vec{h_1}, \vec{h_2}, \vec{h_3})$ is a transformation matrix describing the shape of the box by the vectors $\vec{h_i}$ representing the sides of the box. The volume of the simulation box is given by the determinant of the matrix H

$$V = |H| = \vec{h_1} \cdot \vec{h_2} \times \vec{h_3} \tag{7.4}$$

7.6 Simulation Results

When searching for cubatic order, the most interesting aspect ratios for cylinders are of order unity. Because the overlap criterion involves a time consuming minimization we have chosen to concentrate on a single aspect ratio $L/D = 0.9$.

Figure 7.5 shows the equation of state for this system. For comparison we have also plotted the equation of state obtained from a virial expansion, using the numerical values up to the fifth virial coefficient as obtained in section 7.3 and the equation of state obtained from the Parsons approach, which works very well up to the phase transition.

Simulations are performed on a system of 720 particles, and in each simulation we use 100000 sweeps to get good statistics. In one sweep all particles are moved once on average and one attempt is made to change the box-size or boxshape. In order to get an impression what these systems look like, three snapshots for this system are included in figure 7.6.

For high pressures we start with a perfect AAA-crystal, which we slowly expand. Other crystalline structures are not stable. An ABC-crystal will shifts its planes along each other to form an AAA-structure. The simple cubic phase with cubatic orientations is also not stable and will also deform to a AAA-crystal.

The flip-move is extremely effective. Even for a packing fraction $\phi = 0.7$ one out of every 1000 attempted flips is accepted. But for $\phi = 0.65$ this is already one out of every 100 and increases to about 7% near the transition to the isotropic phase. A simulation without using this flip move showed that at $\phi = 0.65$ particles can achieve a flip via a continuous rotation, but this occurs with a very low probability, only once in a

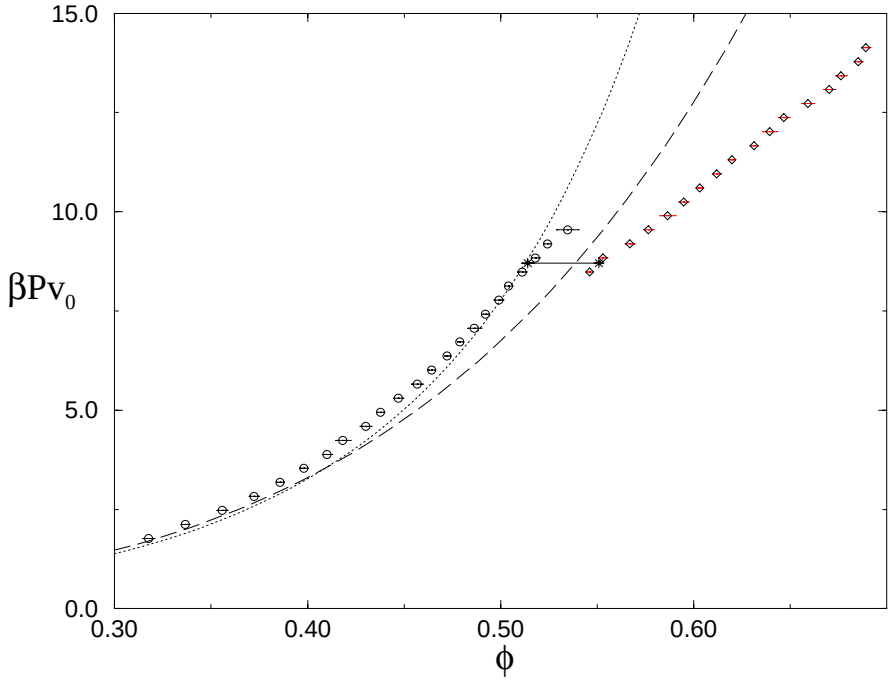

Figure 7.5: The equation of state of cylinders with $L/D = 0.9$ for the isotropic ($\circ$) and crystal ($\diamond$) phase. The solid line denotes the coexistence, the dashed line corresponds to a virial expansion using up to fifth coefficient and the dotted line correspond to the Parsons approach.

simulation of 100000 sweeps. Therefore the introduction of the flip move speeds up this slow 'dynamical' process enormously, leading to a faster convergence to equilibrium.

The high acceptance of the flip move changes the structure of the phase to something new, because particles can to be oriented either parallel or perpendicular to the z-direction as can be seen in figure 7.6. To analyze the structure of the phase we separate the positional and orientational order.

For the orientational order we calculate the nematic order parameter tenser Q defined by

$$Q_{ij} =< \tfrac{2}{3}\hat{n}_i\hat{n}_j - \tfrac{1}{2}\delta_{ij} > \tag{7.5}$$

where $\hat{n}$ are the directors of the particles. This matrix is real, symmetric and traceless. It can therefore be written in the form

$$Q = \begin{pmatrix} N & 0 & 0 \\ 0 & -\frac{1}{2}N + B & 0 \\ 0 & 0 & -\frac{1}{2}N - B \end{pmatrix} \tag{7.6}$$

The maximum eigenvalue N corresponds to the nematic order parameter and the corresponding eigenvector to the nematic axis of the system, and is closely related to the average direction of the particles. B is the biaxial order parameter and will be zero in an uniaxial nematic phase.

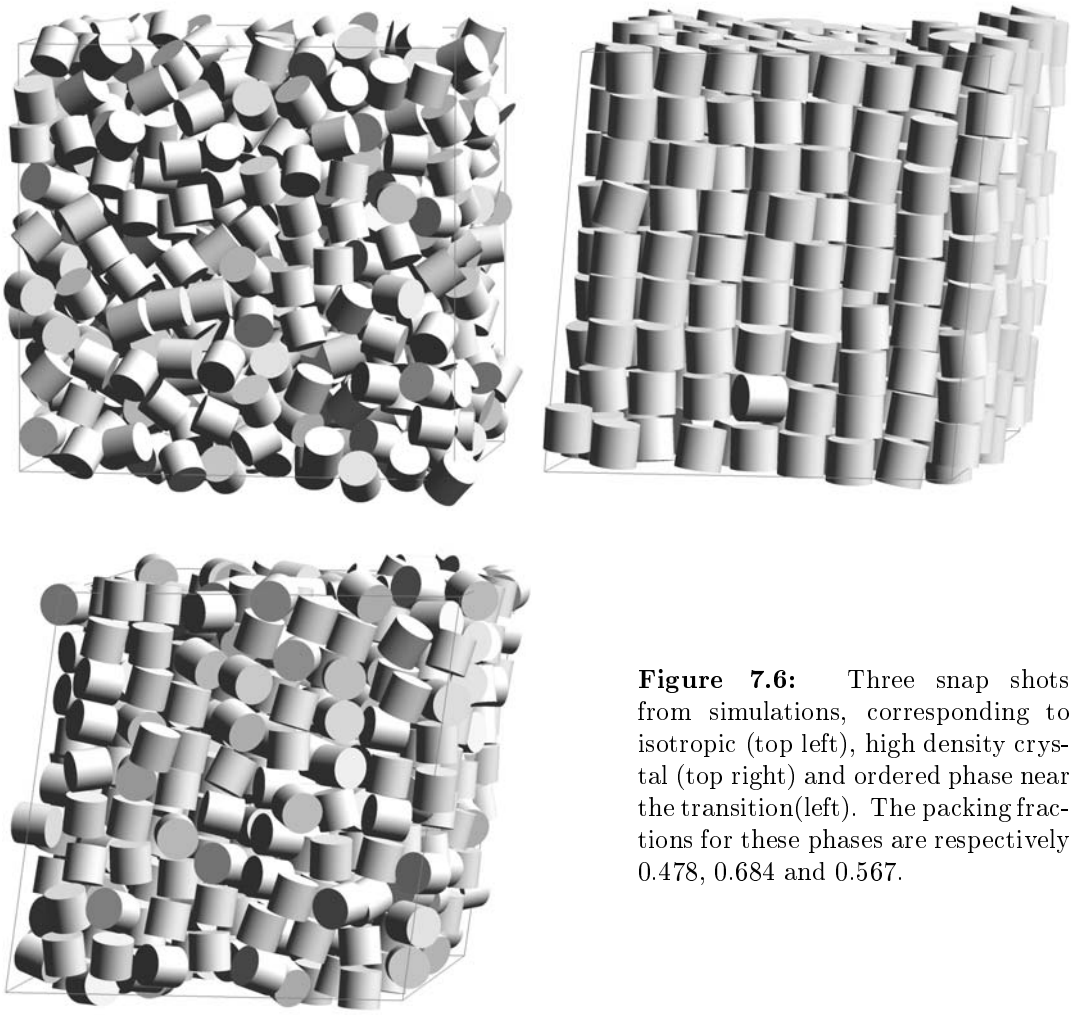

Figure 7.6: Three snap shots from simulations, corresponding to isotropic (top left), high density crystal (top right) and ordered phase near the transition(left). The packing fractions for these phases are respectively 0.478, 0.684 and 0.567.

The cubatic order parameter I_4 which we calculate is a combination of modified spherical harmonics, which is invariant under rotations of the frame. It is a member of a class of invariant order parameters and is defined analogous to the one which was used for the cross-like particles (4.13).

$$I_l = \left\langle \left(\sum_m C_{l,m} C^*_{l,m} \right)^{\frac{1}{2}} \right\rangle \tag{7.7}$$

Although we refer to I_4 as the cubatic order parameter one should realize that a non-zero value does not mean that we have cubatic order. In fact in a perfect nematic phase it is unity. The reason for this is that it is an summation over all $C_{4,m}$, including $C_{4,0} = P_4$ the fourth Legendre polynomial, which in an aligned nematic phase is of order unity. A cubatic phase requires a non-zero I_4 in combination with the absence of nematic order.

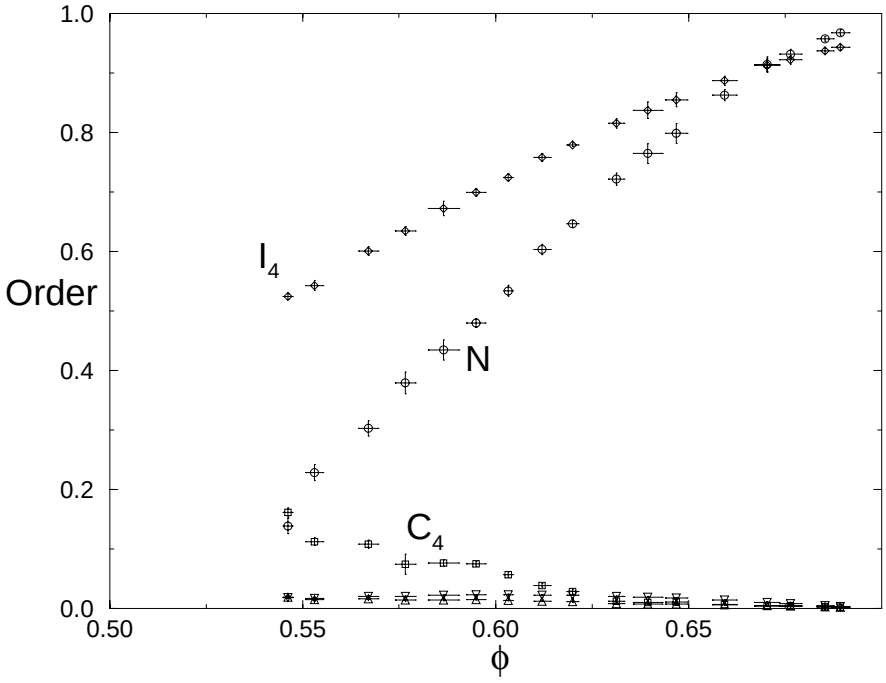

Figure 7.7: The orientational order parameters as function of the packing fraction in the ordered phase. The nematic (○), cubatic (□) and C_4 (◇) order parameters are non-zero, C_2 (△) and C_6 (▽) are negligible small.

In order to detect planar order we finally consider the average of the functions $\sin l\varphi$, where the angles φ of the directors of the particles are measured in the plane perpendicular to the average direction obtained from (7.6)

$$C_l =< |C_{l,l}| > \tag{7.8}$$

This order parameter is invariant under rotation of the system about the average direction.

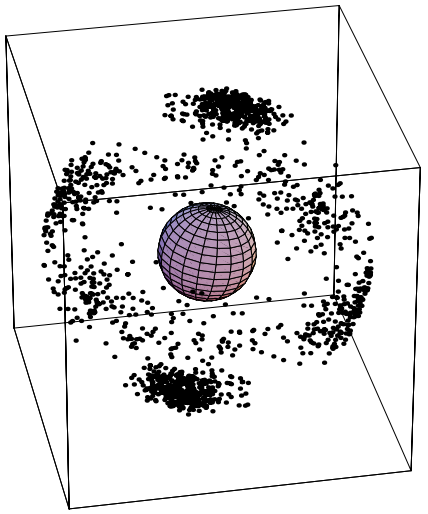

Figure 7.8: The orientational distribution for a configuration at $\phi = 0.567$.

The values of the orientational order parameters are shown in figure 7.7. The nematic order parameter decrease from 1 at high densities continuously to almost zero near the transition point. The cubatic order parameter I_4 has the same behavior, but remains finite, indicating that the orientation distribution does not becomes isotropic but remains ordered. Initially the orientations of the particles in plane are isotropic but for lower densities the number of particles perpendicular to the average direction increases and these particles start to interact. This leads to an additional order in plane. The order is small but significant 4-fold as indicated by the order parameter C_4. The order parameters C_2, which is similar to the biaxial order parameter, and C_6 are both negligible small.

We use the system at packing fraction $\phi = 0.567$ to illustrate the order in the phase near the transition. In figure 7.8 we plotted all orientations of the particles on a unit sphere. It is clear that particles are either along the nematic axis or perpendicular to it.

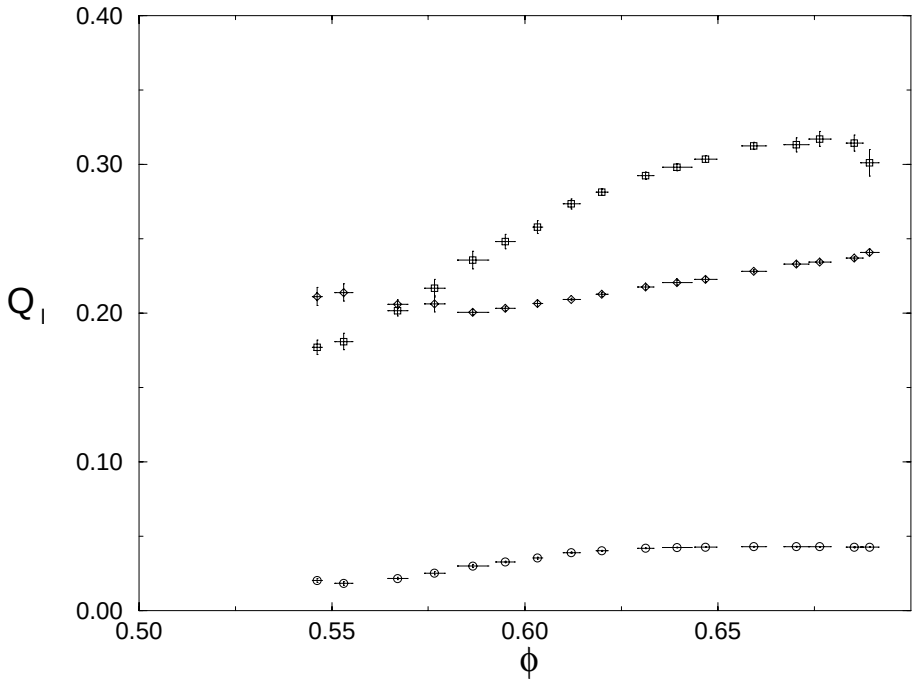

Figure 7.9: The bond orientational order parameters $Q_4(\circ)$, $Q_6(\diamond)$ and $Q_8(\square)$ as function of the packing fraction in the ordered phase.

To characterize the positional order we use the bond orientational order parameters Q_l used by Steinhardt *et al* [52],

$$Q_l = \left\langle \left(\sum_m |C_{l,m}(r)|^2 \right)^{\frac{1}{2}} \right\rangle \tag{7.9}$$

where we determine the polar angles of the vector $\vec{r}$ connecting neighboring particles. Only particles within a distance of twice the length of the particles are used.

The bond orientational order parameters are shown in figure 7.9 and although they are decreasing for decreasing density there is no change indicating any structural difference. This is partially confirmed by projections of the centers of mass of the particles in figure 7.10. The top view shows clearly the hexagonal structure, indicating the presence of columns. The side view shows that columns lie within planes. Observing planes however is much more difficult near the transition to the isotropic phase as can be seen in the front view. This becomes more evident in figure 7.11 where we have determined which pairs of particles are in the same plane according to some criterion. If particles lie in a neighboring columns and the distance along the column is less than 40% of the lengths of the cylinders we consider them to be in the same plane and connect the centers of mass, providing a guide for the eye to spot the planes. The bonds through the boundary conditions are not not drawn but are present as well. On average each particle is connected to 4.9 neighboring particles. In a perfect crystal this number should be 6, while if the columns are distributed randomly, it would, at this density, on average be 4.

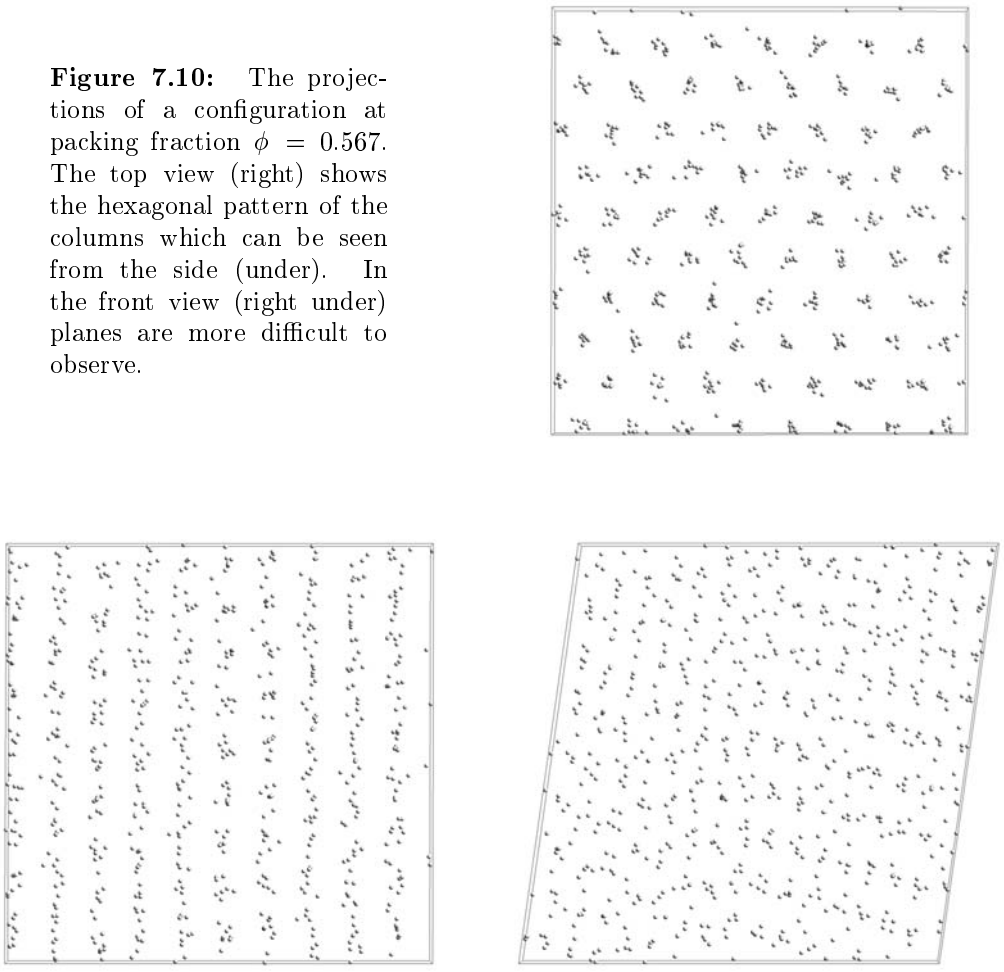

Figure 7.10: The projections of a configuration at packing fraction $\phi = 0.567$. The top view (right) shows the hexagonal pattern of the columns which can be seen from the side (under). In the front view (right under) planes are more difficult to observe.

Finally we show in figure 7.12 the radial distribution function $g(r)$ and the orientational correlation functions $g_2(r)$ and $g_4(r)$, defined by

$$g_l(r) =< P_l(\hat{n}(0) \cdot \hat{n}(r)) > \tag{7.10}$$

Both orientational correlation functions are non-zero over the whole range, although the value of $g_2(r)$ is much smaller. It is tempting to assume that this refers to the absence of nematic order and, because $g_4(r)$ is non-zero some cubatic-like order is present. This is in fact not completely true. $g_2(r)$ is for instance also zero if roughly a third of the particles is aligned along a given direction and the rest is distributed isotropically in the

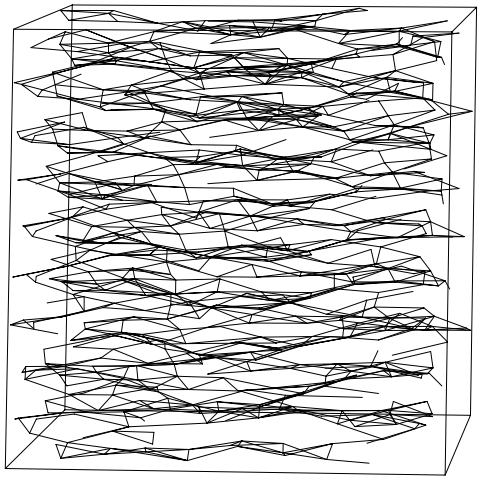

Figure 7.11: In order to visualize the planes, particles within the same plane, according to some criterion, are connected to form a network.

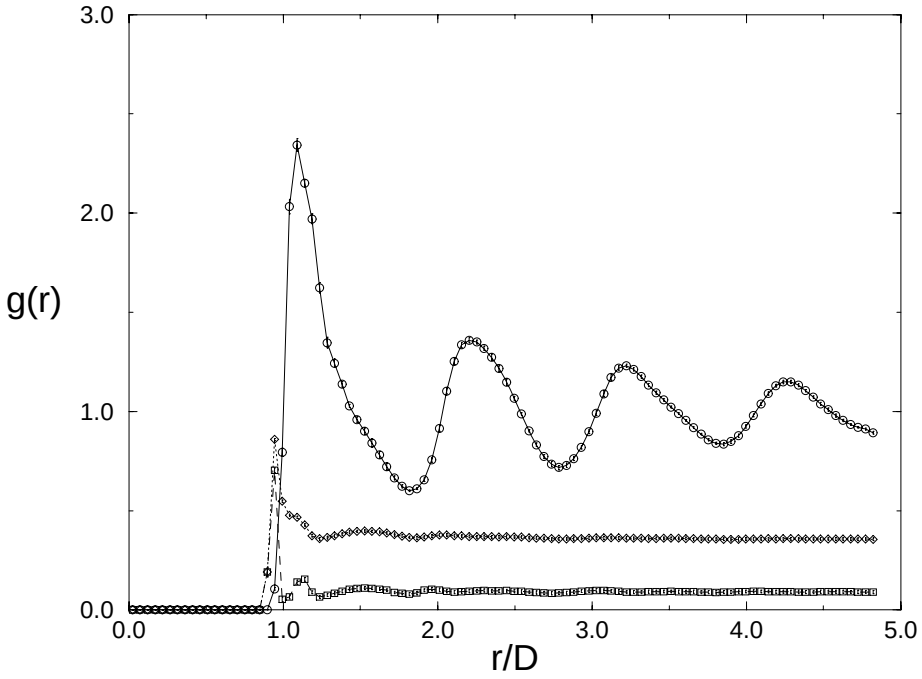

Figure 7.12: The radial distribution function $g(r)$ (○) and the orientational correlation functions $g_2(r)$ (□) and $g_4(r)$ (◇) for $\phi = 0.567$.

plane perpendicular to that direction. This would still be an uniaxial symmetry and therefore a nematic-like phase.

There are two problems left before we can conclude what the nature of this phase is. The first is the positional order which we determined. One could argue that the planes which we indicated are a consequence of the fact that particles are short and therefore it is likely that many particles lie within the same plane using the sketched criterion. If these planes are just an artifact the data could also be interpreted as a columnar phase. In fact during simulations we observe in a single run that some columns slide along their neighbors to displace over one or two times the dimension of the particle.

The second problem is that the orientational symmetry is 4-fold while the positional order is 6-fold symmetric. The 4-fold symmetry can only be explained by interaction of particles in neighboring columns which are both in plane and prefer to be at right angles. The mismatch of both symmetries is then possibly a finite size effect.

In order to check this we performed a simulation using 5760 particles at the same pressure $\beta P v_0 = 9.19$ as a small system with only 720 particles. For the smaller system at $\phi = 0.567 \pm 0.002$ and the C_4 order parameter had a value of 0.108 ± 0.007. The average packing fraction for the large system was $\phi = 0.562 \pm 0.001$ and the order parameter C_4 in this system reduced to 0.073 ± 0.002, compared with the smaller system the order parameter shows a decrease but does not yet become negligible.

7.7 Free Energy Calculation

In order to determine the coexistence between the isotropic liquid and the crystal phase we have find points on the equation of state with equal pressure and chemical potential. To this end we need to determine the free energy. By performing a thermodynamic integration along the equation of state we can evaluate the free energies up to a constant. For this constant we need to determine one reference point.

In the isotropic phase this is easy because we can use the ideal gas as a reference

$$F(\rho) = F_{id}(\rho) + \int_0^\rho d\rho' \frac{P(\rho') - \rho'}{\rho'^2} \tag{7.11}$$

For the crystal phase we use as a reference system an Einstein crystal with the same structure [53], which in our case a perfectly aligned AAA-crystal is. We connect the two systems by a one parameter Hamiltonian which consists of two parts, the coupling of the particles to their equilibrium lattice positions and the alignment for the orientations

$$H_\lambda = \lambda \sum_i (\vec{r}_i - \vec{r}_i^{\,0})^2 + \lambda \sum_i \sin^2(\theta_i). \tag{7.12}$$

where λ is the coupling parameter and $\vec{r}_i^{\,0}$ are the lattice positions of the particles. By slowly increasing the value of λ the system will order according to the imposed field. We used here the same coupling parameter for both fields, but one can also use different parameters.

The free system with $\lambda = 0$ can be related to the Einstein crystal for which $\lambda \gg 1$ by

$$\frac{\beta F(\rho)}{N} = \frac{\beta F_{ein}(\lambda_{max})}{N} - \int_0^{\lambda_{max}} d\lambda < \delta r^2 >_\lambda - \int_0^{\lambda_{max}} d\lambda < \sin^2\theta >_\lambda - \frac{\log V}{N} \tag{7.13}$$

where $< \delta r^2 >_\lambda$ is the mean square displacement and $< \sin^2\theta >_\lambda$ the average sine squared of the angle between the directors of the particles and the direction of the alignment field. The last term corrects for the fact that the center of mass during this simulation needs to be fixed. The value of λ_{max} is chosen such that a system using this Hamiltonian only will not cause any overlaps in the system. For that limit we can derive the value of the free energy of the Einstein crystal

$$\beta F_{ein}(\lambda) = \tfrac{3}{2}\log N - \tfrac{3}{2}(N-1)\log(\frac{\pi}{\beta\lambda}) - N\log(\frac{2\pi}{\beta\lambda}) \tag{7.14}$$

In the case that overlaps do occur, it is possible to correct for this [53]. By simulating the system for different values of λ the integrals in (7.13) can be numerically evaluated. In order to minimize the error we used the Gauss-Legendre quadrature.

The coexistence is obtained is at packing fraction $\phi = 0.514 \pm 0.003$ for the isotropic and $\phi = 0.551 \pm 0.002$ for the crystalline structure,at a pressure $\beta P v_0 = 8.71 \pm 0.05$ (see figure 7.5).

7.8 Polydispersity

In the previous sections we did not find a cubatic phase in a system of hard cylinders with an aspect ratio $L/D = 0.9$. We recall that this aspect ratio was chosen because it is close to the optimal aspect ratio, as far as the excluded volume is concerned, for which the cubatic phase is most likely to occur. Instead a crystalline phase is obtained which melts directly to the isotropic phase. In section 6.5 we discussed the effects of polydispersity on a system of cylinders. The bifurcation theory gave an indication that the isotropic-to-nematic and isotropic-to-cubatic transition shift to lower densities if polydispersity is added to the system of monodisperse cylinders. In this section we will check this numerically by starting in the monodisperse case and adding polydispersity.

For studying continuous mixtures the semigrand ensemble is the most suitable [54, 55]. It is a combination of the canonical and grand canonical ensemble in which the total number of particles N is fixed but the identity of a particle, in this case its shape, is allowed to change. In this fashion a continuous distribution can be obtained.

The way we want to incorporate polydispersity is by keeping the diameters of all particles fixed but the lengths are allowed to change. This is done by imposing an activity-ratio distribution $\exp(-\beta(\mu(L) - \mu(L_0)))$, where $\mu(L)$ is the chemical potential as function of the length L of the cylinders and L_0 is the length of an arbitrary reference component. To a first approximation the resulting distribution function of lengths will be similar to this imposed one [55], hence we will assume a quadratic function

$$\beta(\mu(L) - \mu(L_0)) = -(L - L_0)^2/(2\nu) \tag{7.15}$$

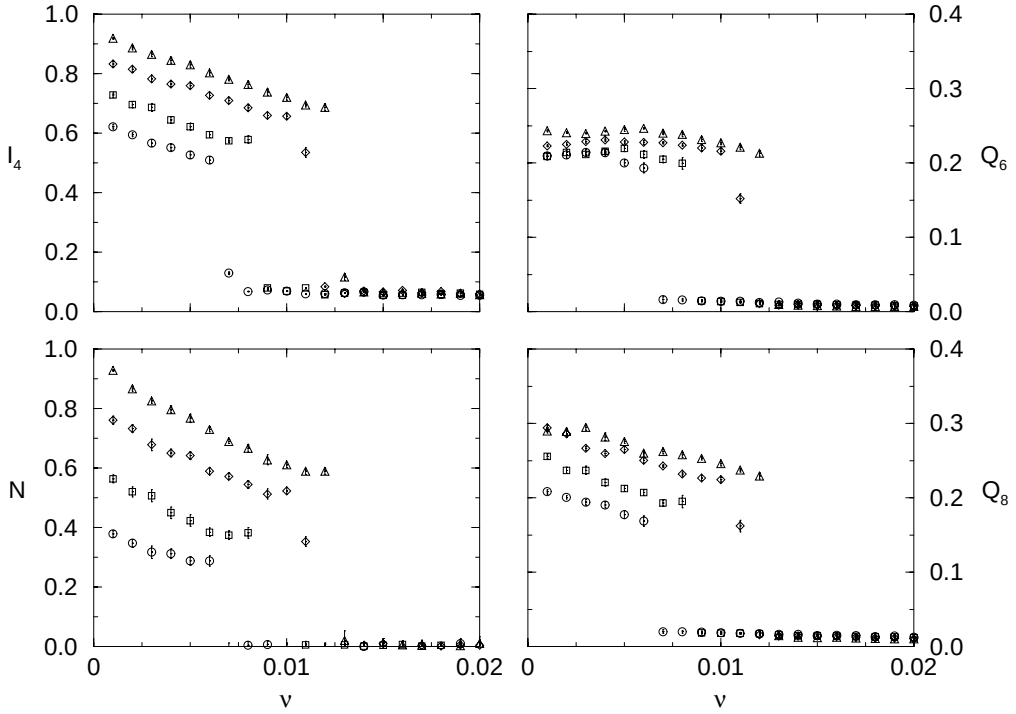

Figure 7.13: The orientational order parameters I_4 and N, and bond orientational order parameters Q_6 and Q_8 as function of the polydispersity parameter ν for pressures $\beta P v_0 = 9.9$ (○), 11.3 (□), 12.7 (◇) and 14.1 (△).

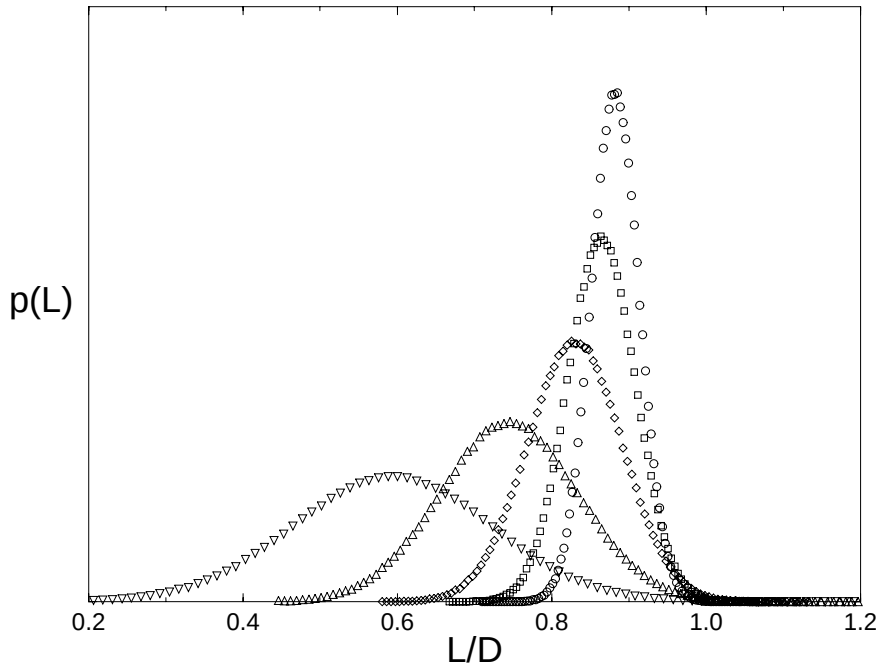

Figure 7.14: The composition distribution functions $p(L)$ at fixed pressure $\beta P v_0 = 9.9$ for $\nu = 0.001$ (○), 0.002 (□), 0.004 (◇), 0.008 (△) and 0.016 (▽).

which for small values of ν will lead to a Gaussian distribution about L_0 with width ν. In the limit $\nu \to 0$ this leads to the monodisperse system with length L_0.

In addition to the moves already discussed we now allow the the lengths of randomly chosen particles to change, which is accepted in the usual way [56].

We did simulations at four different pressures in the stable crystalline region, in which we slowly increased the polydispersity via the parameter ν.

The results for the relevant the most relevant order parameters are summarized in figure 7.13. Similar to the monodisperse case all order parameters vanish at the same time. For the higher pressures a larger value of ν is required to melt the crystal. Although at high enough polydispersity the crystal is destabilized, no ordered phase but the isotropic phase is formed.

For low values for ν the distribution function follows the imposed activity and is a Gaussian distribution at L_0. For increasing values of ν however, it becomes easier to change the length considerably from the reference length L_0 as can be seen in figure 7.14. As a consequence this leads to lower densities and a shift of the peak in the distribution to lower values, away from the aspect ratio $L/D = 0.9$ and a possible cubatic phase. A nematic phase is not observed either. In order to overcome this problem we should fix the peak of the distribution. This can be done by altering the value of L_0 in the imposed activity. This will then lead to a simulation with fixed average composition function.

7.9 Discussion

In this chapter we presented the results of computer simulations for hard cylinders. We first worked out the overlap criterion of these particles. In principle completely the overlap criterion can be solved analytically, but in practice it is more convenient to use a numeric minimization scheme.

We used the overlap criterion to obtain the third, fourth and fifth virial coefficients an compared them with the approximation for these coefficients made by the Parsons approach, showing an acceptable agreement.

In the standard NPT-simulations we introduced the flip-move which rotates a particle directly to a perpendicular orientation. Further more we allowed the box shape to change to an arbitrary parallelepiped for better relaxations in the crystal phase.

We showed the results of simulations for cylinders with an aspect ratio $L/D = 0.9$. The prediction of the equation of state provided by the Parsons approach worked surprisingly well up to the density of the phase transition. At high pressures the system is found in an AAA-crystal. By lowering the pressure particles will reorient due to the flip move and deform the perfect crystal.

The phase has still a distinct 6-fold symmetry for the columns but the layers are less obvious. The orientations are either along the columns or perpendicular to them. Towards the phase transition a weak but significant 4-fold orientational order in plane develops, which may be due to finite size effects.

The phase coexistence was determined at $\phi = 0.514$ in the isotropic and $\phi = 0.551$ for the crystal phase. The theory of chapter 5 predicted for this aspect ratio the isotropic-to-nematic phase transition at $\phi = 0.788$ respectively $\phi = 0.795$. Not only the densities are wrong, which can be accounted for by using a better scaling theory, but also the

wrong symmetry is predicted, caused by the fact that only orientational order was taken into account. No cubatic phase is found.

By imposing activity-ratio distribution, polydispersity is added to the system. Small values of the polydispersity are not strong enough to destabilize the crystal phase. Larger values make it cost less energy to change the aspect ratio's to lower values, which is used by the pressure in order to increase the density. As a consequence the distribution of the particles shifts to smaller aspect ratio's which do not favor the cubatic phase. Instead the crystal melts to the isotropic phase.

The simulations confirm the results of the theory in the sense that there is no isotropic-to-cubatic phase transition, although the reason is quit different. According to the theory this was caused by nematic phase which at high densities is more stable. The true reason however is that at the obtained densities the crystalline order cannot be neglected. The simulations show that the phase transition occurs at a density roughly 50% lower and is to a crystalline phase.

A cubatic phase if possible for cylinders has to be found elsewhere. It can be expected that for cylinders with an aspect ratio $L/D = 0.2$ a cubatic phase will be observed, because there is at these aspect ratios only a small difference in shape between cylinders and cut-spheres.

A Special Functions

Throughout this thesis, the Helmholtz Free energy as a functional of the one particle distribution function is employed. This distribution $\rho(\vec{r},\Omega)$ can always be expanded in a set of suitable functions. In general, it is a function of position and orientation. And the most convenient set of functions to be used depends strongly on the phase under study, the symmetry of the particles, and their interaction.

In case of an homogeneous phase there is no position dependence and the $\vec{r}$ can be integrated out to obtain the one-particle orientational distribution function $\psi(\Omega)$ which is proportional to the fraction of particles with an orientation Ω.

$$\psi(\Omega) = \int \rho(\vec{r},\Omega) d\vec{r} \tag{A.1}$$

For all rigid particles this orientation can be described by the three Euler angles denoted by (α,β,γ), which describe the rotation from a fixed reference frame $\{\hat{x},\hat{y},\hat{z}\}$ to the particle-fixed frame $\{\hat{u},\hat{v},\hat{w}\}$. This rotation consists of a rotation about the z-axis over γ, followed by a rotation about the y-axis over β, and a rotation about the z-axis over α. The invariant measure of this rotation is given by $d\Omega = d\alpha \sin(\beta) d\beta d\gamma$.

A.1 $\mathcal{D}^l_{m,n}$-functions

The set of functions corresponding to the Euler-angles is the set of standard rotation matrix elements, which are denoted by $\mathcal{D}^l_{m,n}(\Omega)$. The complete set is defined for integral and half-integral

values of l and is an extension of the spherical harmonics. For half-integral values the functions change sign for $\beta = 2\pi$ and can be related to spins, but in the case of classical particles these are not needed. The most important properties of these function are listed below. More details can be found in Brink and Satchler [57].

The $\mathcal{D}^l_{m,n}$-functions are defined by

$$\mathcal{D}^l_{m,n}(\alpha\beta\gamma) = e^{-\imath(\alpha m+\gamma n)} d^l_{m,n}(\beta) \tag{A.2}$$

where the function $d^l_{m,n}(\beta)$ is given by

$$d^l_{m,n}(\beta) = \sum_t (-1)^t \frac{\sqrt{(l+m)!(l-m)!(l+n)!(l-n)!}}{(l+m-t)!(l-n-t)!t!(t+n-m)!} \times (\cos\beta/2)^{2l+m-n-2t} (\sin\beta/2)^{2t+n-m} \tag{A.3}$$

and the indices m and n take the values $-l,\ -l+1,\ \cdots,\ l$. The $\mathcal{D}^l_{m,n}$-functions are orthogonal and normalized by

$$\int_0^{2\pi} d\alpha \int_0^{2\pi} d\gamma \int_0^{\pi} \sin(\beta) d\beta (\mathcal{D}^{l'}_{m',n'}(\Omega))^* \mathcal{D}^l_{m,n}(\Omega) = \frac{8\pi^2}{2l+1} \delta_{l,l'} \delta_{m,m'} \delta_{n,n'} \quad \text{(A.4)}$$

Successive rotations Ω_1 and Ω_2 give rise to the following closure relation

$$\mathcal{D}^l_{m,n}(\Omega_2 \Omega_1) = \sum_{p=-l}^{l} \mathcal{D}^l_{m,p}(\Omega_2) \mathcal{D}^l_{p,n}(\Omega_1) \quad \text{(A.5)}$$

For an inverse rotation $\Omega^{-1} = (-\gamma, -\beta, -\alpha)$ we have

$$\mathcal{D}^l_{m,n}(\Omega^{-1}) = \mathcal{D}^l_{n,m}(\Omega)^* = (-1)^{m-n} \mathcal{D}^l_{-n,-m}(\Omega) \quad \text{(A.6)}$$

The last property we want to mention is the integral over three $\mathcal{D}^l_{m,n}$-functions

$$\int \mathcal{D}^l_{m,n}(\Omega) \mathcal{D}^{l'}_{m',n'}(\Omega) \mathcal{D}^{l''}_{m'',n''}(\Omega) d\Omega = 8\pi^2 \begin{pmatrix} l & l' & l'' \\ m & m' & m'' \end{pmatrix} \begin{pmatrix} l & l' & l'' \\ n & n' & n'' \end{pmatrix} \quad \text{(A.7)}$$

where the brackets denote Wigner 3-j symbols.These are only non-zero if the l's values satisfy the triangle inequality and the m's or n's add up to zero.

For the $\mathcal{D}^l_{m,n}$-functions a useful functional can be defined by

$$\mathcal{D}^l_{m,n}[\mathcal{D}^{l'}_{m',n'}](\Omega) \equiv \int d\Omega' \mathcal{D}^l_{m,n}(\Omega'^{-1}\Omega) \mathcal{D}^{l'}_{m',n'}(\Omega') \quad \text{(A.8)}$$

Separating the Ω'^{-1} and Ω by using (A.5), followed by (A.6) will allow evaluation of the integral over Ω' which results in

$$\mathcal{D}^l_{m,n}[\mathcal{D}^{l'}_{m',n'}] = \frac{8\pi^2}{2l+1} \delta_{l,l'} \delta_{m,n'} \mathcal{D}^l_{m',n} \quad \text{(A.9)}$$

The $\mathcal{D}^l_{m,n}$-functions are directly related to the spherical harmonics by

$$\mathcal{D}^l_{m,0}(\alpha, \beta, \gamma) = C^*_{l,m}(\beta, \alpha) = \sqrt{\frac{4\pi}{2l+1}} Y^*_{l,m}(\beta, \alpha) \quad \text{(A.10)}$$

where $C_{l,m}$ are the modified spherical harmonics and in case of both indices of $\mathcal{D}^l_{m,n}$ being 0 they reduce to the Legendre polynomials

$$\mathcal{D}^l_{0,0}(\alpha, \beta, \gamma) = P_l(\cos(\beta)) \quad \text{(A.11)}$$

A.2 Symmetry adapted functions

The number of $\mathcal{D}^l_{m,n}$ related to a specific value of l is $(2l+1)^2$ and hence the number of functions which have to be considered is rapidly increasing. Therefore we like to restrict ourselves to a limited subset of the complete set. Such an appropriate subset will in general always follow directly from the symmetries obeyed by the system we like to study. For instance if we are interested in uniaxial particles we do not really need all three Euler angles to describe the orientation, two of them will satisfy just as well since the third angle only rotates the particle about its axis which will cause no observable effect.

We can exploit such symmetries we can make use in order to create a subset of symmetry adapted functions. Solutions we obtain in the end should always obey the symmetries and we might just as well save time and take the symmetries into account from the start.

The place where we the symmetries come into the problem for our systems is always in the integral of the average excluded volume This excluded volume $\mathcal{E}$ depends only on the relative orientation of the two particles and therefore should not change under transformations which leave the particles invariant. In order to perform a bifurcation analysis we then need to expand this excluded volume in an appropriate set of functions.

$$\mathcal{E}(\Omega_1,\Omega_2) = \mathcal{E}(\Omega_1^{-1}\Omega_2) = \sum_{l,m,n} E_{l,m,n}\mathcal{D}^l_{m,n}(\Omega_1^{-1}\Omega_2) \tag{A.12}$$

where Ω_1 and Ω_2 are the orientations of the particles.

Suppose the particles are invariant under all rotations g of the group G. The excluded volume should therefore not change if we apply any of the rotations g_1 or g_2 from G to the orientations of particles. This leads to a set of equations for the coefficients $E_{l,m,n}$. But instead of having the relations among the coefficients, it is more convenient to use the rotations for creating functions $S^l_{m,n}$ which are invariant under rotations of the group G

$$\begin{aligned} S^l_{m,n}(\Omega) &= \sum_{g_1,g_2\in G} \mathcal{D}^l_{m,n}(g_1^{-1}\Omega g_2) \\ &= \sum_{p,q}\left(\sum_{g_1\in G}\mathcal{D}^l_{m,p}(g_1^{-1})\right)\left(\sum_{g_2\in G}\mathcal{D}^l_{q,n}(g_2)\right)\mathcal{D}^l_{p,q}(\Omega) \end{aligned} \tag{A.13}$$

These functions are identical for several combinations of m and n, hence the total number of different symmetry adapted functions for given value of l is less than the original number of $(2l+1)^2$.

We only made use here of transformations in the form of rotations. Only reflections which conserve parity can be included, since they can be written as a normal rotation as well. Reflections that do not conserve parity however are here forbidden. They change the particle from left-handed to right-handed, which not acceptable in the set of rotation matrix elements.

If we examine the definition of the functional (A.9) more carefully we observe an interesting property in relation with the excluded volume, which can also be used in the form of a functional (2.29)

$$\mathcal{E}[\mathcal{D}^l_{m,n}] = \sum_p E_{l,n,p}\mathcal{D}^l_{m,p} \tag{A.14}$$

The functional decomposes the complete set S of $\mathcal{D}^l_{m,n}$-functions into invariant subspaces $S^l_m = \{\mathcal{D}^l_{m,i}\}$. Moreover for fixed values of l the action of the functional $\mathcal{E}$ on the subspace S^l_m is represented for all values of m by the same matrix $(E_l)_{n,p}$. This decomposition will also be true on a set of symmetry adapted functions and helps to simplify equations which will appear involving the excluded volume.

A.3 $\Delta^l_{m,n}$-functions

In case of the cross-like particles of chapter 3 there are only four transformations which leave the general particle invariant. These are the three rotations about the x-, y- and z-axis over π and the identity. In group theory this group is denoted by D_2 and is on of the dihedral groups [23].

For the elements of the group D_2 we can obtain the following identities

$$\begin{array}{lcll} \mathcal{D}^l_{m,n}(I) & = & \mathcal{D}^l_{m,n}(0,0,0) & = & \delta_{m,n} \\ \mathcal{D}^l_{m,n}(R_x(\pi)) & = & \mathcal{D}^l_{m,n}(0,\pi,\pi) & = & (-1)^l\delta_{m,-n} \\ \mathcal{D}^l_{m,n}(R_y(\pi)) & = & \mathcal{D}^l_{m,n}(0,\pi,0) & = & (-1)^{l+n}\delta_{m,-n} \\ \mathcal{D}^l_{m,n}(R_z(\pi)) & = & \mathcal{D}^l_{m,n}(0,0,\pi) & = & (-1)^n\delta_{m,n} \end{array} \tag{A.15}$$

Performing the first summation over the elements of the group D_2 we get in the definition of the symmetry adapted functions (A.13) we obtain

$$\sum_{g\in D_2} \mathcal{D}^l_{m,p}(g) = (1+(-1)^n)(\delta_{m,p} + (-1)^l\delta_{m,-p}) \tag{A.16}$$

So in order to obtain non-trivial functions we need even values for the index m, and similar for the index n. This leads to the definition of the set of $\Delta^l_{m,n}$-functions

$$\Delta^l_{m,n} = \left(\frac{1}{\sqrt{2}}\right)^{2+\delta_{m,0}+\delta_{n,0}} \left\{\mathcal{D}^l_{m,n} + (-)^l\mathcal{D}^l_{m,-n} + (-)^l\mathcal{D}^l_{-m,n} + \mathcal{D}^l_{-m,-n}\right\}. \tag{A.17}$$

where the prefactor takes care of the normalization. We choose to label all $\Delta^l_{m,n}$-functions with non-negative indices m and n. Naively one might expect that odd values of l are not allowed, just as in the case of Legendre Polynomials where the odd valued polynomials do not have up down symmetry, but here the odd values of l also give rise to non-trivial functions if and only if both indices m and n are non-zero. The choice of the prefactor in (A.17) leads to the following orthogonality relation

$$\int d\Omega \Delta^{l'}_{m',n'}(\Omega)\Delta^l_{m,n}(\Omega) = \frac{8\pi^2}{2l+1}\delta_{l,l'}\delta_{m,m'}\delta_{n,n'} \tag{A.18}$$

From (A.6) we observe that the $\Delta^l_{m,n}$-functions are automatically real valued, leading to a simple relation for inverse orientations

$$\Delta^l_{m,n}(\Omega^{-1}) = \Delta^l_{n,m}(\Omega) \tag{A.19}$$

It is clear that we cannot find a closure relation as (A.5) on the set of $\Delta^l_{m,n}$-functions. The reason is simply that a general rotation will always break the symmetry of the group D_2 and hence introduce functions which are outside the set of $\Delta^l_{m,n}$-functions. There is however a restricted set of rotations which leave our space of functions invariant. This set consists of the elements of the cubic group O. In order to prove this we only need to show that this is true for two generators of this group, which are the rotations over an angle $\pi/2$ about the y- and z-axis. By distinguishing the different combinations of zero and non-zero values for the indices m and n, which are both even it is a simple task to prove that for each element R of the cubic group

$$\begin{aligned}\Delta^l_{m,n}(\Omega R) &= \sum_{p\geq 0} \Delta^l_{m,p}(\Omega)\Delta^l_{p,n}(R) \\ \Delta^l_{m,n}(\Omega R) &= \sum_{p\geq 0} \Delta^l_{m,p}(R)\Delta^l_{p,n}(\Omega)\end{aligned} \tag{A.20}$$

Finally we want a similar expression for the $\Delta^l_{m,n}$-functions as (A.7). Again the only way to obtain this result is by distinguishing the different combinations of zero and non-zero indices

$$\int \Delta^l_{m,n}(\Omega)\Delta^{l'}_{m',n'}(\Omega)\Delta^{l''}_{m'',n''}(\Omega)d\Omega = 8\pi^2 \left(\frac{1}{2}\sqrt{2}\right)^{2-\delta_{0,mm'm''}-\delta_{0,mm'm''}} \times \begin{pmatrix} l & l' & l'' \\ m & \sigma'm' & \sigma''m'' \end{pmatrix} \begin{pmatrix} l & l' & l'' \\ n & \tau'n' & \tau''n'' \end{pmatrix} \tag{A.21}$$

where the brackets denote Wigner 3-j symbols and $\sigma', \sigma'', \tau', \tau''$ are ± 1 and chosen in such a way that $m + \sigma'm' + \sigma''m'' = n + \tau'n' + \tau''n'' = 0$. There is only one possible restriction to this formula, in case $m = 0$ or $n = 0$ the σ's or τ's are not uniquely defined. This causes the 3-j symbols to differ if and only if $l + l' + l''$ is an odd integer, in which case the sign changes. To avoid this one should if possible choose the m and n non-zero by taking a suitable permutation of the $\Delta^l_{m,n}$-functions.

The definition of the functional (A.9) for the $\Delta^l_{m,n}$-functions has the same form

$$\Delta^l_{m,n}[\Delta^{l'}_{m',n'}] = \frac{8\pi^2}{2l+1}\delta_{l,l'}\delta_{m,n'}\Delta^l_{m',n} \tag{A.22}$$

A.4 $C_{l,m}$-functions

For uniaxial particles only two angles are needed, because the third angle γ rotates the particle around its axis and therefore does not change any observable. For these particles it not necessary to describe their orientation by the complete set of $\mathcal{D}^l_{m,n}$. Instead the set of modified spherical harmonics can be used. The orientation is denoted by $\hat{\omega} = (\theta, \varphi)$ the usual polar coordinates and its invariant measure is given by $d\hat{\omega} = d\varphi \sin(\theta) d\theta$. The normalization changes to

$$\int_0^{2\pi} d\varphi \int_0^{\pi} \sin(\theta) d\theta C^*_{l,m}(\hat{\omega}) C_{l,m}(\hat{\omega}) = \frac{4\pi}{2l+1} \delta_{l,l'} \delta_{m,m'} \tag{A.23}$$

If γ is the angle between two directions $\hat{\omega}$ and $\hat{\omega}'$ there exists an addition theorem

$$P_l(\cos\gamma) = \sum_{m=-l}^{l} C^*_{l,m}(\hat{\omega}) C_{l,m}(\hat{\omega}') \tag{A.24}$$

which can easily be derived by using (A.5) with $m = n = 0$ and (A.6) on the argument $\Omega^{-1}\Omega'$.

The definition of the functional also has to be adjusted. On the set of modified spherical harmonics however this can only be defined properly for functions depending only on θ, so the second index has to be zero

$$P_l[C_{l',m'}](\hat{\omega}) \equiv \int d\hat{\omega}' P_l(\hat{\omega}' \cdot \hat{\omega}) C_{l',m'}(\hat{\omega}') \tag{A.25}$$

which now results in

$$P_l[C_{l',m'}] = \frac{4\pi}{2l+1} \delta_{l,l'} C_{l,m'} \tag{A.26}$$

This restriction will however not cause any problems, since the definition of this functional will be used for the excluded volume interaction, which normally depends only on the mutual angle between the directors of the particles and hence can be expanded in Legendre polynomials only.

This set of functions can also be derived from the definition of the symmetry adapted functions by recognizing that the group of rotations which leaves the particle invariant is D_∞. Hence the summations over elements of the symmetry group have to be replaced by integrations over the angle γ.

Bibliography

[1] B.J. Alder and T.E. Wainwright, J. Chem. Phys. **27**, 1208 (1957).

[2] M.H.J. Hagen, E.J. Meijer, G.C.A.M. Mooij, D. Frenkel and H.N.W. Lekkerkerker, Nature **365**, 425 (1993).

[3] P.G. Bolhuis, M.H.J. Hagen and D. Frenkel, Phys. Rev. E **50**, 4880 (1994).

[4] L. Onsager, Ann. N.Y. Acad. Sci. **51**, 627 (1949).

[5] R. Eppenga and D. Frenkel, Mol. Phys. **52**, 1303 (1984).

[6] D. Frenkel and B.M. Mulder, Mol. Phys. **55**, 1171 (1985).

[7] B.M. Mulder and D. Frenkel, Mol. Phys. **55**, 1193 (1985).

[8] J.A.C. Veerman and D. Frenkel, Phys. Rev. A **45**, 5632 (1992).

[9] J.E. Mayer and M.G. Mayer, *Statistical Mechanics*, John Wiley, New York (1977).

[10] R. Evans, Adv. Phys. **28**, 143 (1979).

[11] R. Schneider, *Convex bodies: the Brunn-Minkowski theory*, Cambridge University Press, Cambridge (1993).

[12] R.F. Kayser and H.J. Raveché, Phys. Rev. A **17**, 2067 (1978).

[13] B. Mulder, Phys. Rev. A **39**, 360 (1989).

[14] N. Metropolis, A.W. Rosenbluth, M.N. Rosenbluth, A.H. Teller and E. Teller, J. Chem. Phys. **21**, 1087 (1953).

[15] W.W. Wood and F.R. Parker, J. Chem. Phys. **27**, 720 (1957).

[16] A. Rahman, Phys. Rev. A **136**, 405 (1964).

[17] M.P. Allen and D.J. Tildesley, *Computer simulations of liquids*, Oxford University Press, Oxford (1987).

[18] D. Frenkel and B. Smit, *Understanding Molecular Simulation. From Algorithms to Applications*, Academic Press, Boston (1996).

[19] I.R. McDonald, Mol. Phys. **23**, 41 (1972).

[20] D. Frenkel, 'Statistical mechanics of liquid crystals', in *Liquids, Freezing and Glass Transition*, edited by J.P. Hansen, D. Levesque and J. Zinn-Justin, North-Holland, Amsterdam (1991).

[21] J.P. Straley, Phys. Rev. A **10**, 1881 (1974).

[22] I.S. Gradshteyn and I.M. Ryzhik, *Table of Integrals, Series, and Products*, Academic Press, Inc., San Diego, 5th edition (1994).

[23] M. Hamermesh, *Group Theory*, Addison-Wesley Publ. Comp., Inc., Reading, Massachusettts, 2nd edition (1964).

[24] A. Isihara, J. Chem. Phys. **18**, 1446 (1950).

[25] M.S. Wertheim, Mol. Phys. **83**, 519 (1994).

[26] M.S. Wertheim, J. Chem. Phys. **78**, 4619 (1983).

[27] D. Frenkel, J. Chem. Phys. **91**, 4912 (1987).

[28] D. Frenkel, J. Chem. Phys. **92**, 5314 (1988).

[29] D. Frenkel, Mol. Phys. **60**, 1 (1987).

[30] D. Frenkel, Mol. Phys. **65**, 493 (1988).

[31] F.H. Ree and W.G. Hoover, J. Chem. Phys. **40**, 939 (1964).

[32] G.M. Torrie and J.P. Valleau, J. Comp. Phys. **23**, 187 (1977).

[33] A.P. Lyubartsev, A.A. Martsinovski, S.V. Shekunov and P.N. Vorontsov-Velyaminov, J. Chem. Phys. **96**, 1776 (1992).

[34] E. Marinari and G. Parisi, Europhys. Lett. **19**, 451 (1992).

[35] C.J. Geyer, 'Markov chain monte carlo maximum likelihood', in *Computing Science and Statistics: Proceedings of the 23rd Symposium on the Interface* (1991).

[36] E.F. Gramsbergen, L. Longa and W.H. de Jeu, Physics Reports **135**, 195 (1986).

[37] P. Bolhuis and D. Frenkel, J. Phys. Chem. **106**, 666 (1997).

[38] D. Frenkel and R. Eppenga, Phys. Rev. Lett. **49**, 1089 (1982).

[39] J.D. Parsons, Phys. Rev. A **19**, 1225 (1979).

[40] S.D. Lee, J. Chem. Phys. **87**, 4972 (1987).

[41] G.J. Vroege and H.N.W. Lekkerkerker, Rep. Progr. Phys. **55**, 1241 (1992).

[42] D. Frenkel and J.F. Maguire, Phys. Rev. Lett. **47**, 1025 (1981).

[43] D. Frenkel and J.F. Maguire, Mol. Phys. **3**, 503 (1983).

[44] M.C. Duro, J.A. Martín-Pereda and L.M. Sesé, Phys. Rev. A **37**, 284 (1988).

[45] M.P. Allen, G.T. Evans, D. Frenkel and B.M. Mulder, Adv. Chem. Phys. **86**, 1 (1993).

[46] J. Vieillard-Baron, J. Chem. Phys. **56**, 4729 (1972).

[47] J.W. Perram and M.S. Wertheim, J. Comp. Phys. **58**, 409 (1985).

[48] M. Parrinello and A. Rahman, Phys. Rev. Lett. **45**, 1196 (1980).

[49] M. Parrinello and A. Rahman, J. Appl. Phys. **52**, 7182 (1981).

[50] M. Parrinello and A. Rahman, J. Chem. Phys. **76**, 2662 (1982).

[51] R. Najafabadi and S. Yip, Scripta Metall. **17**, 1199 (1983).

[52] P.J. Steinhardt, D.R. Nelson and M. Ronchetti, Phys. Rev. B **28**, 784 (1983).

[53] D. Frenkel and A.J.C. Ladd, J. Chem. Phys. **81**, 3188 (1984).

[54] J.G. Briano and E.D. Glandt, J. Chem. Phys. **80**, 3336 (1984).

[55] D.A. Kofke and E.D. Glandt, J. Chem. Phys. **87**, 4881 (1987).

[56] D.A. Kofke and E.D. Glandt, Mol. Phys. **87**, 1105 (1988).

[57] D.M. Brink and G.R. Satchler, *Angular Momentum*, Oxford University Press, Oxford, 2nd edition (1968).

Summary

In this thesis the possibility of the existence of a cubatic phase is investigated. This liquid crystal phase has an orientational order with cubic symmetry but no translational order. This phase was discovered during computer simulations of a system of disk-like particles, the cut-spheres, with only hard-core repulsion. So far, however, no experimental system is known which exhibits this phase. This thesis investigates the possibility of the cubatic phase in two other systems.

In chapter 1 the background of the complex fluids is sketched, including the discovery of the cubatic phase. In chapter 2 the basic theoretical framework of this thesis is introduced, in particular the statistical mechanical background of density functional theory. We then proceed to derive the Helmholtz free energy functional in the second virial approach. This is the basis of all theoretical work in this thesis. We also introduce the bifurcation analysis, a simple but powerful tool to study phase transitions in complex liquids.

In chapter 3 this technique is applied to a system of "Onsager crosses", particles consisting of three elongated perpendicular rods. By using bifurcation analysis, a free energy minimization and Gaussian approximation the orientational phase behavior of these particles is mapped out in the limit where the rods are infinitely long. We find four different ordered phases: the nematic, the biaxial, the D_4 phase and the cubatic phase. The latter is found when the three constituting rods have approximately the same length.

In chapter 4 the validity of the assumptions made in chapter 3 is checked for finite aspect ratios by calculating the second and higher virial coefficients of perfect crosses. In addition the parameter hopping method is introduced as a tool to overcome problems in simulating these cross-like particles. Although in principle a useful simulation technique for glasses, the entanglement of the crosses are beyond its capacity. No indication for the cubatic phase or any other type of ordering is observed. A mechanically stable crystal could be constructed, but did not form spontaneously.

Chapter 5 describes the theory of monodisperse cylinders as an Ansatz to explain the cubatic phase of the stacks formed by cut-spheres. The preference for cylinders with aspect ratios of order unity to be parallel is only slightly larger than for those particles to be perpendicular. Although the bifurcation analysis was promising, trial functions indicated that for all aspect ratio's the isotropic-to-cubatic transition is preceded by the isotropic-to-nematic transition.

Chapter 6 describes in a simple way how to incorporate the formation of stacks in systems of cylinders, by combining the description of such system at the different levels of monomers and clusters. According to the bifurcation theory the instability of the isotropic system shifts to lower densities and for thin cylinders near this point stacks are formed, which possibly can form the cubatic phase. We discuss the effect of polydispersity on the bifurcation analysis. Also in this case, the instability of the isotropic phase

shifts to lower density. It was shown not to depend on the actual distribution, but only on the average length and the mean-squared length.

In chapter 7 cylinders the virial coefficients of cylinders are calculated and the outcome was compared with the results from the Parsons approach. Cylinders with an aspect ratio of 0.9 are simulated and showed that the Parsons approach works up to the first order phase transition to a crystalline phase. This phase is an AAA-crystal but in which planes are not straight but fluctuating. The particles tend to orient in, or perpendicular to, the layers. The orientational distribution exhibits a weak but significant 4-fold symmetry. On increasing pressure the system slowly evolves to the conventional AAA-crystal. No indication of a cubatic phase is found. The introduction of polydispersity via an imposed activity ratio led to a destabilization of the crystal phase. On increasing the width of the imposed activity, the distribution of particle lengths, shifts to lower aspect ratios and away from unity. The ordered phase melts, also in this case directly to an isotropic phase.

Samenvatting voor Iedereen

"Hallo, hoe gaat het? Wat doe jij zo tegenwoordig?"
"Ik ben nu bezig met mijn promotie onderzoek."
"Gôh, wat leuk. En wat doe je dan precies?"
"Ik probeer met behulp van theorie en computersimulaties het gedrag van vloeibare kristallen te beschrijven."
"Jaajaah, klinkt wel ingewikkeld."
Meestal is dit het einde van het gesprek over mijn werk. Een enkele keer is iemand meer geinteresseerd en vraagt verder, maar over het algemeen neemt het gesprek een andere wending. Men gaat er namelijk vanuit dat een eventuele uitleg toch te moeilijk is om te begrijpen.

Speciaal voor deze mensen zal ik hier proberen een idee te geven van de zaken waar ik mij de afgelopen jaren mee bezig heb gehouden en die in dit proefschrift worden beschreven. Om dit te bereiken zal ik gebruik maken van analogiën. Het probleem met analogiën is dat ze welliswaar verhelderend kunnen zijn, maar toch vaak de waarheid geweld aan doen. Dat risico neem ik dan maar.

We starten met de 'atomaire hypothese', de aanname dat ieder zuiver materiaal, is opgebouwd uit kleine identieke deeltjes. Deze deeltjes zijn zo klein dat we ze niet kunnen zien met het blote oog, en zelfs niet met een microscoop. Deze kleine deeltjes noemen we *moleculen*. Deze moleculen zijn zelf opgebouwd uit nog weer kleinere deeltjes die we *atomen* noemen. Die atomen kunnen we beschrijven als hele kleine bolletjes, die afhankelijk van het soort, een andere grootte hebben. Doordat moleculen zijn opgebouwd uit deze bouwsteentjes zijn die over het algemeen niet bolvormig. Sommige moleculen, zoals zuurstof, bestaan uit slechts twee tegen elkaar geplakte atomen. Andere moleculen, zoals die van plastic, worden gevormd door hele lange ketens van atomen. Omdat de ketens duizenden of miljoenen atomen lang zijn en soms maar enkele atomen breed zijn dit net draadjes en ze zijn makkelijk te buigen zonder dat ze meteen breken. Weer andere moleculen, bijvoorbeeld die van cholesterol, bestaan uit slechts enkele tientallen atomen en hebben de vorm van een kort, dik stokje en zijn helemaal niet buigzaam.

Hoewel de meeste materialen duidelijk verschillen van elkaar zijn er ook overeenkomsten. Zo kunnen de meeste in drie verschillende toestanden voorkomen, of zoals wij dat noemen *fasen*. We onderscheiden de *vaste*, de *vloeibare* en de *gasvormige* fase. Het bekendste voorbeeld uit het dagelijks leven waarvan we alle drie de vormen kennen is water. Water is vloeibaar maar als we het voldoende afkoelen (0^0C) bevriest het tot ijs, de vaste fase, en als we het verwarmen tot (100^0C) gaat het koken en wordt waterdamp, de gasvormige fase. Voor veel andere stoffen zijn we die drie fasen niet gewend omdat ze normaal maar in een van de drie toestanden voorkomen. De zuurstof in de lucht bijvoorbeeld wordt pas vloeibaar bij een temperatuur van -183^oC en indien we het nog verder afkoelen tot -219^oC wordt het vast. Yzer daarentegen moeten we verwarmen tot 1538^oC om het vloeibaar te maken en pas bij 2861^oC wordt het gasvormig.

Indien we de drie verschillende verschijningsvormen met elkaar vergelijken vinden we dat over het algemeen de vaste vorm het hoogst soortelijk gewicht heeft. Dus als zuivere stoffen uit identieke moleculen bestaan, dan moeten er meer moleculen in een kubieke meter vaste stof zitten dan in een zelfde volume van de vloeistof of de damp.Een uitzondering hierop is water, immers de vaste vorm, ijs, blijft op water drijven en moet dus een lagere dichtheid hebben.

Wat verder opvalt is dat terwijl vloeistoffen en gassen de vorm aan nemen van een glas of container waarin ze zitten, vaste stoffen een vorm hebben die slechts met moeite kan worden veranderd.

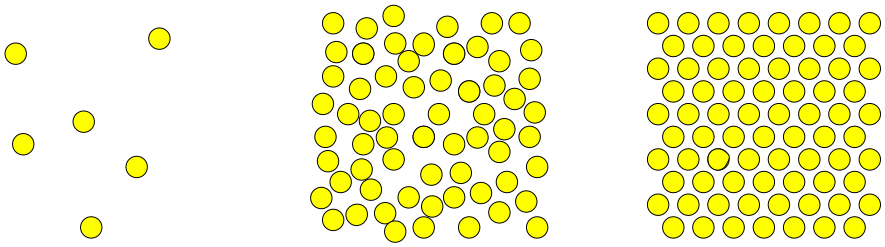

In bovenstaande figuur is op een simpele manier weergegeven hoe een gas, vloeistof en vaste stof er uitzien als we dit zouden bekijken op de schaal van de moleculen. De moleculen worden hier afgebeeld als bolletjes.

Omdat een gas een lage dichtheid heeft zijn de moleculen ver van elkaar verwijderd. Voor een vloeistof zitten de moleculen veel dichter opeen maar lijken op een willekeurige manier gestapeld. De dichtheid van een vaste stof is echter nog hoger. Om al die deeltjes een plaats te geven moeten ze netjes in een rij gaan zitten. Dit is te vergelijken met een doos suikerklontjes. Als er maar een paar klontjes in de doos zitten liggen ze willekeurig door de doos verspreid. Maar als we er een heleboel bij gooien zullen ze tegen elkaar komen te liggen. Als we toch nog meer klontjes in de doos willen doen moeten we ze netjes op een zelfde manier op een rij leggen. We zeggen dan ook wel dat in een gas en vloeistof de deeltjes *ongeordend* zijn, terwijl ze in een vaste stof op een nette, geordende manier gerangschikt zijn die we *kristallijn* noemen.

In werkelijkheid zitten moleculen echter helemaal niet stil maar bewegen of trillen en botsen hierbij voortdurend tegen elkaar, net als biljartballen. Hoe hoger de temperatuur is, des te sneller bewegen ze. In een gas en vloeistof zullen ze kris-kras door elkaar bewegen maar in een vaste stof is, zoals in het plaatje te zien is, niet veel ruimte. De deeltjes zullen als gevolg daarvan voortdurend tegen hun buren weerkaatsen en daardoor min of meer op de zelfde plaats blijven.

Het is nu ook een intuïtief duidelijk waarom een gas nauwelijks weerstand biedt als we er met een hand door heen bewegen. Immers als we dit doen zal onze hand tegen de moleculen aan botsen, wat wij als een zwakke weerstand ervaren. In een vloeistof is de dichtheid veel hoger en zal onze hand tegen veel meer moleculen aanbotsen en dus een grotere weerstand voelen. Als we het zelfde bij een vaste stof proberen botst onze hand tegen de buitenste laag moleculen aan en probeert die te verplaatsen. In tegenstelling tot in de vloeistof en het gas kunnen deze deeltjes echter niet ver van hun plaats voordat ze tegen buren aanbotsen, en die weer tegen hun buren, enz. Met als gevolg dat, zodra we de buitenste laag willen verplaatsen, we het hele object moeten verplaatsen.

Overigens zijn moleculen geen gewone biljartballen. Op korte afstand van elkaar zullen ze elkaar namelijk afstoten, wat lijkt op botsen, maar op grotere afstand van elkaar trekken ze elkaar een beetje aan.

Wat we tot nu toe gezien hebben is dat er drie verschillende fasen zijn, waarvan de gasvormige en vloeibare fase ongeordend zijn en de vaste fase geordend. Wat we hiervoor hebben aangenomen is dat ieder materiaal uit kleine deeltjes bestaat, moleculen, die we als een soort biljartballetjes kunnen beschouwen. Indien we op ieder moment weten op welke plaats de deeltjes zitten en hoe groot ze zijn weten we in principe genoeg om zo'n systeem van bolletjes te beschrijven. Zoals eerder vermeld echter, zijn de meeste moleculen helemaal niet bolvormig, maar bijvoorbeeld staafjes. Dit betekend dat we niet alleen hun positie moeten weten maar ook in welke richting ze wijzen.

Dit opent nieuwe perspectieven, want in de geordende fase van een vaste stof hebben we eigenlijk alleen maar gekeken naar de orde in de posities van de deeltjes, maar nu zijn er ook nog de orientaties van de deeltjes waar we naar kunnen kijken. Ook nu zorgt de dichtheid, het aantal deeltjes per volume, ervoor dat er orde ontstaat. Als we bijvoorbeeld lucifers in een doosje gooien zullen ze niet alleen willekeurig door elkaar komen te liggen maar ook allemaal in verschillende richtingen wijzen. We kunnen vervolgens zo'n doosje schudden en hoewel na afloop ze anders zullen liggen, zal er nog steeds geen enkele orde zijn. Als we dit proces herhalen en er steeds meer lucifers bij gooien komt er een moment dat de lucifers gelijk gaan richten. Er is een geordende fase onstaan waarbij ook de orientaties van de deeltjes meedoen. Iets dergelijks gebeurt met sommige staafachtige moleculen. In onderstaande figuur heb ik drie mogelijke fasen van dit soort deeltjes geschetst.

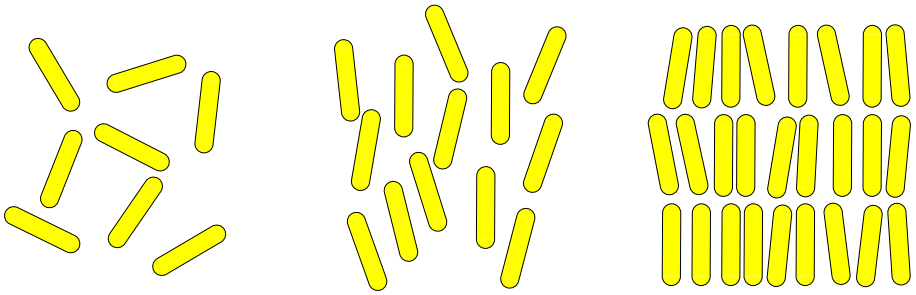

In het linkse plaatje zijn de deeltjes helemaal niet geordend. In het middelste plaatje wijzen alle deeltjes gemiddeld in de zelfde richting, maar zijn de posities van de middelpunten van de deeltjes ongeordend. Dit type ordening noemen we een *nematische* fase. In het rechtse plaatje is een *smectische* fase geschetst, daarin zijn zowel de orientaties als de posities geordend. De deeltjes wijzen allemaal de zelfde kant op en liggen in laagjes. Dit soort fasen die niet volledig maar slechts ten dele geordend zijn noemen we *vloeibare kristallen*. Ze bezitten zowel eigenschappen van vloeistoffen als van kristallen. Zo is er duidelijk een soort orde aanwezig maar kunnen we een vloeibaar kristal wel roeren. Dit soort vloeibare kristallen wordt tegenwoordig gebruikt in de beeldschermpjes van rekenapparaten en kwartshorloges en zijn soms beter bekend onder de engelse naam 'liquid crystal display' (LCD).

In 1991 werd een nieuw type vloeibaar kristal ontdekt. Niet in een experiment, maar in een computersimulatie waarbij de deeltjes de vorm hebben van een soort schijfjes. In onderstaande figuur staat een moment opname van een simulatie van deze fase weergegeven.

Net zoals in de nematische fase zijn de posities van de schijfjes ongeordend terwijl de orientaties wel een orde vertonen. Deze is echter anders dan in een nematische fase. Terwijl in de laatste de deeltjes allemaal in min of meer een en dezelfde richting wijzen lijken de schijfjes in deze nieuwe fase in drie verschillende richtingen te kunnen wijzen. Die richtingen zijn bovendien onderling loodrecht, net als de ribben van een kubus. Deze fase werd dan ook de *kubatische* fase genoemd. Tot op heden is deze fase nog nooit in een bestaand systeem aangetoond. Het is deze fase waar dit proefschrift aan gewijd is.

In het eerste deel van dit proefschrift bekijken we deeltjes in de vorm van kruisjes. Kruisjes hebben van nature al drie verschillende richtingen waarin ze wijzen. Het idee is dat als lucifers naast elkaar in dezelfde richting willen liggen dit misschien ook wel zo is voor deze kruisjes en op die manier dus een kubatische fase vormen. Volgens de theorie die we ontwikkeld hebben is dit inderdaad het geval indien de staafjes die het kruisje vormen heel erg lang zijn. De computersimulaties voor kleine kruisjes echter, laten zien dat die geen kubatische fase kunnen vormen.

In het tweede deel van van dit proefschrift bekijken we deeltjes die de vorm hebben van cylindertjes, die even lang als breed zijn. Als je deze deeltjes van boven bekijkt lijken ze rond, terwijl van de zijkant op vierkantjes lijken. Hoewel de theorie aanvankelijk veelbelovend leek te zijn, bleken ze toch geen kubatische fase te kunnen vormen. Dit werd nog eens bevestigd door computersimulaties, die overigens wel een ander interessante fase lieten zien.